Josip Juraj Strossmayer University of Osijek

University of Dubrovnik

Ruđer Bošković Institute

Doctoral Programme of Molecular Biosciences

Marin Kutnjak

Roles of the ACRC and SPRTN proteases and the p97 segregase in DNA-protein crosslink repair

Doctoral thesis

Osijek, 2026

Sveučilište Josipa Jurja Strossmayera u Osijeku

Sveučilište u Dubrovniku

Institut Ruđer Bošković

Doktorski studij Molekularne bioznanosti

Marin Kutnjak

Uloge proteaza ACRC i SPRTN te segregaze p97 u popravku unakrsnih veza DNA i proteina

Doktorski rad

Osijek, 2026.

Josip Juraj Strossmayer University of Osijek

University of Dubrovnik

Ruđer Bošković Institute

Doctoral Programme of Molecular Biosciences

Marin Kutnjak

Roles of the ACRC and SPRTN proteases and the p97 segregase in DNA-protein crosslink repair

Doctoral thesis

Osijek, 2026

TEMELJNA DOKUMENTACIJSKA KARTICA

Sveučilište Josipa Jurja Strossmayera u Osijeku **Doktorski rad**
Sveučilište u Dubrovniku
Institut Ruđer Bošković
Doktorski studij Molekularne bioznanosti

Znanstveno područje: Interdisciplinarno područje znanosti
Znanstvena polja: biologija, kemija

Uloge proteaza ACRC i SPRTN te segregaze p97 u popravku unakrsnih veza DNA i proteina

Marin Kutnjak

Doktorski rad je izrađen u: Laboratoriju za molekularnu ekotoksikologiju Zavoda za istraživanje mora i okoliša Instituta Ruđer Bošković, Zagreb

Mentor: dr. sc. Marta Popović, viša znanstvena suradnica

Kratki sažetak doktorskog rada:
Ovo istraživanje ispituje uloge proteaza ACRC i SPRTN te segregaze p97 u popravku unakrsnih veza DNA i proteina u stanicama čovjeka i u zebrici kao komplementarnim modelnim sustavima. Utvrdili smo da je ACRC esencijalna proteaza za rani razvoj kralježnjaka koja sudjeluje u popravku endogenih DPC-ova. Pokazano je da ATPaza p97 doprinosi popravku više vrsta staničnih DPC-ova. Interakcija SPRTN-a i p97 putem SHP motiva mogla bi biti važna za popravak nekih endogenih DPC-ova *in vivo*.

Broj stranica: 125
Broj slika: 25
Broj tablica: 0
Broj literaturnih navoda: 151
Jezik izvornika: engleski
Ključne riječi: unakrsne veze DNA i proteina (DPC-ovi), popravak DPC-ova, proteaza ACRC, proteaza SPRTN, segregaza p97, zebrica (*Danio rerio*)

Datum javne obrane:

Povjerenstvo za javnu obranu:
1.
2.
3.
4. (zamjena)

Doktorski rad je pohranjen u: Nacionalnoj i sveučilišnoj knjižnici Zagreb, Ul. Hrvatske bratske zajednice 4, Zagreb; Gradskoj i sveučilišnoj knjižnici Osijek, Europska avenija 24, Osijek; Sveučilištu Josipa Jurja Strossmayera u Osijeku, Trg sv. Trojstva 3, Osijek

BASIC DOCUMENTATION CARD

Josip Juraj Strossmayer University of Osijek **PhD thesis**
University of Dubrovnik
Ruđer Bošković Institute
Doctoral Study of Molecular biosciences

Scientific Area: Interdisciplinary area of science
Scientific Fields: Biology, Chemistry

Roles of the ACRC and SPRTN proteases and the p97 segregase in DNA-protein crosslink repair

Marin Kutnjak

Thesis performed at: Laboratory for Molecular Ecotoxicology, Division for Marine and Environmental Research, Ruđer Bošković Institute, Zagreb

Supervisor: Dr. Marta Popović, Senior Research Associate

Short abstract:
This study investigates the roles of the ACRC and SPRTN proteases and the p97 segregase in DNA-protein crosslink repair in human cells and zebrafish as complementary model systems. We identified ACRC as an essential protease in early vertebrate development that repairs endogenous DPCs. The ATPase p97 was shown to be an important contributor to the repair of multiple cellular DPCs. The SPRTN-p97 interaction via the SHP motif could be important for the repair of some endogenous DPCs *in vivo*.

Number of pages: 125
Number of figures: 25
Number of tables: 0
Number of references: 151
Original in: English
Key words: DNA-protein crosslinks (DPCs), DPC repair, ACRC protease, SPRTN protease, p97 segregase, zebrafish (*Danio rerio*)

Date of the thesis defense:

Reviewers:
1.
2.
3.
4. (substitute)

Thesis deposited in: National and University Library in Zagreb, Ul. Hrvatske bratske zajednice 4, Zagreb; City and University Library of Osijek, Europska avenija 24, Osijek; Josip Juraj Strossmayer University of Osijek, Trg sv. Trojstva 3, Osijek

CONTENTS

1. INTRODUCTION

1.1. DNA damage and DNA repair

The DNA molecule contains the genetic information required by living organisms for growth, differentiation, survival, and cell division. DNA is a sensitive molecule located in a chemically highly reactive environment. It is continuously subjected to damage under the influence of various endogenous and exogenous factors. Loss of DNA integrity results in diverse disruptions of cellular processes and, consequently, cell death and diseases such as malignant tumors, diabetes, accelerated aging, or neurodegeneration (Jackson & Bartek, 2009).

Mammalian cells are estimated to sustain on the order of 10^5 DNA lesions per day. These lesions include chemically modified bases and nucleotide-level errors, such as mismatches and small insertions/deletions; abasic (AP, apurinic/apyrimidinic) sites; bulky helix-distorting lesions (e.g., cyclobutane pyrimidine dimers and 6-4 photoproducts) and intrastrand crosslinks; DNA interstrand crosslinks (ICLs); DNA single-strand breaks (SSBs); DNA double-strand breaks (DSBs); and **DNA-protein crosslinks (DPCs)**. Base damage can arise through spontaneous hydrolysis, deamination, oxidation, and alkylation, whereas ultraviolet (UV) radiation and certain chemical mutagens, including polycyclic aromatic hydrocarbons (PAHs) and some chemotherapeutic agents, generate bulky helix-distorting lesions. AP sites are the most frequent endogenous lesions. SSBs are likewise common and arise either directly, for example through oxidative damage to the DNA backbone, or indirectly during repair of damaged bases, whereas DSBs are much less frequent under physiological conditions but are among the most deleterious lesions. Particularly toxic are covalent crosslinks: ICLs prevent strand separation and thereby block replication and transcription, while DPCs constitute a highly heterogeneous class of bulky lesions. Thus, DNA lesions differ markedly in both abundance and biological impact, ranging from highly frequent small base lesions that are usually repaired efficiently to rarer bulky or crosslinked lesions that pose major barriers to replication and transcription and therefore disproportionately threaten genome stability (Chen et al., 2024; Hoch, 2023; Q. Li et al., 2023).

To preserve genomic integrity, a sophisticated genome-maintenance system has emerged in organisms, comprising several DNA damage response (DDR) and DNA damage tolerance (DDT) pathways. Different DDR pathways are involved in the recognition and repair

of specific types of DNA lesions, for example base excision repair (BER), single-strand break repair (SSBR), nucleotide excision repair (NER), and mismatch repair (MMR), which primarily resolve lesions that do not involve DSBs. These repair pathways typically act via excision and resynthesis of a short tract on one DNA strand. DNA interstrand crosslinks are processed by the Fanconi anemia (FA) pathway, while DSBs are mainly repaired by homology-directed repair (HDR) and classical non-homologous end joining (c-NHEJ). Additional DSB repair pathways include alternative end joining/microhomology-mediated end joining (alt-EJ/MMEJ), single-strand annealing (SSA), and, in specific contexts, break-induced replication (BIR) (Fielden et al., 2018; Q. Li et al., 2023). In addition to these DDR pathways, cells also employ DDT mechanisms, such as translesion DNA synthesis (TLS) and template switching, to bypass lesions during replication. At present, most known DDR pathways are relatively well characterized. However, it is still not entirely clear how cells repair DNA-protein crosslinks, even though DPCs are highly prevalent DNA lesions and their presence is highly cytotoxic (Fielden et al., 2018; Vaz et al., 2017). **DPC repair (DPCR)** is a rapidly evolving field: its major pathways have now been established, but many aspects of pathway choice, coordination, and lesion-specific processing remain incompletely understood.

1.2. DNA-protein crosslinks (DPCs)

The genomes of organisms are continuously exposed to various forms of DNA damage. DPCs are frequent DNA lesions that arise when a protein, regardless of its size or other properties, becomes irreversibly covalently bound to DNA. They are highly heterogeneous lesions that vary widely in the size of the crosslinked protein, the chemistry of the crosslink between the protein and DNA, and the topology of the surrounding DNA, which may be intact or contain a single-strand or double-strand break. DPCs can arise endogenously or upon exposure to exogenous physical or chemical crosslinking agents (DPC inducers). Endogenous DPC inducers include (i) by-products of cellular metabolic reactions, such as reactive oxygen species (ROS), reactive nitrogen species (RNS), and aldehydes (e.g., formaldehyde generated during histone demethylation, acetaldehyde, malondialdehyde, and acrolein), and (ii) structural DNA lesions, including abasic sites, oxanines (deaminated guanines), nicks in the DNA strand, and DNA strand breaks. Exogenous DPC inducers include, for example, ultraviolet radiation, ionizing radiation (IR), transition metals, aldehydes derived from environmental contaminants, and various chemotherapeutic agents, such as cisplatin derivatives, nitrogen mustards, 5-aza-

2’-deoxycytidine (5-aza-dC), camptothecin, and etoposide (Kühbacher & Duxin, 2020; Perry & Ghosal, 2022).

DPCs are among the most abundant DNA lesions in cells. Abasic sites are the most frequent DNA lesions; these arise endogenously at a rate of about 10 000 events per cell per day in the human genome and can themselves act as endogenous DPC inducers in cells, as their reactive aldehydic form can react with nearby protein amino groups, such as lysine side chains or protein N-termini, to form covalent DNA-protein adducts, typically via Schiff base formation (Nakamura & Nakamura, 2020). DPCs occur at a frequency of approximately 6 000 events per day in the genome of each mammalian cell. In a molecular context, these lesions are large and constitute a physical barrier to DNA-associated processes, including replication, transcription, DNA repair, recombination, and chromatin remodeling. Therefore, DPC repair pathways are exceptionally important for preventing genomic instability (i.e., maintaining genomic integrity), which can ultimately contribute to the development of various diseases. The consequences of unrepaired DPCs are partly understood, whereas the components, regulation, and mechanisms of DPC repair pathways remain relatively underexplored, despite attracting increasing research interest in recent years. At the cellular level, impaired DPC repair may lead to SSBs, DSBs, genome instability, and ultimately cell death, whereas at the organismal level it has been associated with cancer, premature aging, and neurodegenerative disorders (Ruggiano & Ramadan, 2021; Vaz et al., 2017).

1.2.1. Non-enzymatic and enzymatic DPCs

DPCs arise when proteins become irreversibly covalently crosslinked to DNA either after exposure to physical (e.g., UV radiation) or chemical agents (e.g., aldehydes), giving rise to **non-enzymatic DPCs**, or as a consequence of abortive/aberrant enzymatic reactions, resulting in enzymatic DPCs (Stingele & Jentsch, 2015) (Figure 1). In non-enzymatic DPCs, in principle any protein, regardless of its size, structure, or function, can become crosslinked to DNA if it is in close proximity during exposure to a DPC-inducing agent.

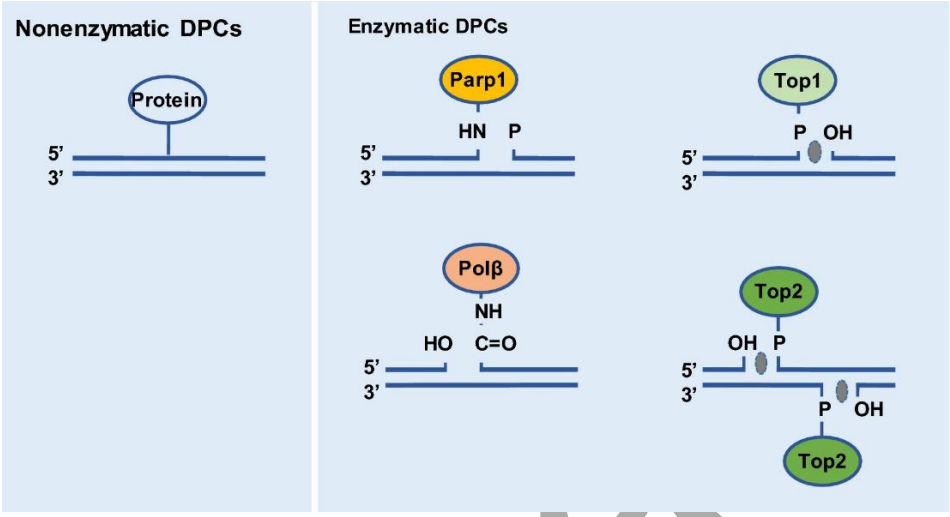

Figure 1. Schematic overview of non-enzymatic and enzymatic DNA-protein crosslinks (DPCs). Non-enzymatic DPCs can involve proteins nonspecifically crosslinked to DNA, whereas enzymatic DPCs can arise from trapped covalent intermediates of DNA-processing enzymes. Adapted from (H. Zhang et al., 2020)

Formaldehyde (FA) is one of the most potent DPC inducers. It promotes crosslinking of numerous proteins and is therefore non-specific. Formaldehyde is naturally present in the cellular environment because it is generated by endogenous cellular processes such as lipid peroxidation and the demethylation of DNA, RNA, and histones. Exposure to formaldehyde can also be exogenous, for example through smoking, polluted air, industrial resins, paints, adhesives, and certain food, cosmetic, and construction products (Ruggiano & Ramadan, 2021). It has been estimated that the normal endogenous concentration of formaldehyde in the blood of humans, rhesus monkeys, and rats (*Rattus norvegicus*) is around 100 µM, whereas in rat liver and nasal mucosa it can reach up to 400 µM (Heck & Casanova, 2004). Formaldehyde-induced DPC formation proceeds through reversible Schiff base intermediates formed on either protein or DNA amino groups, which subsequently react with the other biomolecule to generate a methylene crosslink (Figure 2) (Tretyakova et al., 2015). Formaldehyde generated during endogenous cellular processes can readily be found in close proximity to DNA. Therefore, DPC formation in cells is continuous, and cells must possess mechanisms to repair these lesions in order to avoid their negative consequences.

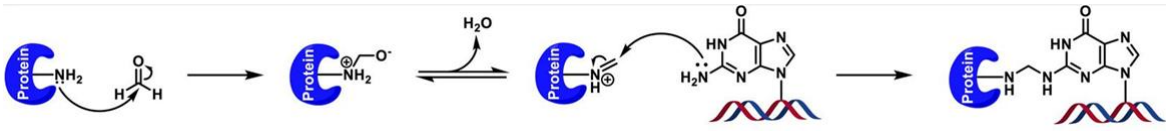

Figure 2. Mechanism of formaldehyde-induced DNA-protein crosslink formation. Formaldehyde reacts reversibly with a protein amino group to form a Schiff base intermediate, which subsequently reacts with an exocyclic amino group of a DNA base to generate a methylene bridge linking the protein to DNA (adapted from (Tretyakova et al., 2015)).

1.2.1.1. Enzymatic DPCs

Enzymatic DPCs can be induced endogenously when enzymes that interact with DNA during their normal catalytic cycles encounter a distortion in the DNA helix (e.g., abasic sites) or locally elevated concentrations of aldehydes or ROS. Exogenously, they can be induced by chemotherapeutic agents that bind to a particular enzyme and promote irreversible covalent attachment of the enzyme to the DNA backbone. Well-known examples of enzymatic DPCs are trapped topoisomerase 1 cleavage complexes (**TOP1ccs**) and topoisomerase 2 cleavage complexes (**TOP2ccs**). The TOP1 and TOP2 enzymes relax DNA supercoils during replication and transcription. Relaxation is achieved through the transient cleavage of DNA followed by religation of the cleaved ends. TOP1 introduces a single-strand break and becomes covalently linked to the 3' end of DNA, whereas TOP2 introduces a double-strand break and becomes covalently linked to the 5' end of DNA (Ashour et al., 2015; Wojtaszek & Williams, 2024). During the normal catalytic cycle of topoisomerases, a reversible covalent intermediate, TOP1cc or TOP2cc, is formed, in which the catalytic tyrosine residue of the enzyme is linked to the phosphate group of a DNA nucleotide by a phosphotyrosyl bond (which is a phosphodiester bond). When religation fails, this normally transient intermediate becomes stabilized or trapped, giving rise to an enzymatic DNA-protein crosslink termed a **TOP1-DPC** or **TOP2-DPC**. Such trapping can occur spontaneously when DNA is damaged, leading to persistence of the covalent intermediate. However, this process can also be induced by certain chemotherapeutic agents, such as camptothecin (CPT), which inhibits TOP1, and etoposide (ETO), which inhibits TOP2 (Nitiss, 2009; Pommier, 2009; Wojtaszek & Williams, 2024). Camptothecin derivatives, including irinotecan and topotecan, and etoposide are topoisomerase-targeting chemotherapeutic agents that act as topoisomerase poisons by trapping TOP1ccs and TOP2ccs, respectively. Clinically, irinotecan is used mainly in the treatment of metastatic colorectal cancer, topotecan in the treatment of certain ovarian, small-cell lung, and cervical cancers, and etoposide in the treatment of small-cell lung cancer and refractory testicular cancer (Stingele et al., 2017). Enzymatic DPCs also include DNMT1 (DNA methyltransferase 1), the major maintenance DNA methyltransferase, which becomes covalently trapped on DNA following exposure to 5-aza-dC. Because 5-aza-dC acts as a

cytosine analogue and DNMT1 pseudosubstrate, it blocks completion of the methylation reaction, inhibits maintenance methylation at CpG sites, and leads to the formation of **DNMT1-DPCs**. Clinically, 5-aza-dC (decitabine) is used as a hypomethylating chemotherapeutic agent, particularly for myelodysplastic syndromes and acute myeloid leukemia (Maslov et al., 2012; Santi et al., 1984). Poly(ADP-ribose) polymerase 1 (PARP1) is a DNA strand-break sensor that catalyzes poly(ADP-ribosyl)ation (PARylation), generating PAR chains that recruit and coordinate DNA repair factors at damage sites. Inhibition of PARP1 catalytic activity can lead to **PARP1 trapping**: formation of long-lived **PARP1-DNA complexes** at breaks (DPC-like protein-DNA obstacles, although not covalent crosslinks). Talazoparib is reported to produce the greatest degree of PARP1 trapping among first-generation PARP inhibitors (PARPi) (Ray & Opyrchal, 2025). Another enzymatic DPC involves the protein **HMCES** (5-hydroxymethylcytosine-binding, ES-cell-specific), which functions as a sensor of abasic sites in single-stranded DNA (ssDNA) and forms a covalent DNA-protein crosslink at these lesions (Mohni et al., 2019).

Compounds that induce DPCs commonly have important applications in biomedicine, particularly as chemotherapeutic agents for the treatment of malignant tumors. These compounds inhibit specific proteins through different mechanisms, including promotion of DNA-protein crosslinking (i.e., DPC formation) and protein trapping on DNA. Induced DPCs can obstruct DNA replication in tumor cells and trigger replication stress and DNA damage responses, ultimately resulting in cell cycle arrest, inhibition of tumor cell proliferation, cytotoxicity, and apoptosis. Examples of clinically used anticancer agents that induce DPCs or DPC-like lesions include irinotecan and topotecan, which act as TOP1 poisons; etoposide, doxorubicin, and mitoxantrone, which act as TOP2 poisons; 5-aza-dC (decitabine), which traps DNMT1 on DNA; olaparib and talazoparib, which are PARP inhibitors that can trap PARP on DNA; and cisplatin, which can promote crosslinking of various proteins to DNA-platinum complexes (Fielden et al., 2018). Their efficacy could be further increased if DPC inducers were used in combination with inhibitors of enzymes involved in DPC repair (nucleases, unfoldases/segregases, proteases, and esterases). Research aimed at elucidating the mechanisms of enzymes involved in DPC repair and identifying their inhibitors therefore has strong potential to uncover promising approaches that could be exploited to design new chemotherapeutics for the treatment of malignant diseases.

1.3. DPC repair

Impaired DPC repair results in sensitivity to agents that induce DNA-protein crosslinks, errors in DNA replication, and cell-cycle abnormalities, which represent early steps toward the development of chromosomal instability and tumorigenesis (Ide et al., 2018). For this reason, cells employ multiple pathways to repair such lesions. In cells, DPCs are repaired by proteases, nucleases (including NER-associated nucleases), and/or esterases. In proteolytic DPC repair, the protein component of the lesion is degraded, and the residual peptide adduct is then removed from DNA by the NER machinery or by the tyrosyl-DNA phosphodiesterases TDP1 and TDP2. In nucleolytic DPC repair, nucleases excise the DNA segment containing the crosslinked protein, after which the resulting DNA damage is repaired by canonical pathways for single-strand or double-strand breaks. In addition to lesion removal pathways, cells may also tolerate some peptide-DNA adducts by bypassing them during DNA replication. **Translesion DNA synthesis** (**TLS**) is a **DNA damage tolerance** (**DDT**) mechanism in which the replicative DNA polymerase is replaced by specialized TLS polymerases, which generally have lower processivity and fidelity and are therefore often error-prone. TLS polymerases can bypass DNA lesions during replication by inserting nucleotides opposite damaged templates. TLS has been primarily associated with bypass of relatively small obstacles (e.g., pyrimidine dimers and abasic sites), and until recently there was little evidence that TLS polymerases can efficiently bypass crosslinked peptides, which represent larger lesions. Recently, however, human TLS polymerases **Pol η**, **Pol ι**, and **Pol κ** were shown to bypass a model 15-mer peptide-DNA crosslink *in vitro*. Pol ι and Pol κ inserted only the correct nucleotide opposite the lesion, whereas Pol η was less selective at insertion but still supported error-free full-length bypass, because only correctly paired products were extended to completion (Ghodke et al., 2021). Consistent with this, another recent study showed that a model 5-formylcytosine (5fC)-conjugated DNA-peptide crosslink was efficiently bypassed in human HEK293T cells, and that the associated mutagenic TLS was markedly reduced in cells deficient for **Pol η**, **Pol ι**, or **Pol ζ** (Bacurio et al., 2024). It is therefore possible that, following DPC proteolysis, TLS polymerases may enable replication to continue in the presence of a smaller peptide remnant, thereby preventing replication fork stalling and potential fork collapse.

1.3.1. DPC proteases

DPC proteases resolve DNA-protein crosslinks by proteolytically degrading the crosslinked protein in a process termed DPC proteolysis (Stingele et al., 2017; Vaz et al., 2017).

Interest in this pathway increased markedly following the identification of the yeast metalloprotease **Wss1** (weak suppressor of Smt3-1) (Stingele et al., 2014) and its functional homolog in higher eukaryotes, **SPRTN** (SprT-like N-terminal domain, also known as SPARTAN or DVC1), which contains an N-terminal SprT domain (Lopez-Mosqueda et al., 2016; Maskey et al., 2017; Stingele et al., 2016; Vaz et al., 2016). Both proteases harbor an intrinsic metalloprotease active site within specialized, yet phylogenetically distinct, protease domains: the WLM (Wss1p-like metalloprotease) domain of Wss1 and the SprT domain of SPRTN (Vaz et al., 2017). Their proteolytic activity is DNA-dependent, but they display no defined specificity for a particular DNA nucleotide sequence or for a specific amino-acid sequence in the protein substrate, consistent with the heterogeneous nature of DPC lesions (Vaz et al., 2016). The apparent absence of strict sequence specificity is likely beneficial because a wide variety of proteins can form crosslinks with DNA. At the same time, however, it increases the possibility of off-target proteolysis of chromatin-associated proteins that perform essential cellular functions. DPC proteolysis therefore needs to be tightly regulated to minimize unintended cleavage. However, the mechanisms governing this regulation remain underexplored. Moreover, DPC proteases have been reported to act not only on *bona fide* DPCs but also on other nucleoprotein obstacles, including proteins that are tightly (though noncovalently) bound to DNA, such as trapped PARP1-DNA complexes (Saha et al., 2021). Collectively, recent findings indicate that DPC proteases play multiple roles in safeguarding genome integrity (Ruggiano & Ramadan, 2021). These roles are discussed in detail in separate chapters.

1.3.2. Nucleases

Pathways involving **nucleases**, such as **nucleotide excision repair** and an **MRE11**-dependent pathway (meiotic recombination 11; MRE11 is otherwise involved in homologous recombination), operate in prokaryotic and eukaryotic cells. NER is currently considered to have only a limited role in DPC repair because it can process only small DPCs (< 16 kDa in mammalian cells). It has therefore been proposed that DPC proteases and/or proteasome act first to partially degrade the protein component of the DPC, after which NER enzymes excise a stretch of nucleotides to which a smaller peptide remnant remains attached (Vaz et al., 2017). Recently, transcription-coupled nucleotide excision repair factors have been implicated in transcription-coupled DPC repair (Carnie et al., 2024; Oka et al., 2024; van Sluis et al., 2024). The mammalian nuclease **APE2** (Apn2 is the yeast ortholog in *Saccharomyces cerevisiae*) has

been implicated as a major enzyme that reverses endogenous 3'-blocked DNA termini. These lesions can arise from TOP1-dependent processing of genomic ribonucleotides and from TOP1-DPCs, yielding blocked 3' ends that cannot be extended or ligated. *In vitro*, APE2 and TDP1 poorly process intact TOP1-DPC, but both efficiently act on proteolytically degraded TOP1-DPC (Álvarez-Quilón et al., 2020). It is also possible that the 5' endonuclease **XPF-ERCC1** (xeroderma pigmentosum group F-complementing protein partnered with ERCC1, excision repair cross-complementing group 1) is involved in the repair of TOP1-induced DNA damage via a pathway distinct from TDP1-dependent processing, consistent with an incision-based mechanism for excision of TOP1-linked lesions. XPF-ERCC1 is a heterodimeric endonuclease best known for making the 5' incision in the NER pathway (Y.-W. Zhang et al., 2011). In the repair of DNA-protein crosslinks at double-strand breaks (e.g., TOP2- or Spo11-linked DSB ends), the nuclease **MRE11** acts within the MRN complex (MRE11/RAD50/NBS1 (Nijmegen breakage syndrome 1)). Notably, MRN endonuclease activity is stimulated at protein-blocked 5' ends, consistent with a mechanism in which the protein adduct itself promotes incision-based processing of blocked DSB termini (Aparicio et al., 2016; Deshpande et al., 2016; Hoa et al., 2016).

1.3.3. Tyrosyl-DNA phosphodiesterases

The previously mentioned TOP1-DPC and TOP2-DPC can be repaired by **tyrosyl-DNA phosphodiesterases 1 and 2 (TDP1 and TDP2)**, which hydrolyze the phosphotyrosyl linkage between the catalytic tyrosine of the trapped topoisomerase and the DNA backbone. TDP1 primarily resolves 3'-phosphotyrosyl adducts (characteristic of TOP1cc), whereas TDP2 preferentially cleaves 5'-phosphotyrosyl adducts (characteristic of TOP2cc). Because the phosphotyrosyl bond is generally inaccessible within intact, native topoisomerase-DNA complexes, efficient processing by TDP1/TDP2 typically requires prior proteolytic degradation of the trapped topoisomerase and/or protein unfolding/denaturation to expose the scissile linkage (Gao et al., 2014; Pommier et al., 2014). Recently, it was shown that Tdp1 removes Top1-DPCs and histone H3-DPCs, whereas Tdp2 removes Top2-DPCs *in vivo* (Anticevic et al., 2023, 2024). In addition, the SUMO E3 ligase **ZATT** (zinc finger protein associated with TDP2 and TOP2), also known as **ZNF451** (zinc finger protein 451), has been shown to promote TOP2-DPC repair *in vitro*. ZATT-mediated SUMOylation of TOP2-DPCs enhances recruitment and activity of TDP2, likely by altering the conformation of TOP2-DPCs and making the crosslink site accessible to TDP2-mediated excision (Schellenberg et al., 2017).

Consistent with this, Park et al. (2023) showed in human cells that ZATT contributes to the processing of etoposide-induced TOP2-DPCs and influences TOP2 turnover after treatment (Park et al., 2023).

1.4. SPRTN protease

Wss1 and SPRTN (Figure 3) were the first DPC proteases identified and remain the best-characterized enzymes shown to directly proteolyze the protein component of DNA-protein crosslinks. Proteolytic DPC repair was first established in yeast, where the DNA-dependent metalloprotease Wss1 promotes replication-coupled degradation of DPCs (Stingele et al., 2014). Replication assays in *Xenopus* egg extracts subsequently indicated a comparable replication-coupled DPC proteolysis activity in metazoans (animals) (Duxin et al., 2014), and follow-up studies identified SPRTN as a central DNA-dependent protease in this pathway (Lopez-Mosqueda et al., 2016; Stingele et al., 2016; Vaz et al., 2016). Although Wss1 and SPRTN share a related metalloprotease core and similar DNA-dependent activation, phylogenetic analyses indicate they are not strict orthologs but rather distantly related functional homologs (Fielden et al., 2018; Reinking et al., 2020; Vaz et al., 2017).

Sequence similarity between Wss1 and SPRTN is largely restricted to their protease domains, most notably around the conserved metalloprotease active site that contains the characteristic HEXXH motif (Vaz et al., 2016). Loss of Wss1 and SPRTN increases sensitivity to formaldehyde, a potent inducer of DPCs, consistent with a general role for both enzymes in DPC repair. This notion is reinforced by *in vitro* cleavage assays showing that Wss1 and SPRTN can proteolyze a broad range of diverse DNA-binding protein substrates (Lopez-Mosqueda et al., 2016; Stingele et al., 2014, 2016; Vaz et al., 2016). Structural studies of the yeast Wss1 protease domain (WLM) show a conserved Zn-dependent metalloprotease catalytic core but no obvious substrate-binding cleft. Together with the highly variable surface electrostatic properties outside the catalytic patch, this is consistent with broad substrate tolerance (Yang et al., 2017). *In vitro*, Wss1 can cleave several DNA-binding proteins in a DNA-dependent manner, including TOP1 and chromatin-associated proteins such as histone H1 and HMG (high-mobility group) proteins (Stingele et al., 2014).

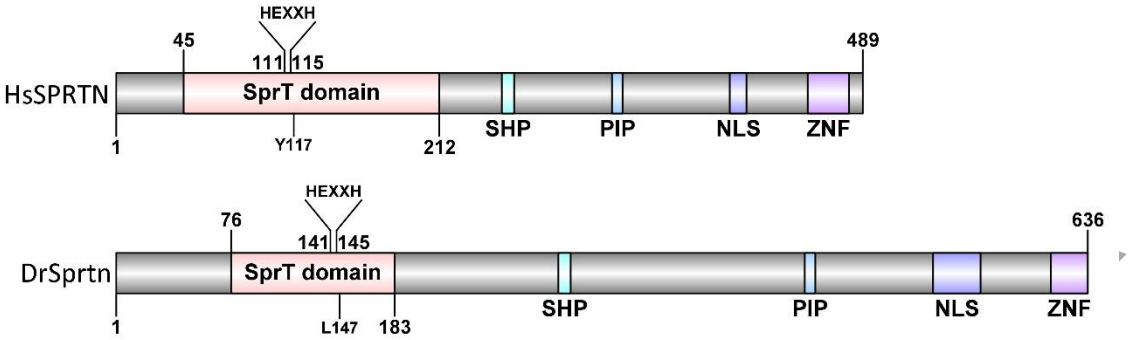

Figure 3. Comparison of the domain organization of human and zebrafish SPRTN proteins. *Hs*SPRTN, human SPRTN (*Homo sapiens*; UniProt Q9H040); *Dr*Sprtn, zebrafish Sprtn (*Danio rerio*; UniProt A0A0G2L7I0). The SprT domain was annotated based on InterPro and NCBI CD-Search analyses. Conserved motifs and functional elements are indicated: SHP, p97-interacting SHP box; PIP, PCNA-interacting protein box; NLS, nuclear localization signal; ZNF, UBZ4-type ubiquitin-binding zinc finger. The conserved HEXXH motif of the protease core is also indicated (H, histidine; E, glutamate; X, any amino acid). Y117 in human SPRTN and the corresponding L147 residue in zebrafish Sprtn are shown. Numbers indicate amino acid positions delimiting the indicated protein regions or marking specific residues. Schematic representations were generated using IBS 1.0.3 (Illustrator for Biological Sequences).

SPRTN is also a DNA-dependent metalloprotease with broad substrate scope. Reported SPRTN substrates include core histones (H2A, H2B, H3, and H4) and histone H1, the topoisomerases TOP1 and TOP2, and several additional DNA- or chromatin-associated proteins such as HMG1, HLTF (helicase-like transcription factor), and FAN1 (Fanconi anemia-associated nuclease) (Mórocz et al., 2017; Stingele et al., 2016; Vaz et al., 2016). DPC proteolysis reduces the bulk of the lesion but typically leaves a peptide residue crosslinked to DNA, the size of which is not well defined. Although this residual peptide-DNA adduct is a smaller barrier to replication and transcription than the full-length crosslinked protein, it generally still requires downstream processing by nucleases and/or tyrosyl-DNA phosphodiesterases (Vaz et al., 2017). Recently, it was shown that Sprtn participates in Top1-DPC repair *in vivo* in the zebrafish model, followed by Tdp1-mediated excision of the crosslinked peptide after exposure to the DPC inducers camptothecin and formaldehyde (Anticevic et al., 2023). In some cases, translesion DNA synthesis can bypass the crosslinked peptides generated by SPRTN-mediated proteolysis without further downstream processing, albeit in an error-prone and potentially mutagenic manner.

1.5. ACRC protease

The existence of multiple DPC proteases suggests that cells require distinct enzymes to counteract DPC-associated cytotoxicity, which is expected given the heterogeneity of proteins that can become crosslinked to DNA and the high frequency of these lesions. Although SPRTN is not strictly sequence-specific, it preferentially proteolytically processes DNA-binding proteins in poorly structured regions enriched in lysine, arginine, and serine residues (Vaz et al., 2016). The presence of additional proteases could therefore broaden the substrate range by enabling efficient processing of crosslinked proteins that lack these features, ultimately helping to prevent genome instability. Despite phylogenetic divergence, DPC proteases share some common features, most notably DNA binding and a modular domain architecture with interaction motifs, suggesting partially overlapping functions and potentially related modes of regulation (Ruggiano & Ramadan, 2021). Finally, this framework provides a rationale for context-specific proteases such as **ACRC/GCNA** (acidic repeat-containing protein/germ cell nuclear antigen), which may complement SPRTN-dependent DPC proteolysis in those settings.

1.5.1. Role of ACRC

ACRC is a highly conserved eukaryotic protein that contains a C-terminal SprT protease domain throughout the metazoan lineage, except in a few rodent species (Carmell et al., 2016; Fielden et al., 2018; Otten et al., 2025). In metazoans, ACRC is thought to be expressed mainly in germ cells and in early embryonic or other proliferative/pluripotent cells (Bhargava et al., 2020; Borgermann et al., 2019; Carmell et al., 2016; Dokshin et al., 2020). Accordingly, most studies to date have relied on animal models rather than human somatic cell lines. Although *ACRC* appears dispensable for viability in cultured mammalian cells, targeted loss (knockout) of *ACRC* causes severe germline/early-embryo phenotypes, including maternal-effect embryonic lethality in *Drosophila melanogaster*, *Caenorhabditis elegans*, and zebrafish (*Danio rerio*) (Bhargava et al., 2020; Supina Pavić, 2023).

In *D. melanogaster*, loss of *acrc* leads to replication stress and elevated DNA damage in germ cells, as reflected by increased nuclear RPA (replication protein A) foci (indicative of ssDNA at stalled or processed replication forks) and increased H2Av phosphorylation (γH2Av, a γH2AX analog and widely used marker of DSBs), as well as hypersensitivity to hydroxyurea (HU), an inhibitor of ribonucleotide reductase (which depletes dNTP pools and promotes fork stalling). *Acrc* deficiency also causes genome instability, including mitotic chromosome

segregation defects and micronucleus formation in early *Drosophila* embryos. In *C. elegans*, disruption of *acrc* is associated with elevated genome instability (e.g., increased mutation signatures/instability and chromosomal abnormalities) and defects in brood size/embryonic viability. These phenotypes generally reduce reproductive potential. Finally, in *C. elegans*, fertility and embryonic viability defects are further exacerbated when *dvc-1* (the *SPRTN* homolog) is mutated in addition to *acrc*, consistent with partially nonredundant genome-protection pathways (Bhargava et al., 2020; Dokshin et al., 2020). In *Drosophila*, embryos derived from females mutant for the *acrc* and the *SPRTN* homolog maternal haploid (*mh*) fail to complete embryogenesis. Loss of the *acrc* elevates total DPC levels in germ cells and early embryos in flies, worms, and zebrafish (Bhargava et al., 2020), and available evidence implicates TOP2-DPC as a key endogenous lesion in these germline/early-embryo contexts (Bhargava et al., 2020; Dokshin et al., 2020). In *C. elegans*, *dvc-1* and *acrc* mutants are both sensitive to formaldehyde, suggesting partial functional overlap between Dvc-1 and Acrc in formaldehyde tolerance (Borgermann et al., 2019).

To examine ACRC function in a vertebrate model, Bhargava et al. (2020) generated zebrafish *acrc* mutant alleles, including a 7-bp deletion and a complex insertion, that introduce early frameshifts and are predicted to yield severely truncated proteins. The progeny of mutant females showed fully penetrant maternal-effect defects, with widespread morphological abnormalities and embryonic death (100%), regardless of the paternal genotype (wild-type or *acrc* homozygous mutants). Consistent with chromosome instability, DAPI (4’,6-diamidino-2-phenylindole) analysis of early embryos (64 – 128 cell stage) revealed asynchronous mitotic divisions and extensive chromosome tangling/bridging. These results indicate that zebrafish *acrc* mutation causes maternal-effect lethality, characterized by pronounced chromosomal instability. A similar phenotype was observed by the same researchers in *Drosophila* and *C. elegans*, indicating that ACRC supports genome stability in germline/early-embryo contexts across species. Thus, Acrc is likely essential for early zebrafish embryonic development through a maternal effect. In other words, maternally provided *acrc* gene products (Acrc mRNA and/or Acrc protein) deposited in the oocyte cytoplasm influence offspring phenotype and are required for early embryogenesis (Supina Pavić, 2023), although the underlying mechanisms remain unknown. To test whether Acrc loss is associated with elevated DPC levels, the authors performed the RADAR assay (rapid approach to DNA adduct recovery) on zebrafish embryos lysed at the 1000-cell stage and observed modestly increased total DPC levels in mutants (Bhargava et al., 2020).

The mouse (*Mus musculus*) ortholog of ACRC lacks the SprT domain and is predicted to be entirely disordered. Male Acrc mutant mice are viable but exhibit impaired fertility, with most mutant males being sterile, suggesting that Acrc's intrinsically disordered region (IDR) plays an important role in male fertility in mice (Carmell et al., 2016). Ribeiro and Crossan (2023) reported that mouse Acrc is dispensable for resistance of mouse embryonic stem cells to formaldehyde and etoposide, supporting a protease-independent role in mice. Instead, mouse Acrc binds core histones, has histone-chaperone activity, associates with nascent DNA and PCNA (proliferating cell nuclear antigen), and helps maintain normal S-phase progression in undifferentiated spermatogonia, pointing to an additional role in chromatin handling during DNA replication (Ribeiro & Crossan, 2023).

Germ cells and early embryos are likely especially sensitive to genome instability resulting from DPC accumulation, because lesions arising at these stages can be propagated to offspring (germline) or broadly amplified across the rapidly dividing cells of the developing organism. Moreover, extensive gene-expression reprogramming during embryogenesis, together with active histone demethylation, can increase endogenous formaldehyde production, potentially elevating DPC formation in these contexts. Preventing the persistence and inheritance of such lesions may therefore help explain why cells deploy multiple DPC proteases with partially overlapping, context-dependent functions (Ruggiano & Ramadan, 2021).

1.5.2. Evolutionary conservation and domain architecture of ACRC

Early in metazoan embryogenesis, primordial germ cells segregate from somatic cells and follow a distinct developmental program that preserves genome integrity across generations. ACRC is an ancient eukaryotic protein family that likely arose early in eukaryotic evolution and has been reported to be conserved across ~1.5 billion years of evolution. Because it is highly expressed in metazoan germ cells, ACRC is thought to be primarily associated with sexual reproduction and fertility (Bhargava et al., 2020; Carmell et al., 2016). ACRC contains an N-terminal acidic intrinsically disordered region (IDR) that remains conserved despite substantial divergence in primary amino-acid sequence between species. In most metazoans, except in certain mouse and rat species, ACRC orthologs also contain a C-terminal SprT protease domain (Figure 4), a zinc finger (ZnF) motif, and an HMG box (high mobility group box). The HMG box and ZnF are well-established DNA-binding motifs (Bhargava et al., 2020; Otten et al., 2025). Although ACRC's domain organization is known, relatively little is understood about its cellular functions. Recent work has implicated ACRC in DPC repair.

However, direct evidence of ACRC proteolytic activity is still lacking, and its high-resolution 3D structure has not yet been determined.

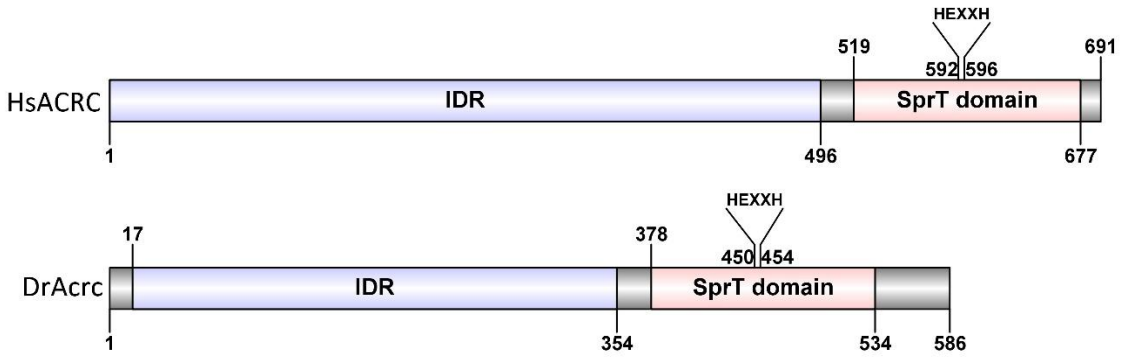

Figure 4. Comparison of the domain organization of human and zebrafish ACRC proteins. *Hs*ACRC, human ACRC (*Homo sapiens*; UniProt Q96QF7); *Dr*Acrc, zebrafish Acrc (*Danio rerio*; UniProt A0A0R4IWG9). The SprT domain was annotated based on InterPro and NCBI CD-Search analyses, whereas intrinsically disordered regions (IDRs) were annotated based on MobiDB predictions. The conserved HEXXH motif of the protease core is indicated (H, histidine; E, glutamate; X, any amino acid). Numbers indicate amino acid positions delimiting the indicated protein regions. Schematic representations were generated using IBS 1.0.3 (Illustrator for Biological Sequences).

Fielden et al. (2018) performed a phylogenetic analysis of SprT and WLM domain sequences across multiple species and concluded that ACRC orthologs cluster much more closely with SPRTN-family (SPRT) orthologs than with Wss1-family (WLM) orthologs. They identified ACRC orthologs in archaea and eukaryotes, but not in bacteria. Using *in silico* molecular modeling, they further reported that the predicted 3D structure of the protease core of the human ACRC SprT domain closely resembles that of the human SPRTN SprT domain (Figure 5). The modeled ACRC protease core comprises two α-helices containing three histidines (predicted to coordinate Zn^{2+}) and the catalytic glutamate, consistent with the SPRTN protease core. The first two histidines (H) together with the glutamate (E) form the HEXXH motif, a hallmark of zinc-dependent metalloproteases. Despite these similarities at the level of the protease core, SPRTN and ACRC differ substantially in overall sequence and domain architecture. Notably, the SprT domain is N-terminal in SPRTN but C-terminal in ACRC (Fielden et al., 2018). Moreover, MobiDB predictions indicate that human ACRC is largely disordered, with approximately 72% of its residues displaying disorder propensity, mainly within the N-terminal two-thirds of the protein that constitute the IDR, whereas SPRTN is only partially disordered, with approximately 53% of its residues displaying disorder propensity, predominantly in its C-terminal region.

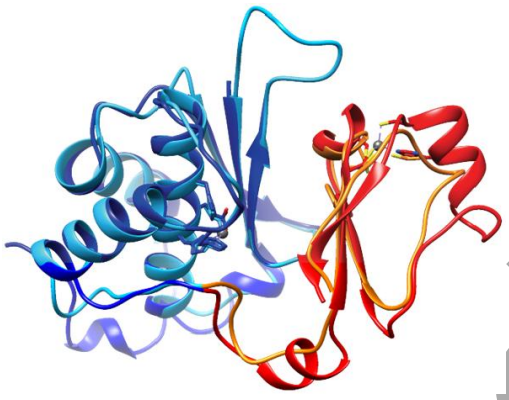

Figure 5. Superimposition of the SprT domain structure of human SPRTN (PDB: 6MDX) with a predicted structure of the SprT domain of human ACRC. The metalloprotease subdomain (protease core) of SPRTN is shown in blue and that of ACRC in light blue; the zinc-binding subdomain of SPRTN is shown in red and that of ACRC in orange. Zinc ions are depicted as grey spheres, and zinc-coordinating residues as grey sticks. The figure was prepared by Dr. Nives Ivić (Proteros biostructures GmbH, Martinsried, Germany) using MODELLER (personal communication).

1.6. The 26S proteasome and other candidate DPC proteases

1.6.1. 26S proteasome

The **26S proteasome** is the principal proteolytic machine of the ubiquitin-proteasome system, degrading a wide range of cellular proteins that have been targeted for turnover by ubiquitin modification. Beyond its central role in maintaining protein and amino acid homeostasis, the proteasome regulates numerous cellular processes, including the cell cycle, DNA replication, transcription, signal transduction, and stress responses (Bard et al., 2018). Emerging evidence also implicates the proteasome in DNA-protein crosslink repair (Larsen et al., 2019; Mohni et al., 2019; Oka et al., 2024; Prasad et al., 2019; Sun et al., 2020). For example, the HMCES-DPC formed at abasic sites in ssDNA is ubiquitylated and resolved by proteasome-mediated degradation (Mohni et al., 2019). In replication-coupled experiments in *Xenopus* egg extracts, model DPCs are polyubiquitylated during DNA replication, which promotes proteasome recruitment and DPC degradation; in addition, SPRTN provides a distinct, ubiquitylation-independent proteolysis pathway (Larsen et al., 2019). HMCES binds abasic sites in ssDNA at replication forks, via interactions with ssDNA and PCNA, and forms a covalent HMCES-DNA crosslink that shields the lesion from error-prone processing. By doing so, HMCES suppresses translesion synthesis across AP sites and blocks endonuclease action that could otherwise generate mutations and double-strand breaks. The resulting

HMCES-DNA crosslink is subsequently ubiquitylated and resolved through ubiquitin-dependent, proteasome-mediated degradation (Mohni et al., 2019). However, Donsbach et al. (2023) showed that HMCES-DPCs can also be resolved by a DNA-context-dependent non-proteolytic release mechanism, in which reversal of the crosslink is catalyzed by a conserved glutamate residue in the HMCES active site. HMCES remains stably crosslinked in ssDNA and at ssDNA-dsDNA junctions, where it protects AP sites from cleavage, but is released once the lesion is transferred into dsDNA after fork bypass, thereby permitting downstream AP-site repair (Donsbach et al., 2023). Larsen et al. (2019) used replication-coupled assays in *Xenopus* egg extracts to show that model DPCs can be proteolytically degraded during DNA replication by either the 26S proteasome or the metalloprotease SPRTN, which function as independent DPC proteases. In the *Xenopus* egg extract system with model DPC substrates used in this study, proteasomal targeting of DPCs required extensive DPC polyubiquitylation (partially dependent on the E3 ligase activity of TRAIP (TRAF-interacting protein)), whereas SPRTN-mediated DPC degradation could occur without ubiquitylation of the crosslinked protein and instead depended on nascent-strand extension to within a few nucleotides of the lesion (Larsen et al., 2019). In contrast, in proliferating human cell lines with formaldehyde-induced chromatin DPCs, Ruggiano et al. (2021) found that ubiquitylation was required for SPRTN recruitment to repair foci and efficient replication-coupled DPC repair (Ruggiano et al., 2021). Nevertheless, although several studies have suggested that the proteasome contributes to proteolytic DPC repair, the extent and context dependence of this contribution remain unclear.

1.6.2. Other candidate DPC proteases: FAM111A/B and DDI1/2

In addition to the yeast protease Wss1 and the metazoan proteases SPRTN and ACRC, several other proteases have recently emerged as candidate factors in DNA-protein crosslink repair, including the serine proteases **FAM111A** and **FAM111B** (family with sequence similarity 111 member A/B) and the aspartyl proteases **DDI1** and **DDI2** (DNA damage inducible 1/2) in humans, along with their orthologs in other species. Among the genes encoding these proteases, *SPRTN* is the only one currently considered essential for mammalian cell viability (Reinking et al., 2020; Torrecilla et al., 2024). Evidence linking these newly identified proteases to DPC repair is, however, largely indirect and often based on phenotypes such as hypersensitivity to DPC-inducing agents and increased DPC accumulation in mutant cells or organisms. Importantly, for none of these candidates has a direct proteolytic role in DPC repair been unambiguously demonstrated using *in vitro* substrate cleavage assays. As the number of

candidate DPC proteases continues to grow, a key open question arises: to what extent do their functions overlap (are they substrate- and/or context-specific), and how are their activities distributed across cell-cycle phases and developmental stages?

Biochemical evidence that FAM111A/B or DDI1/2 proteins directly proteolyze *bona fide* DPC substrates remains limited. Unlike SPRTN and ACRC, FAM111A/B and DDI1/2 do not contain a SprT domain. Nevertheless, both the FAM111 and DDI families have well-established catalytic activity. FAM111A is an active serine protease that undergoes autocatalytic self-cleavage *in vitro* and in cells (Hoffmann et al., 2020; Kojima et al., 2020), whereas yeast Ddi1 and human DDI2 are aspartyl proteases that cleave polyubiquitylated protein substrates *in vitro*, preferentially requiring long ubiquitin chains (Dirac-Svejstrup et al., 2020; Yip et al., 2020). Multiple studies further indicate that disease- or function-associated mutations in genes encoding yeast Ddi1 (Serbyn et al., 2020) and human FAM111A (Hoffmann et al., 2020; Kojima et al., 2020) alter their protease function and cellular tolerance to DPC lesions. Recent work showed that oxidative stress inducers (including H_2O_2, NaOCl, menadione, and plumbagin) increase DPC levels in both *S. cerevisiae* and *Candida albicans*. Under these conditions, Wss1 and **Ddi1** promoted fungal survival and DPC tolerance in partially redundant pathways, with Wss1 playing the more prominent role (Sukted et al., 2025). Another study identified a PARP1-dependent, replication-independent DPC repair pathway in *Xenopus* egg extracts that targets DPCs on ssDNA gaps, as well as TOP1cc-like lesions flanked by a DNA nick, for PARylation, subsequent ubiquitylation, and proteolytic removal. Within this pathway, **DDI2** was shown to act as a backup protease for ubiquitylated DPC substrates, particularly PARylated gapped M.HpaII (DNA methyltransferase HpaII)-DPCs, when proteasomal processing was compromised (Fábián et al., 2024).

1.7. Context-dependent functions of DPC proteases

1.7.1. DPC proteases in S phase

DPCs can stall the CMG (CDC45-MCM2-7-GINS) replicative helicase and/or replicative DNA polymerases during DNA synthesis, depending on the size of the adduct and its position relative to the replication fork (Duxin et al., 2014; Nakano et al., 2013). Consistent with this, actively proliferating cells (i.e., cells traversing S phase) are more sensitive to DPC-inducing agents such as formaldehyde and to TOP1 poisoning by camptothecin than

nondividing cells (Hsiang et al., 1989; Kumari et al., 2012; Vaz et al., 2016). If not resolved, DPCs can act as persistent replication barriers that prolong fork stalling, promote fork collapse, and ultimately generate double-strand breaks and genome instability (Cortez, 2019). In yeast, **Wss1** promotes tolerance to formaldehyde-induced DPCs and helps cells complete S phase (Stingele et al., 2014). In yeast cells, **Ddi1** has been reported to be recruited in an S-phase-dependent manner to damage sites to promote removal of a Top1cc-like model DPC (Serbyn et al., 2020). Initial studies suggested that **FAM111A** acts during S phase (Kojima et al., 2020). More recent work shows that FAM111A localizes to replication forks and that its dimerization-dependent serine protease activity helps prevent fork stalling at protein obstacles in cells, including CPT-stabilized TOP1ccs (Palani et al., 2024). However, among metazoan DPC repair factors, replication-coupled DPC proteolysis has been demonstrated most directly for **SPRTN**: SPRTN co-purifies with core replisome components and is detected on nascent DNA by iPOND (isolation of proteins on nascent DNA), where it moves with the replisome during DNA synthesis (Vaz et al., 2016). Despite this, how SPRTN is specifically directed to DPCs at replication forks remains unresolved.

ACRC also appears to function during S phase. In *Drosophila*, loss of Acrc is associated with replication stress in proliferating germ cells, reflected by increased nuclear RPA foci and elevated γH2Av, and by hypersensitivity to hydroxyurea. In *C. elegans*, disruption of Acrc is likewise linked to replication-associated genome instability, including increased microsatellite repeat-length changes. RADAR-based DPC profiling in *Drosophila* further revealed enrichment of TOP2- and MCM-associated DPCs (e.g., MCM3) in Acrc mutant ovaries and early embryos, consistent with a role in mitigating nucleoprotein obstacles during replication (Bhargava et al., 2020). In human U2OS cells, ectopically expressed ACRC is recruited to 5-aza-dC-induced DNMT1-DPCs in a SUMO/SIM-dependent manner, consistent with a potential function in processing these lesions. However, its functional contribution to DNMT1-DNA adduct clearance remains unresolved (Borgermann et al., 2019). DNMT1-DPCs arise behind replication forks, where DNMT1 is recruited to newly synthesized (hemimethylated) DNA to maintain cytosine methylation patterns, and it can become covalently trapped when 5-aza-dC is incorporated into DNA in place of cytosine (Maslov et al., 2012). It remains to be established whether ACRC plays a direct and physiologically relevant role in resolving DNMT1-DPCs, and which additional DPC substrates it targets during S phase. Notably, because human ACRC retains a SprT domain whereas mouse Acrc does not, mammalian ACRC proteins may combine replication-associated chromatin functions with proteolytic activity in a species-specific

manner. Thus, at least in mammals, ACRC may support S-phase genome maintenance not only through DPC processing but also through nonproteolytic roles linked to chromatin dynamics during DNA replication (Ribeiro & Crossan, 2023). More broadly, it is still unclear why multiple DPC proteases operate during S phase and what functional distinctions separate the ACRC- and SPRTN-dependent pathways.

1.7.2. DPC proteases outside S phase

Despite strong evidence supporting a role for **SPRTN** in replication-coupled DPC proteolysis (Stingele et al., 2016; Vaz et al., 2016), it is unlikely that SPRTN's functions are restricted to S phase. Indeed, biallelic germline (inherited) mutations in *SPRTN* are linked to early-onset hepatocellular carcinoma in humans (Lessel et al., 2014), whereas partial loss of SPRTN in mice, as seen in SPRTN hypomorphic mice, leads to DPC accumulation and spontaneous liver tumorigenesis (complete knockout of SPRTN in mice is embryonically lethal) (Maskey et al., 2014, 2017). The liver may be particularly susceptible because it is a major organ for formaldehyde handling and metabolism, which can increase exposure to aldehyde-driven DPC formation and thereby heighten the requirement for efficient DPC processing pathways (Maskey et al., 2017). However, most adult hepatocytes are long-lived quiescent cells (i.e., largely in G0) (Berasain & Avila, 2015; Grisham, 1962) and therefore do not normally enter S phase, suggesting that SPRTN may also have replication-independent functions. Supporting this idea, Weickert et al. (2023) identified a role for SPRTN in replication-independent, global-genome DPC repair that does not depend on replication-coupled recognition of the lesion. This replication-independent SPRTN-dependent DPC cleavage pathway requires SUMO-targeted ubiquitylation of the protein adduct and operates alongside proteasomal DPC degradation. Moreover, RJALS (Ruijs-Aalfs syndrome)-associated SPRTN variants with defective ubiquitin binding compromise global-genome DPC repair and show synthetic lethality when proteasomal DPC repair capacity is reduced (Weickert et al., 2023). Further supporting replication-independent functions of SPRTN, Tomaskovic et al. (2026) showed that SPRTN is required not only during S phase but also during mitosis, where SPRTN depletion in cells leads to the accumulation of spontaneous mitotic DPCs, including TOP2A-associated lesions, and prevents efficient resolution of formaldehyde-induced DPCs in M phase. Acute depletion of SPRTN specifically during mitosis was sufficient to induce chromosome segregation defects and micronuclei formation, indicating a mitotic role rather than merely processing lesions carried over from S phase. These micronuclei accumulated

persistent DPCs and DNA damage, underwent nuclear envelope defects and rupture, and were linked to cytosolic DNA release and cGAS-STING (cyclic GMP-AMP synthase-stimulator of interferon genes) activation, thereby connecting unresolved mitotic DPCs to inflammatory signaling and to the progeroid phenotypes observed in a knock-in mouse model of RJALS (SPRTN-Y118C/Y118C). Unresolved DPCs promote chromosome missegregation and micronucleus formation, and when damaged DNA leaks from these structures into the cytosol, it is detected by cGAS, which catalyzes cGAMP synthesis, leading to STING activation and inflammatory signaling (Tomaskovic et al., 2026). Consistent with the latter, in *Drosophila* maternal-effect mutations in *mh* (the *SPRTN* homolog) cause loss of the paternal chromosomes during the first zygotic mitosis, resulting in haploid embryonic lethality. This paternal chromosome loss has been attributed to defective condensation of paternal DNA during mitosis, although the underlying mechanism remains unresolved (Delabaere et al., 2014).

ACRC may also function outside S phase. In *C. elegans* embryos, Acrc is cell-cycle regulated and becomes enriched on condensed chromosomes during M phase, where it colocalizes with Top2. In addition, TOP2α/β peptides were recovered in anti-ACRC immunoprecipitations from mouse ESCs (embryonic stem cells), and Acrc co-immunoprecipitates with Top2 in *C. elegans*, supporting a conserved physical association between ACRC and TOP2. Because TOP2 activity is required for sister-chromatid decatenation in mitosis, TOP2-linked lesions are expected to be prominent at this stage. Consistent with Acrc promoting Top2-DPC resolution, *C. elegans* Acrc mutants are hypersensitive to the Top2 poison etoposide but not to the Top1 poison camptothecin (Dokshin et al., 2020). In summary, the evidence gathered so far indicates that DPC proteases are important for maintaining genome integrity during DNA replication and may also act outside S phase of the cell cycle.

1.7.3. DPC proteases and transcription

DPCs can obstruct not only DNA replication but also transcription (Ide et al., 2018). Because transcriptional stalling and mutagenesis can compromise genome stability (Brégeon & Doetsch, 2011), understanding how DPCs affect RNA polymerases progression is important. However, this remains largely unexplored. Still, several observations implicate DPC proteases in transcription-associated processes. In yeast, the largest and catalytic subunit of RNA polymerase II (Rpb1) has been proposed as a substrate of the proteases Ddi1 and Wss1 upon hydroxyurea treatment, and Ddi1 was shown to interact with Rpb1 by co-immunoprecipitation (Serbyn et al., 2020). RNA polymerase II (RNAPII) is the enzyme that transcribes protein-

coding genes into precursor mRNA, and also produces many non-coding RNAs (e.g., some snRNAs/lncRNAs) in eukaryotic cells. In human cells, FAM111A has likewise been linked to RNA polymerase II: FAM111A overexpression reduces RPB1 (POLR2A) levels on chromatin, and the two proteins also interact (Hoffmann et al., 2020).

Supporting the idea that DPCs can be handled during transcription, Oka et al. (2024) showed that formaldehyde-induced DPCs are preferentially removed from actively transcribed regions by a transcription-coupled pathway involving canonical TCR factors, p97, and the proteasome (Oka et al., 2024). Recent work has begun to define transcription-coupled DPC repair (TC-DPC repair) in mammalian cells: DPCs stall RNAPII, promote RNAPII ubiquitylation and degradation, and are preferentially removed from actively transcribed genes in a CSB/CSA-dependent manner. Notably, this pathway appears independent of downstream transcription-coupled NER factors, including UVSSA (UV-stimulated scaffold protein A) and XPA (xeroderma pigmentosum group A protein), and relies on the $CRL4^{CSA}$ ubiquitin ligase and the proteasome, rather than SPRTN. CSB (Cockayne syndrome group B protein) and CSA (Cockayne syndrome group A protein) are Cockayne syndrome proteins that respond to RNAPII stalling at DNA lesions and coordinate transcription-coupled DNA repair, with CSA acting as a substrate receptor within the CRL4 (Cullin-RING E3 ubiquitin ligase 4) complex (Carnie et al., 2024; van Sluis et al., 2024). Cockayne syndrome is a rare inherited disorder caused by defects in transcription-coupled DNA repair, leading to developmental and neurological problems with photosensitivity, growth failure, and premature aging-like features (Wilson et al., 2016).

1.7.4. DPC proteases and cleavage of proteins tightly bound to DNA

Mass spectrometry (MS)-based profiling of proteins covalently bound to nucleic acids has been instrumental in identifying the proteins most frequently recovered in DPCs. Analyses of the endogenous adductome in human cells (Kiianitsa & Maizels, 2020), together with DPC profiling in SPRTN-deficient HeLa cells (Vaz et al., 2016) and ACRC-deficient models (Bhargava et al., 2020), showed that topoisomerases, histones, and subunits of the MCM complex within the CMG replicative helicase are among the most prevalent DPC components. It is expected that such screens will be enriched for DNA-binding proteins, because factors that operate in close proximity to DNA are more likely than others to become irreversibly covalently crosslinked to it. However, proteins near DNA can also associate with it tightly without forming a covalent crosslink. In such cases, protein-DNA association is maintained by non-covalent

forces, primarily electrostatic interactions and hydrogen bonds, with additional contributions from van der Waals contacts and, in some contexts, hydrophobic effects. The relative contributions of these interactions, and the practical distinction between genuinely crosslinked versus tightly bound (but non-crosslinked) proteins, remain incompletely characterized. Several studies suggest that DPC proteases may also promote genome stability by cleaving proteins that are tightly associated with DNA, thereby helping to prevent replication-associated defects. For example, Wss1 has been proposed to cleave tightly bound histones (Maddi et al., 2020), whereas SPRTN (Saha et al., 2021) and FAM111A (Kojima et al., 2020) have been reported to target trapped PARP1-DNA complexes. SPRTN can also cleave CHK1 (checkpoint kinase 1) (Halder et al., 2019) and has been implicated in proteolysis of the nuclease MRE11, generating a truncated MRE11 form with diminished DNA-binding and nuclease activity (Na et al., 2021).

1.7.5. Regulation of DPC proteases

Because active DPC proteases pose an inherent risk to cellular proteins, cells employ multiple mechanisms to constrain their activity. Wss1 and SPRTN are DNA-activated proteases whose catalytic activity is stimulated upon **binding to ssDNA and dsDNA** (double-stranded DNA) (Stingele et al., 2016; Vaz et al., 2016), thereby restricting proteolysis to DNA-proximal substrates and helping protect nuclear proteins away from chromatin (Li et al. 2019). In addition, both proteases undergo DNA-dependent **trans-autoproteolysis** (self-cleavage *in trans*), in which one protease molecule cleaves another molecule of the same protease. This may terminate protease activity when the enzymes are recruited to chromatin that lacks DPCs, that is, when proteolysis is not required. Together, these features suggest a finely balanced interplay between DPC repair-promoting activation and inactivation through self-cleavage, although the underlying regulatory mechanisms remain incompletely understood (Stingele et al., 2016).

Another major layer of regulation involves **post-translational modifications** (**PTMs**) – phosphorylation, ubiquitylation, SUMOylation, and acetylation – of DPC proteases, their substrates, and their **interaction partners**. SPRTN, for example, interacts with PCNA, the ATPase p97, and TEX264 (testis expressed 264) (Ruggiano & Ramadan, 2021). During replication, TEX264 recognizes TOP1-DPCs on chromatin and recruits SPRTN and p97 to the lesion, enabling subsequent processing by TDP1, which hydrolyzes the phosphotyrosyl linkage after SPRTN-mediated proteolysis has reduced the crosslinked protein to a peptide adduct (Fielden et al., 2020). TEX264 has also been identified as a nucleophagy receptor that senses

TOP1-DPCs at replication forks and promotes their p97-dependent delivery to lysosomes for selective autophagic degradation in an ATR (ataxia telangiectasia and Rad3-related)- and MRE11-dependent, proteasome-independent manner (Lascaux et al., 2024).

PTMs are thought to regulate the recruitment, retention, and activation of DPC proteases at sites of DNA damage. DPC proteases can recognize ubiquitin via ubiquitin-associated (UBA) or ubiquitin-binding zinc finger (UBZ) domains and SUMO (small ubiquitin-like modifier) via SUMO-interacting motifs (SIMs) (Borgermann et al., 2019; Stingele et al., 2014, 2016). Consistently, DPC-inducing agents such as formaldehyde and 5-aza-dC trigger signaling cascades that promote ubiquitylation and/or SUMOylation of crosslinked proteins (Borgermann et al., 2019; Ruggiano et al., 2021; Sun et al., 2020). ACRC colocalizes at DNMT1 chromatin foci induced by 5-aza-dC, and this localization depends on DPC SUMOylation and on SIMs in ACRC (Borgermann et al., 2019). SPRTN likewise forms nuclear foci after formaldehyde exposure, and this response is abolished by pharmacological inhibition of the ubiquitylation pathway, although the extent to which its UBZ domain directly mediates recruitment to DPC sites in cells remains unclear (Borgermann et al., 2019; Ruggiano et al., 2021). Recent *in vitro* reconstitution studies suggest that DPC ubiquitylation can directly allosterically activate SPRTN, including variants lacking the MIU (motif interacting with ubiquitin) and UBZ modules, in part through ubiquitin binding to an allosteric interface at the back of the SprT protease domain (USD), which stabilizes an open, active conformation (Dürauer et al., 2025). Song et al. (2025) further proposed that SPRTN achieves substrate selectivity through a dual ubiquitin-recognition mode, in which the C-terminal UBZ functions as a high-affinity ubiquitin sensor, while the USD interface binds ubiquitin chains via avidity, creating a chain-length-dependent threshold that preferentially activates SPRTN on polyubiquitylated DPCs and helps spare replisome components (Song et al., 2025).

DPC proteases themselves are also post-translationally modified. **SPRTN** exists in unmodified and monoubiquitylated forms under normal conditions, whereas DPC induction promotes its **deubiquitylation** and relocalization to chromatin (Stingele et al., 2016). A phosphorylation-based feedback loop has also been proposed in which SPRTN cleaves the inhibitory C-terminus of CHK1, promoting CHK1 eviction from replicative chromatin and generating kinase-active N-terminal CHK1 fragments. Full-length CHK1 and/or these fragments then **phosphorylate** the C-terminal regulatory region of SPRTN, thereby enhancing SPRTN recruitment to chromatin and supporting DPC repair during DNA replication (Halder et al., 2019). SPRTN is additionally regulated by acetylation: Huang et al. (2020) showed that

DPC-inducing treatment promotes VCPIP1 (VCP-interacting protein 1)-dependent deubiquitylation of SPRTN, which is a prerequisite for subsequent **acetylation** of SPRTN at K230. This acetylation promotes SPRTN association with chromatin and supports efficient TOP1-DPC removal and DPC repair (Huang et al., 2020). Moreover, SPRTN is regulated in a cell-cycle-dependent manner by **APC/C-Cdh1-mediated proteolysis** (APC/C, anaphase-promoting complex/cyclosome; Cdh1, Cdc20 homolog 1). APC/C-Cdh1 is an E3 ubiquitin ligase complex that promotes proteasomal degradation of specific cell-cycle regulators, particularly from mitotic exit through G1. SPRTN levels are highest in S and G2 phase, decline rapidly upon mitotic exit, are reduced by Cdh1 overexpression, and increase upon Cdh1 depletion. In addition, SPRTN interacts with Cdh1 and can be ubiquitylated by APC/C-Cdh1 *in vitro*. Together, these findings indicate that APC/C-Cdh1 targets SPRTN for degradation, thereby restricting its expression to S, G2, and early M phases, when its replication-associated functions are required (Mosbech et al., 2012). Overall, available evidence suggests that DPC protease activity can be tuned by post-translational modifications of the proteases themselves, their substrates, and their interaction partners.

1.8. DPC proteases in human disease

Replication stress is a major contributor to tumorigenesis and cancer-associated genome instability (Gaillard et al., 2015). Replication stress can be driven by obstacles encountered by replication forks, including proteins that are irreversibly covalently crosslinked to DNA or tightly associated with it. Accordingly, several human disorders support a link between defective DPC repair, elevated replication stress, and cancer predisposition.

Mutations in the human ***SPRTN*** gene cause a rare autosomal recessive progeroid disorder, RJALS (Ruijs-Aalfs syndrome). RJALS was the first and remains the only well-established human disorder directly linking defective proteolytic DPC repair to disease, resulting from biallelic hypomorphic SPRTN variants (Vaz et al., 2016). Clinically, patients exhibit features of premature ageing (including cataracts, greying hair, and lipodystrophy) and are predisposed to early-onset hepatocellular carcinoma. At the cellular level, RJALS patient-derived cells display replication stress, elevated double-strand breaks, chromosomal aberrations, and increased total DPC levels (Lessel et al., 2014).

Mutations in ***FAM111A*** cause KCS2 (Kenny-Caffey syndrome type 2), a rare autosomal dominant disorder marked by short stature, hypoparathyroidism, hypocalcemia, and

skeletal abnormalities. Heterozygous *FAM111A* variants have also been reported in patients with OCS (osteocraniostenosis), also termed GCLEB (gracile bone dysplasia). GCLEB is typically neonatal-lethal due to severe skeletal abnormalities (Isojima et al., 2014; Unger et al., 2013). It has been proposed that KCS2- and GCLEB-associated mutations dysregulate the proteolytic activity of FAM111A, and more recent studies support a gain-of-function (hyperactive protease) model (Nie et al., 2020). However, the extent to which altered protease activity directly drives the full spectrum of disease phenotypes remains to be conclusively established.

Alterations affecting ***ACRC*** have been associated with pediatric germ cell tumors (GCTs). In humans, *ACRC* is located on the X chromosome. Notably, in a subset of pediatric GCTs profiled for both copy number and DNA methylation, *ACRC* showed copy-number loss and/or promoter hypermethylation in 66% of cases, which correlated with reduced *ACRC* expression, and low *ACRC* expression was significantly associated with poor survival (Bhargava et al., 2020). In addition to pediatric GCTs, seven rare *ACRC* gene variants have been identified in men with primary spermatogenic failure (SPGF), suggesting a role for ACRC in human male infertility (Hardy et al., 2021). Consistent with this, Ribeiro and Crossan (2023) showed that mouse Acrc is required for maintenance of undifferentiated spermatogonia and normal S-phase progression, thereby offering a plausible framework linking Acrc dysfunction to defective spermatogenesis (Ribeiro & Crossan, 2023). Together, these observations implicate ACRC in maintaining genome stability in germ cells. However, whether these disease associations reflect a direct role for ACRC in DPC repair remains to be determined.

1.9. p97 segregase/unfoldase

p97, also known as **VCP** (valosin-containing protein) and termed **Cdc48** (cell division cycle 48) in yeast, is a highly abundant and evolutionarily conserved member of the **AAA+ ATPase family** (ATPases associated with diverse cellular activities) that functions as an ATP-driven segregase/unfoldase in multiple protein quality-control and genome-maintenance pathways. Structurally, p97 forms a barrel-shaped **homohexamer** composed of six identical subunits arranged into **two stacked rings around a central pore** (Figure 6). Each subunit contains an **N-terminal (N) domain** that mediates cofactor binding and recognition of ubiquitylated substrates, **two ATPase domains**, **D1 and D2**, connected by linker regions, and a short **C-terminal tail** (Figure 7). The D1 domain is primarily required for oligomerization and hexamer assembly, whereas the D2 domain provides most of the ATP hydrolysis activity that drives substrate processing. Through ATP-dependent conformational changes, p97 engages ubiquitylated substrates and remodels them, typically by coupling substrate unfolding to their extraction from membranes, chromatin, or protein assemblies, thereby facilitating their degradation, recycling, or relocalization. In addition, the N-domain can adopt distinct conformational states that help regulate cofactor binding and p97 activity. Consistent with its broad cellular roles, p97 is indispensable for mammalian development and cell survival, and pathogenic p97 variants are associated with multisystem proteinopathy and other neurodegenerative phenotypes, while dysregulated p97 expression or activity has also been linked to cancer (Costantini et al., 2021; Noireterre & Stutz, 2024; Pontifex et al., 2024).

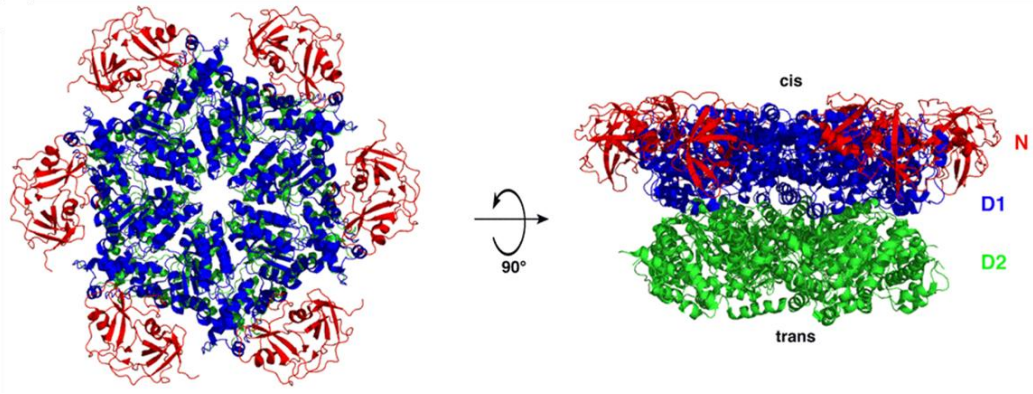

Figure 6. Hexameric structure of Cdc48/p97. Cdc48 is the yeast ortholog of metazoan p97/VCP. Each monomer comprises an N-terminal (N) domain and two AAA ATPase domains, D1 and D2. The N-terminal (D1) face of the central pore is referred to as the cis side and the C-terminal (D2) face as the trans side (adapted from (Bodnar & Rapoport, 2017)).

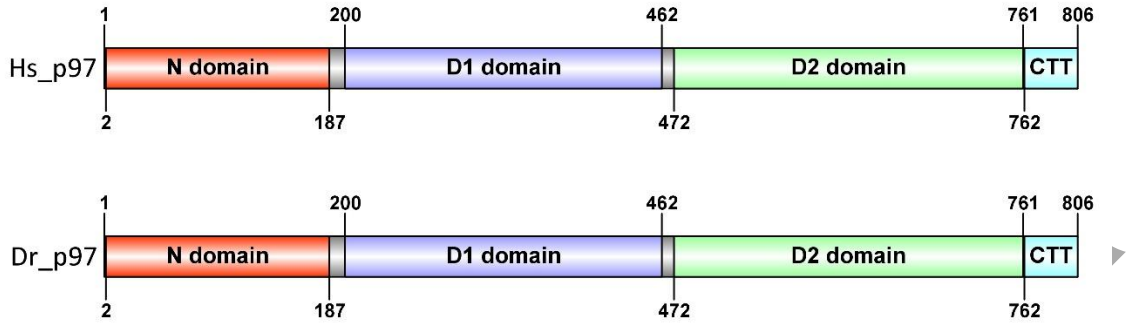

Figure 7. Comparison of the domain organization of human and zebrafish p97 proteins. *Hs*_p97, human p97 (*Homo sapiens*; UniProt P55072); *Dr*_p97, zebrafish p97 (*Danio rerio*; UniProt Q7ZU99). Domain organization was annotated based on InterPro and NCBI CD-Search analyses. The N domain, D1 ATPase domain, D2 ATPase domain, and C-terminal tail (CTT) are indicated. Numbers indicate amino acid positions delimiting the indicated protein regions. Schematic representations were generated using IBS 1.0.3 (Illustrator for Biological Sequences).

In the prevailing model of p97 action, the heterodimeric cofactor **UFD1** (ubiquitin fusion degradation 1)**-NPL4** (nuclear protein localization protein 4) (**UN**) binds to the cis side of the hexamer and recognizes a sufficiently long substrate-attached polyubiquitin chain. Polyubiquitin binding stimulates the ATPase, increasing ATP hydrolysis in the D2 domain while decreasing it in D1. ATP hydrolysis in D2 then drives translocation of the substrate polypeptide through the central pore, thereby unfolding it and promoting its extraction from membranes, chromatin, or stable protein assemblies. By contrast, ATP hydrolysis in D1 is largely dispensable for substrate unfolding and pore translocation, but appears important for subsequent substrate release, likely by promoting N-domain rearrangements that allow deubiquitylating enzymes (DUBs) to access and trim the ubiquitin chain. Release of the processed substrate requires cooperation with deubiquitylating enzymes, which trim the ubiquitin chain without necessarily removing it completely, so that the released substrate may remain oligoubiquitylated before transfer to downstream factors and, ultimately, the proteasome (Bodnar & Rapoport, 2017). Through association with numerous cofactors, including UFD1-NPL4, p47, UBXD1 (UBX domain-containing protein 1), and proteins carrying UBX (ubiquitin regulatory X domain), UBXL (UBX-like domain), VIM (VCP/p97-interacting motif), or VBM (VCP/p97-binding motif) interaction motifs or domains, p97 functions as a central cellular segregase that extracts ubiquitylated proteins from membranes, chromatin, and other protein assemblies, thereby promoting their degradation, recycling, refolding, or relocalization (Costantini et al., 2021; Noireterre & Stutz, 2024).

Consistent with its broad cofactor network, p97 functions as an ATP-driven segregase in numerous cellular pathways. These include **endoplasmic reticulum-associated protein degradation** (**ERAD**), mitochondria-associated and ribosome-associated degradation, autophagy and lysophagy, endosomal trafficking, lipid droplet biogenesis, Golgi assembly, chromatin-associated degradation, cell-cycle progression, DNA replication, and multiple DNA damage response pathways (Costantini et al., 2021; Noireterre & Stutz, 2024; Pontifex et al., 2024).

1.9.1. p97 in DPC repair

Importantly for genome stability, p97 has been shown to **extract** or promote the turnover of several chromatin-associated protein substrates. In human cells, p97, together with the proteasome, mediates repair-independent eviction of lesion-stalled **RNA polymerase II** from chromatin in response to transcription-blocking lesions, particularly when transcription-coupled repair is compromised (Zhu et al., 2024). It also extracts sterically trapped **Ku70/Ku80 rings** during DNA double-strand break repair (van den Boom et al., 2016), removes the **DNA polymerase α/primase complex** from chromatin during unperturbed DNA replication (Rodríguez-Acebes et al., 2025), and extracts ubiquitylated **Aurora B kinase** from chromatin during mitotic exit, thereby promoting chromatin decondensation and nuclear envelope reformation (Ramadan et al., 2007). Together, these findings highlight p97 as a central ATP-driven segregase that couples protein extraction from chromatin to downstream pathways such as degradation, recycling, or functional inactivation, and thereby supports intracellular proteostasis and chromatin integrity (Costantini et al., 2021).

The role of p97 in **DPC repair** remains incompletely understood. Nevertheless, available evidence indicates that p97 contributes to the processing of at least several chromatin-bound **DPC** or **DPC-like substrates**, often together with UFD1-NPL4 and, in some contexts, SPRTN (Noireterre & Stutz, 2024). Recent work showed that p97 ATPase activity likely remodels TOP1 to facilitate SPRTN-mediated proteolysis of **TOP1-DPCs**, while **TEX264 recruits p97 and SPRTN** to SUMOylated TOP1-DPCs (Fielden et al., 2020). More recently, the same group showed that p97 also functions in a SPRTN-independent pathway in which TEX264 directs TOP1-DPCs to lysosomes through selective nucleophagy (Lascaux et al., 2024). p97 has also been implicated in the processing of **TOP2-DPCs** in human cells, as its inhibition causes persistence of etoposide-induced TOP2A- and TOP2B-DPCs and increases levels of ubiquitylated TOP2-DPCs (Swan et al., 2021). p97 has further been implicated in the

processing of 5-aza-dC-induced **DNMT1-DPCs**, as inhibition of its ATPase activity blocks overall DNMT1-DPC repair (Weickert et al., 2023). In human cells, Krastev et al. (2022) showed that **trapped PARP1** is sequentially SUMOylated by PIAS4 (protein inhibitor of activated STAT 4) and then ubiquitylated by RNF4 (RING finger protein 4), modifications that promote UFD1-dependent recruitment of p97 and subsequent removal of trapped PARP1 from chromatin (Krastev et al., 2022). More recently, Oka et al. (2024) showed that p97, together with the proteasome, is required for transcription-coupled removal of formaldehyde-induced DPCs from actively transcribed genes, indicating that p97 also contributes to the repair of **DPCs during transcription** (Oka et al., 2024). Importantly, Kröning et al. (2022) demonstrated in a purified *in vitro* system that p97, together with its ubiquitin adaptor UFD1-NPL4, can unfold a **tightly folded polyubiquitylated Eos protein** crosslinked to DNA and thereby facilitate its proteolysis by **SPRTN** (Kröning et al., 2022). Thus, direct functional cooperation between p97 and SPRTN has been demonstrated biochemically for a model DPC substrate *in vitro*. However, whether this mechanism broadly applies to endogenous cellular DPCs, and in which biological contexts p97 acts together with SPRTN *in vivo*, remains to be established.

1.9.2. Interaction of p97 and SPRTN

Two studies suggest that p97 and SPRTN might cooperate in the processing of some DPCs (Fielden et al., 2020; Kröning et al., 2022). In human cells, SPRTN interacts with p97 through a conserved **SHP box motif** (Figure 3) that mediates binding to the N-terminal domain of p97. Mosbech et al. (2012) identified p97 as a prominent SPRTN-interacting protein by SILAC (stable isotope labeling by amino acids in cell culture)-based mass spectrometry and confirmed this interaction by co-immunoprecipitation. They further showed that mutation of the SHP box (F253A/L260A) abolished p97 binding, consistent with SPRTN functioning as a p97 adaptor. In parallel, Davis et al. (2012) showed that SPRTN recruits the p97-UFD1-NPL4 complex to sites of DNA damage and promotes dissociation of Pol η from damaged chromatin (Davis et al., 2012). Notably, p97 binding was not required for SPRTN recruitment to stalled replication forks. Instead, SPRTN promoted relocalization of p97 to UV-induced, PCNA-positive nuclear foci during S phase and facilitated the p97-dependent removal of Pol η from these sites (Mosbech et al., 2012). These studies established an early functional link between SPRTN and p97. Functional cooperation between p97 and SPRTN in DPC repair has been demonstrated *in vitro* (Kröning et al., 2022) and is also supported in cells for TOP1-DPC repair

(Fielden et al., 2020), although the broader importance of this interaction in DPC repair remains to be established.

1.10. Zebrafish (*Danio rerio*) as a model organism

An animal species is considered a useful model organism for studying human diseases and biological processes if it reliably represents a broader group of organisms while remaining experimentally tractable. Desirable features include a high-quality sequenced genome, similarity in body plan, organs, physiology, and signaling pathways to the target organisms, orthology of the genes under study, simple and cost-effective maintenance, and suitability for genetic manipulation and phenotypic analysis (Flinn et al., 2008). Although some questions can be addressed using alternative systems such as cultured cell lines, animal models remain essential for studying diseases and biological processes at the level of the whole organism without exposing humans to experimental risk (Lieschke & Currie, 2007). Because mammalian research is relatively expensive and raises bioethical concerns, other animal model organisms, including invertebrates and fish, are widely used. At the same time, the mouse remains one of the most important vertebrate model organisms because, as a mammal, it more closely resembles humans in terms of anatomy, physiology, tissue organization, and disease manifestation. Owing to this close evolutionary and physiological relationship, mouse models are particularly valuable for studies requiring high translational relevance, especially in the context of mammalian development, complex organ physiology, and disease mechanisms. Their use is generally more costly, time-consuming, and ethically demanding than work with zebrafish (Standley et al., 2024). As a vertebrate, zebrafish (*Danio rerio* (Hamilton, 1822)) (Figure 8) shares important developmental pathways, physiological processes, and organ systems with humans and is therefore widely used as a model organism in laboratories worldwide. Its use helps reduce research time and cost, and it has been applied to studies of gene function, organ development, tumor biology, toxicology, novel therapeutics, human diseases and disorders, and aquaculture-related topics (Bozkurt, 2020).

Zebrafish is a small tropical freshwater fish of the carp family (Cyprinidae). The species was formerly referred to as *Brachydanio rerio*, but after synonymization of *Brachydanio* with *Danio*, *Danio rerio* became the accepted name (Chu, 1981). Zebrafish is native to South Asia and has become a widely used model organism largely because of its practical and experimental advantages. It reaches sexual maturity in approximately two and a half months, which enables relatively rapid generation of transgenic lines, and a healthy breeding pair can produce 200 – 300 fertilized eggs per week (Bozkurt, 2020). Embryogenesis is completed by 72 h post-fertilization (hpf), visible pigmentation appears between approximately 30 and 72 hpf (Hill et al., 2005), and by convention zebrafish are considered embryos until 72 hpf, after which they

are referred to as larvae. Under laboratory conditions, adult zebrafish typically weigh between 0.5 and 0.9 g and have a fork length (FL) of 22 – 38 mm (Ribas & Piferrer, 2014). Zebrafish typically live for about 2 – 3 years, although under favorable laboratory conditions they may live longer (Zhao et al., 2024). A major advantage of zebrafish is that embryos and larvae are transparent (Figure 18), which facilitates a wide range of assays and screening approaches. In addition, external fertilization and development outside the maternal body enable straightforward experimental manipulation of embryos and observation of cellular processes during embryogenesis. Zebrafish also exhibit sexual dimorphism. Although sex differences are difficult to detect in juvenile fish, adult individuals can usually be distinguished easily. Males are generally smaller and more slender, with a more elongated body and golden-blue stripes, whereas females are larger and rounder, with a white abdomen and silver-blue stripes (Ribas & Piferrer, 2014).

Figure 8. Adult zebrafish (*Danio rerio* (Hamilton, 1822)), a vertebrate model organism widely used in biomedical research (adapted from (White & Patton, 2023)).

Although zebrafish is a relatively simple vertebrate model compared with other vertebrate systems, it offers several important advantages, most notably external embryogenesis, the transparency of embryos and larvae, and broad similarities to human physiology, despite notable exceptions such as the absence of lungs, mammary glands, prostate, uterus, and placenta. Embryos, larvae, and adults are all small, making husbandry more cost-effective than in larger animal models, while the time required to obtain a new generation is relatively short. Microinjection of fertilized eggs (zygotes) is also relatively straightforward and economical. The transparency of embryos and larvae greatly facilitates developmental studies, as embryogenesis can be directly observed and experimentally manipulated (Bozkurt, 2020). The zebrafish genome has been sequenced to high quality, and many molecular biology

techniques are now well established in this model, including gene knockdown and knockout methods, as well as, to some extent, gene knock-in approaches (Lantz-McPeak et al., 2015). Zebrafish is widely used to identify genes involved in the development of muscle, bone, and adipose tissue, in nutrient metabolism, and in processes related to disease, stress, and behavior. Moreover, compounds that affect fish physiology can be tested in zebrafish (Bozkurt, 2020).

The haploid zebrafish genome is organized into 25 chromosomes and contains approximately 1.37 Gb of DNA (Zebrafish Genome Assembly GRCz11, https://www.ncbi.nlm.nih.gov/grc/zebrafish/data), which is less than half the size of the human haploid genome (approximately 3.10 Gb) (Human Genome Assembly GRCh38.p14, https://www.ncbi.nlm.nih.gov/grc/human/data). Current Ensembl annotation lists 25 592 protein-coding genes in zebrafish (https://www.ensembl.org/Danio_rerio/Info/Annotation). Two key community resources for zebrafish researchers are the Zebrafish Information Network (ZFIN), the central zebrafish genetic and genomic database, and the Zebrafish International Resource Center (ZIRC), a repository and distribution center for zebrafish lines and related materials.

Approximately 71.4% of human genes have at least one zebrafish ortholog (Howe et al., 2013). Notably, orthologs of genes involved in all known human DNA repair pathways are present in zebrafish, and approximately 99% of human DNA repair genes have zebrafish orthologs (Abugable et al., 2019; Pei & Strauss, 2013). The human and zebrafish ACRC, SPRTN, and p97 proteins are orthologs and display conserved core domain architecture (Figures 3, 4, 7), suggesting that their functions are evolutionarily conserved. Zebrafish is therefore a suitable model organism for studying the roles of these proteins.

1.11. Research objectives

The aim of this study was to improve our understanding of the factors involved in the repair of DNA-protein crosslinks (DPCs) at both the cellular and organismal levels, using human cells and zebrafish (*Danio rerio*) as model systems. The specific objectives were:

1. To investigate the role of the putative protease ACRC in DPC repair using zebrafish as a model organism, and to determine the importance of the putative protease core of ACRC for protein function.
2. To investigate the role of the segregase p97 in DPC repair using human cells and zebrafish as model systems.
3. To determine whether the interaction between the protease SPRTN and the segregase p97 is important for DPC repair using human cells and zebrafish as model systems.

This study is expected to advance our understanding of DPC repair at the cellular and organismal levels. By using human cells and zebrafish as model systems, it aimed to clarify the specific contributions of ACRC, SPRTN, and p97, as well as the functional relationships among these proteins, in DPC repair. A better understanding of how different proteins contribute to DPC repair may provide important insight into tumorigenesis, ageing, and neurodegenerative diseases, and may also support the development of new therapeutic strategies for human diseases.

2. MATERIALS AND METHODS

2.1. Biological models

2.1.1. Human cell lines

HEK293T (human embryonic kidney 293T) **WT cells** were used for the initial SPRTN rescue experiments because they grow rapidly and are highly amenable to transient transfection, which makes them suitable for combined siRNA-mediated silencing and plasmid-based overexpression assays (Thomas & Smart, 2005). In this thesis, they were therefore used as a convenient screening system for testing the effects of SPRTN depletion and re-expression of different SPRTN constructs. These cells have an average doubling time of approximately 24 h (Cervera et al., 2011).

HeLa (from Henrietta Lacks) **WT cells** were used as the main human-cell model for pharmacological inhibition of p97 and analysis of endogenous DNA-protein crosslink accumulation. Their robust growth and well-established use in cell-biological studies (Masters, 2002) made them suitable for short inhibitor treatments followed by DPC isolation and quantification. HeLa cells are human cervical adenocarcinoma cells with reported doubling times usually between 20 and 30 h (Allier et al., 2018).

HeLa ΔSPRTN cells were used as a SPRTN-deficient rescue background for analysis of SPRTN-WT, SPRTN-SHPmut, and SPRTN-E112A constructs. HeLa ΔSPRTN cells were originally generated by Vaz et al. (2016) as a CRISPR/Cas9-created SPRTN-deficient HeLa model for analysis of DPC repair. HeLa cells are triploid for chromosome 1, and disruption of *SPRTN* in this system affected two of the three endogenous alleles, so the resulting line represents a partial *SPRTN* knockout. Consistent with this, one intact *SPRTN* allele remains and residual endogenous SPRTN expression is still present (Vaz et al., 2016). HeLa ΔSPRTN cells were a kind gift from the laboratory of Professor Kristijan Ramadan, Department of Oncology, University of Oxford.

2.1.1.1. Cell culture conditions

HEK293T, HeLa WT, and HeLa ΔSPRTN cells were maintained as adherent cultures in high-glucose Dulbecco's Modified Eagle's medium supplemented with 10% fetal bovine

serum [DMEM high glucose with L-glutamine and sodium pyruvate (Capricorn Scientific, DMEM-HPA); fetal bovine serum (Capricorn Scientific, FBS-GI-12A)]. Cells were cultured at 37 °C in a humidified incubator with 5% CO_2 and were routinely passaged approximately twice per week. For subculturing, cells were detached using prewarmed trypsin-EDTA [0.25% trypsin-EDTA solution (Sigma-Aldrich, T4049)], after which trypsinization was stopped by addition of complete growth medium. The resulting cell suspension was then either reseeded into fresh culture flasks (25 or 75 cm^2) for continued cultivation or used for subsequent experiments and reseeded.

2.1.2. Zebrafish and zebrafish husbandry

Unless stated otherwise, wild-type *Danio rerio* of the AB strain were used in this work, whereas mutant lines are described separately in the relevant sections. The original AB fish were obtained from the European Zebrafish Resource Center (EZRC, Karlsruhe, Germany).

2.1.2.1. Maintenance of adult fish and embryos

Adult zebrafish were kept in a recirculating water system at 28.5 °C under a 14 h light/10 h dark photoperiod and were maintained under standard zebrafish husbandry conditions, including regular monitoring of temperature, pH, and conductivity (Aleström et al., 2020).

Embryos were obtained by natural mating and raised in E3 embryo medium (5 mM NaCl, 0.17 mM KCl, 0.33 mM $CaCl_2$, and 0.33 mM $MgSO_4$) in Petri dishes in the incubator at 28.5 °C until further use. Juvenile fish were fed size-appropriate microparticulate diets according to age, and adult fish were maintained on the routine feeding schedule used in the facility. From 6 to 15 days post-hatch, juvenile fish were fed three times daily with Gemma Micro 75 (Skretting; distributed by Zebcare, 12459). From 15 to 30 days post-hatch, fish were fed three times daily with Gemma Micro 150 (Skretting; distributed by Zebcare, 12456), whereas fish older than 30 days post-hatch were fed once daily with Gemma Micro 300 (Skretting; distributed by Zebcare, 12457).

All procedures involving zebrafish were carried out in accordance with Directive 2010/63/EU on the protection of animals used for scientific purposes, as amended by Commission Delegated Directive (EU) 2024/1262, and the Croatian Animal Protection Act (NN 102/17, 32/19), under project license HR-POK-023.

2.2. Treatment of cells and zebrafish embryos with p97 inhibitors

Two chemically distinct small-molecule inhibitors of p97 were used in this study. NMS-873 is a potent allosteric p97 inhibitor from the triazole class that enables acute pharmacological inhibition of p97 activity (Magnaghi et al., 2013). CB-5083 is a potent, selective ATP-competitive p97 inhibitor that preferentially targets the D2 ATPase domain (Anderson et al., 2015). Stock solutions of both inhibitors were prepared in dimethyl sulfoxide (DMSO, Kemika, 453201) at 50 mM, aliquoted, and stored at -20 °C. To minimize loss of compound stability, repeated freeze-thawing of individual aliquots was avoided.

For pharmacological inhibition of p97 in human cells, HeLa cells were seeded into T-150 culture flasks at a density of 1.2 × 10^6 cells per flask and cultured for 48 h before treatment. Cells were then exposed for 6 h to NMS-873 (Sigma-Aldrich, SML1128-5MG) or CB-5083 (Tocris Bioscience, 7379) in serum-free medium. Based on preliminary MTT analyses, 10 μM NMS-873 and 5 μM CB-5083 were chosen for subsequent DPC experiments, whereas 5 and 10 μM of both inhibitors were tested in cytotoxicity assays. Because both compounds were dissolved in DMSO, the corresponding vehicle control contained 0.02% DMSO. After treatment, cells were washed twice with 1× PBS, collected, and dry-frozen at -80 °C until RADAR isolation.

For *in vivo* p97 inhibitor treatment, wild-type zebrafish embryos were manually dechorionated at 24 hpf (1 dpf) with forceps under a stereomicroscope and subsequently exposed to NMS-873 or CB-5083. For each condition, 30 – 35 embryos per well were placed in 6-well plates containing inhibitor diluted in E3 embryo medium and incubated at 28.5 °C. In titration experiments, embryos were treated for 6 h with NMS-873 at 5, 10, or 20 μM, or with CB-5083 at 5, 10, 20, 40, or 60 μM. For subsequent DPC experiments, embryos were treated for 6 h with 20 μM NMS-873 or 20 μM CB-5083. At 30 hpf, embryos were briefly washed twice with E3 medium, collected, and dry-frozen at -80 °C until RADAR isolation.

2.3. MTT viability assay

The colorimetric MTT assay was used, as previously described (Wang et al., 2010), to assess the cytotoxicity of p97 inhibitor treatment in HeLa cells. In this assay, metabolically active cells reduce the yellow tetrazolium salt MTT (3-(4,5-dimethylthiazol-2-yl)-2,5-diphenyltetrazolium bromide) to insoluble purple formazan. Metabolically active cells reduce

MTT to insoluble purple formazan through the action of NAD(P)H-dependent oxidoreductase enzymes. After solubilization of the formed crystals, the signal is quantified spectrophotometrically by measuring absorbance in the 500 – 600 nm range. Higher absorbance reflects a greater number of viable, metabolically active cells.

HeLa cells were seeded in 96-well plates at 7,000 cells per well for experiments that included a 20 h recovery period after treatment, and at 10,000 cells per well for experiments performed without recovery. Cells were then treated for 6 h with the p97 inhibitors NMS-873 or CB-5083 at final concentrations of 5 μM or 10 μM. In experiments including recovery, the inhibitor-containing medium was replaced after 6 h and the cells were further incubated for 20 h before viability measurement. Cell viability was then determined by incubation with 100 μL of 5 mg/mL MTT solution (Alfa Aesar, L11939) for 3 h. The solution was then removed, and the resulting formazan crystals were dissolved in 500 μL isopropanol (Kemika, 1622601), followed by shaking at 350 rpm for 15 min using a plate shaker-thermostat (BioSan, PST-60HL-4). Absorbance was measured at 578 nm, with 750 nm used as the reference wavelength, using a microplate reader (Tecan, Infinite M200). Absorbance values were normalized to untreated control cells and used as an indicator of relative cell viability.

2.4. Gene silencing by siRNA transfection

Endogenous SPRTN was silenced in HEK293T cells by transfection of small interfering RNA (siRNA) prior to plasmid transfection with SPRTN expression constructs used for analysis of the SHP motif and related functional assays. Silencing efficiency was evaluated by quantitative polymerase chain reaction (qPCR) using gene-specific primers. HEK293T cells were seeded in 75 cm² culture flasks at 76,800 cells per flask, and 24 h later they were transfected with 10 nM siRNA targeting SPRTN (ON-TARGETplus Human SPRTN siRNA, Dharmacon/Horizon Discovery, L-015442-02-0005; sequence: 5'-CAUCAAAGUCAAAAGCGAA-3'). For siRNA delivery, DharmaFECT transfection reagent (Dharmacon, USA) was used according to the manufacturer's instructions. Briefly, siRNA was diluted in Opti-MEM reduced-serum medium (Gibco, 31985070) to prepare solution A, while DharmaFECT reagent was diluted in Opti-MEM to prepare solution B. The two solutions were then combined and added to the cells to achieve a final siRNA concentration of 10 nM. Cells were subsequently incubated for 24 h at 37 °C in 5% CO_2, after which they were transfected with plasmid DNA.

2.5. Plasmid transfection by polyethyleneimine (PEI)

Plasmid transfection was performed in HEK293T and HeLa ΔSPRTN cells to express different SPRTN variants used for analysis of the SHP motif and the proteolytic activity of SPRTN. In HEK293T cells, plasmid transfection was carried out 24 h after siRNA transfection. HeLa ΔSPRTN cells were seeded in 75 cm² culture flasks at 600,000 cells per flask and transfected with plasmid DNA 24 h after seeding. The expression constructs SPRTN-WT, SPRTN-SHPmut, and SPRTN-E112A were cloned in the pcDNA3.1/HisA backbone, and 6.25 µg of plasmid DNA was used per flask for each construct. For transfection, 6.25 µg of plasmid DNA was diluted in PBS, while 25× PEI transfection reagent (1 mg/mL stock) was first diluted 1:25 in PBS in a separate tube (Tom et al., 2008). The resulting DNA:PBS and PEI:PBS solutions were then mixed in a 1:1 ratio, mixed by low-speed vortexing three times for 3 s, and incubated for 15 min at room temperature to allow formation of PEI-DNA complexes. After removal of the culture medium, the transfection mixture was added to the cells in DMEM without FBS. After 4 h incubation, the transfection medium was replaced with complete growth medium. Forty-eight hours after plasmid transfection, cells were washed twice with 1× PBS, collected, and dry-frozen at -80 °C for subsequent DPC isolation using the modified RADAR assay. A small aliquot of cells was collected in parallel for qPCR analysis to verify SPRTN overexpression and assess the efficiency of SPRTN silencing.

2.6. RNA isolation, reverse transcription, and qPCR analysis

2.6.1. Verification of *SPRTN* overexpression in HEK293T and HeLa ΔSPRTN cells and *SPRTN* silencing in HEK293T cells

Total RNA was isolated using the Total RNA Isolation Kit (NEB, T2010) according to the manufacturer's instructions. RNA concentration was measured using BioSpec-nano spectrophotometer (Shimadzu), and RNA integrity was assessed by agarose gel electrophoresis. For each sample, purified total RNA was reverse transcribed into cDNA using the ProtoScript II First Strand cDNA Synthesis Kit (NEB, E6560) with a 1:1 mixture of oligo(dT) and random hexamer primers.

SPRTN expression was quantified by relative qPCR in technical triplicates, using 5 ng cDNA per reaction. Human *SPRTN* was amplified with the following primers: *HsSPRTN* forward 5'-GAGGTGGATGAGTATCGGCG-3' and reverse 5'-

GGGTTCCCTGTTAGTAGCTCG-3' (primer efficiency 2.01). As the reference gene, *HsRANBP2* was used with primers forward 5'-TGTAGTGATACTGATGAAGACAATGG-3' and reverse 5'-TTGTGCTAGTTATTTCTTCTGTCTGAG-3' (primer efficiency 1.97). qPCR was performed on a 7300 Real-Time PCR System (Applied Biosystems) using Power SYBR Green PCR Master Mix (Applied Biosystems, 4367659) according to the manufacturer's instructions. The cycling conditions were as follows: an initial denaturation step at 95 °C for 10 min, followed by 40 cycles of 95 °C for 15 s and 60 °C for 1 min; amplification was followed by melting-curve analysis.

qPCR data were processed using 7500 Fast System SDS software (Applied Biosystems) and relative expression levels were calculated using the Q-Gene method (Muller et al., 2002; Simon, 2003), according to the following formula for mean normalized expression (MNE): $MNE = E(R)^{Ct(R)} / E(gene)^{Ct(gene)}$, where E(R) is the amplification efficiency of the reference gene, Ct(R) is the average Ct value of the reference gene for a given sample, E(gene) is the amplification efficiency of the gene of interest, and Ct(gene) is the average Ct value of the gene of interest for that sample. For graphical presentation, MNE values were presented as fold change relative to the control sample, i.e. HEK293T WT or HeLa ΔSPRTN, as indicated for each experiment.

2.7. Gene silencing in zebrafish embryos using morpholino oligonucleotides and mRNA microinjection

Morpholino oligonucleotides are synthetic antisense oligomers that suppress gene expression by hybridizing to complementary RNA sequences. Depending on their design, they can either inhibit translation by targeting the 5'-UTR or start-codon region of the mRNA, or interfere with pre-mRNA splicing by binding to exon-intron junctions (Moulton, 2007). For silencing of zebrafish Sprtn, two morpholinos were used: a translation-blocking morpholino targeting the 5'-UTR (5'-TCGGTCTGCTTTAGTAACAACAGTT-3') and a splice-blocking morpholino targeting the exon 2-intron 2 boundary (5'-AGAGAGGCATATTTAACCAACCTGA-3'). Both morpholinos were obtained from Gene Tools (USA). For microinjection, a premixed solution containing 250 μM of each Sprtn morpholino, 300 mM KCl, and 0.015% phenol red was injected into one-cell-stage zebrafish embryos.

For silencing of p97, embryos were injected in the same manner with a splice-blocking morpholino targeting the exon 5-intron 5 boundary (5'-ATTTGTCAATTTACTCGCCTCTCGC-3'). The p97 morpholino was used at a final concentration of 150 μM in the same solution (300 mM KCl and 0.015% phenol red). p97 morpholino-injected embryos were used to examine the contribution of p97 to DNA repair *in vivo* and were collected at 30 hpf and dry-frozen at -80 °C for subsequent RADAR analysis. Likewise, embryos injected with Sprtn morpholinos were used in rescue experiments designed to assess the contribution of the SPRTN-p97 interaction, and were also collected at 30 hpf and dry-frozen at -80 °C for RADAR analysis.

For these rescue and overexpression experiments, embryos injected with Sprtn morpholinos were co-injected at the one-cell stage with *in vitro* synthesized mRNA encoding zebrafish Sprtn-WT, Sprtn-SHPmut, or Sprtn-L147A. Zebrafish WT and *acrc* mutant embryos were injected with mRNA constructs used for Acrc rescue and domain analysis, including zebrafish Acrc-WT, Acrc-E451A, Acrc-SprT, Acrc-ΔSprT, and Acrc-ΔC, as well as DrSprtn and MmAcrc.

All microinjections were performed using a FemtoJet® 4x microinjection system (Eppendorf) with Femtotips™ microinjection capillary tips (Eppendorf). Approximately 1 nL of the respective premixed solution was injected into the yolk of 1- to 4-cell-stage embryos. mRNA used for injection was synthesized *in vitro* from purified linearized plasmids by SP6 transcription using the HiScribe SP6 RNA Synthesis Kit (NEB, E2070S) together with the ARCA cap analog kit (NEB, S1411) to improve mRNA stability. The resulting RNA was purified using the RNA Cleanup Kit (NEB, T2040) and injected into 1- to 4-cell-stage embryos in a volume of 1 nL. Injection solutions contained 300 mM KCl and 0.015% phenol red. For Acrc constructs, mRNA was injected at 250 ng/μL, whereas Sprtn constructs were injected at 100 ng/μL.

2.8. Generation and maintenance of zebrafish *acrc* mutant lines

For analysis of the role of Acrc in DNA-protein crosslink repair *in vivo*, zebrafish wild-type fish and two genetically modified zebrafish lines carrying mutations in *acrc* were used. One mutant line carried an in-frame deletion of 12 nucleotides in *acrc* exon 12, resulting in deletion of amino acids 451-454 (ΔEMCH) within the predicted catalytic core of the SprT domain (Figure 9). This allele was designated *rbi5*. The deleted EMCH residues form part of

the conserved HEXXH motif, and E451 corresponds to the predicted catalytic glutamate. The second mutant line was represented by two exon 12 alleles, *rbi8* and *rbi9*, which introduced frameshifts and premature stop codons at amino acid positions 477 and 472, respectively, in the 586-amino-acid Acrc protein (Figure 9). These mutations resulted in C-terminally truncated Acrc proteins downstream of E451. The mutant zebrafish lines were generated by CRISPR/Cas9-mediated genome editing. This work was initiated before the start of the present PhD project as part of the doctoral work of Dr. Christine Supina Pavić (Supina Pavić, 2023). At that stage, guide RNAs targeting the putative protease core of zebrafish Acrc were designed, synthesized (Modzelewski et al., 2018), and used for microinjection into 1-cell-stage embryos together with Cas9 protein (EnGen® Spy Cas9 NLS, NEB, M0646T). Two guides targeting *acrc* exon 12 were used: DrACRC sgRNA_1 (5'-GGAGCATAAAGCCTCCAGAA-3'), which gave rise to the *rbi8* and *rbi9* alleles, and DrACRC sgRNA_2 (5'-GGCCGCATGACACATTTCA-3'), which generated the *rbi5* allele. For mutagenesis, 1 nL of an injection mixture containing guide RNA (180 ng/µL), Cas9 protein (600 ng/µL), and 300 mM KCl was injected into embryos at the 1-cell stage.

Injected F0 fish were raised to sexual maturity, and founders transmitting *acrc* mutations were subsequently identified. During the present PhD project, the breeding and characterization of these lines were completed. F0 founders were crossed to obtain the F1 generation, heterozygous carriers were identified, and subsequent crosses were performed to obtain homozygous F2 fish required for further analyses. Adult fish from the F1, F2, and subsequent generations were genotyped by PCR amplification and sequencing of genomic DNA obtained from tail-fin tissue. For analysis of injected embryos, lysis was performed with proteinase K (Alpha Aesar, J63710; 0.5 mg/mL) in digestion buffer (10 mM Tris-HCl, pH 8.5, 50 mM KCl, 0.3% Tween-20) for 3 h at 55 °C, followed by PCR and sequencing using the primers Geno_acrc_F (5'-ACAGATCGGTTACGGGATAC-3') and Geno_acrc_R (5'-TTGATGTCATAACTGTGGCA-3').

Three alleles were selected for further maintenance, and experiments were subsequently performed either with the $acrc^{rbi5/rbi5}$ line or with the $acrc^{rbi8/rbi9}$ line. Both mutant lines showed the same major phenotype, similar rescue patterns, and comparable accumulation of DNA-protein crosslinks, and both were therefore used in the study. Homozygous mutant males and females were used for maintenance of the lines, and their homozygous embryos were used in downstream analyses of DPC accumulation. In addition, rescue of the early embryonic phenotype by injection of *in vitro* transcribed Acrc-WT mRNA allowed survival of embryos

from both mutant lines to adulthood, which further enabled propagation and long-term maintenance of the mutant lines.

2.9. Western blot analysis of zebrafish tissues

Western blot analysis was performed on ovarian lysates obtained from WT zebrafish and from both *acrc* mutant lines. Zebrafish ovaries were analyzed individually, with one ovary processed per sample. Each ovary was lysed in 500 µL RIPA buffer containing 150 mM NaCl, 1% Triton X-100, 0.5% sodium deoxycholate, 50 mM Tris-HCl (pH 8.0), and 0.5% SDS, supplemented with protease inhibitors (leupeptin, 1 µg/mL; pepstatin, 1 µg/mL; chymostatin, 1 µg/mL; aprotinin, 10 µg/mL; PMSF, 1 mM) and phosphatase inhibitors (sodium fluoride, 2 mM; sodium pyrophosphate, 2 mM; sodium orthovanadate, 5 mM). Tissue homogenization was performed using an Ultra-Turrax T25 homogenizer in three 10 s cycles at medium intensity, followed by sonication with an MSE probe sonicator in three 3 s cycles at low power. Lysates were then centrifuged at 10,000 × g for 7 min at 4 °C, and the supernatants were collected for further analysis. Total protein concentration was determined using the Pierce Detergent Compatible Bradford Assay Kit (Thermo Fisher Scientific, 23246) according to the manufacturer's instructions.

Protein samples were separated on homemade 5 – 18% SDS-polyacrylamide gradient gels at 120 V for 90 min using a Mini-PROTEAN 3 Cell electrophoresis system (Bio-Rad). Precision Plus Protein Dual Color Standards spanning 10 – 250 kDa (Bio-Rad, 1610374) were used to estimate protein size. Samples were subsequently transferred to PVDF membranes (Roche, 03010040001) by wet transfer using a Mini Trans-Blot system (Bio-Rad). Membranes were blocked in 5% low-fat milk in TBST (20 mM Tris-HCl, pH 7.5; 150 mM NaCl; 0.1% Tween 20) for 2 h at room temperature and then incubated with primary antibodies diluted in 2.5% BSA in TBST overnight at 4 °C. After incubation with HRP-conjugated secondary antibodies for 1 h, membranes were washed three times for 10 min in TBST. Signal detection was performed using ECL blotting substrate (Bio-Rad, 1705061) according to the manufacturer's instructions, and chemiluminescence was recorded using a ChemiDoc XRS+ System (Bio-Rad, 1708299).

For detection of Acrc and histone H3 as a loading control, 25 µg of total protein was loaded per sample. The following primary antibodies were used: anti-ACRC (Sigma-Aldrich, SAB1403429; 1:6000) and anti-histone H3 (Cell Signaling Technology, 9715; 1:3000). For

secondary detection, HRP-conjugated anti-mouse antibody (Sigma-Aldrich, A9044; 1:100000) was used with the anti-ACRC antibody, whereas HRP-conjugated anti-rabbit antibody (Sigma-Aldrich, A0545; 1:100000) was used for histone H3 detection.

2.10. DPC isolation using the modified RADAR method

DNA-protein crosslinks (DPCs) were isolated using a modified RADAR (rapid approach to DNA adduct recovery) assay, based on the original method of Kiianitsa and Maizels (Kiianitsa & Maizels, 2013, 2020) and further optimized in our laboratory for improved reproducibility and for application to zebrafish embryos (Anticevic et al., 2023). In this study, this modified protocol was applied to human cell lines and to zebrafish embryos collected at 6 hpf and 30 hpf.

For DPC isolation from human cell lines, cell pellets were lysed in 1 mL of prewarmed DPC lysis buffer containing 6 M guanidinium isothiocyanate, 10 mM Tris-HCl (pH 6.8), 20 mM EDTA, 4% Triton X-100, 1% N-lauroylsarcosine sodium, and 5% β-mercaptoethanol, and incubated for 10 min at 55 °C with vigorous mixing. For zebrafish samples, DPCs were isolated either from 50 embryos per sample at 6 hpf (WT and *acrc* mutant embryos) or from 25 embryos per sample at 30 hpf, using the same lysis buffer and incubation conditions. After lysis, DPC-containing DNA was precipitated by addition of an equal volume of 96% ethanol and collected by centrifugation at 10,000 × g for 10 min at 4 °C. The resulting DNA pellets were washed four times with wash buffer (20 mM Tris-HCl, pH 7.5, 50 mM NaCl, 1 mM EDTA, 50% ethanol) using the same centrifugation conditions. After a brief drying for 5 min at 40 °C, the pellets were dissolved in 850 µl of 8 mM NaOH. To facilitate solubilization, samples were sonicated using an MSE probe sonicator at low power. For human cell samples and 30 hpf embryo samples, sonication was performed once for 8 s, whereas 6 hpf embryo samples were sonicated ten times for 8 s.

For DNA quantification, a 50 µL aliquot of each DPC isolate was treated with proteinase K (20 mg/mL, Fisher Scientific, BP1700-100) for 3 h at 55 °C, and DNA concentration was measured using the PicoGreen assay according to the manufacturer's instructions (Invitrogen, P7581). The remaining samples were normalized to the same amount of DNA and then treated with benzonase nuclease (Millipore, E1014) for 1 h at 37 °C to remove DNA. After benzonase treatment, samples were snap-frozen in liquid nitrogen and subjected to overnight lyophilization using a FreeZone 2.5 lyophilizer (Labconco, USA) at approximately -50 °C and

5 Pa vacuum. Lyophilized DPC samples were finally dissolved in SDS loading buffer containing 4 M urea, 62.5 mM Tris-HCl (pH 6.8), 1 mM EDTA, and 2% SDS.

2.11. Detection and quantification of DPCs

2.11.1. Silver staining

DNA-normalized DPC isolates obtained by the modified RADAR method were used for analysis of both total cellular DPCs and selected specific DPC species. Total DPCs were resolved on 5 – 18% SDS-polyacrylamide gradient gels and visualized using the ProteoSilver™ Silver Stain Kit (Sigma-Aldrich, PROTSIL1) according to the manufacturer's instructions. For 6 hpf zebrafish embryo samples, a DPC equivalent of 25 ng total DNA was loaded per lane for silver staining, whereas for 30 hpf embryo samples and human cell samples, a DPC equivalent of 200 ng total DNA was loaded.

2.11.2. Western blotting and dot blotting

Specific DPC species were detected by western blotting or dot blotting. Histone H3-DPCs were analyzed by western blotting and dot blotting. Ku80-, PARP1-/Parp1-, TOP1/Top1-, DNMT1/Dnmt1-, TOP2/Top2-, POLR3A/Polr3a-, and MCM2/Mcm2-DPCs were analyzed by dot blotting with protein-specific antibodies. For 6 hpf embryo samples, a DPC equivalent of 25 ng total DNA was used for detection of histone H3, Parp1, Top1, Top2, Dnmt1, Polr3a, and Mcm2. For 30 hpf embryo samples and human cell samples, a DPC equivalent of 200 ng total DNA was used for histone H3 analysis, whereas a DPC equivalent of 500 ng total DNA was used for Ku80, PARP1/Parp1, TOP1/Top1, DNMT1/Dnmt1, TOP2/Top2, POLR3A/Polr3a, and MCM2/Mcm2.

For western blot analysis, DPC samples were separated on 5 – 18% SDS-polyacrylamide gradient gels and transferred to PVDF membranes (Roche, 03010040001). Membranes were blocked in 5% low-fat milk in TBST (20 mM Tris-HCl, pH 7.5, 150 mM NaCl, 0.1% Tween 20) for 2 h at room temperature, followed by incubation with primary antibody diluted in 2.5% BSA in TBST overnight at 4 °C. After incubation with HRP-conjugated secondary antibody for 1 h, membranes were washed three times for 10 min in TBST. Chemiluminescent detection was performed using ECL blotting substrate (Bio-Rad,

1705061) and recorded with the ChemiDoc™ XRS+ System (Bio-Rad, 1708299). Histone H3 was detected using anti-histone H3 (Cell Signaling Technology, 9715; 1:3000).

For dot blot analysis, 200 µL of each DPC sample diluted in TBST was loaded per well onto nitrocellulose membranes (GE Healthcare, 10-6000-02) using the Bio-Dot microfiltration device (Bio-Rad Laboratories, CA, USA) and applied by vacuum at 700 mbar. After blocking in 5% low-fat milk in TBST, membranes were incubated with primary antibodies in 2.5% BSA/TBST overnight at 4 °C, followed by HRP-conjugated secondary antibodies and chemiluminescent detection as described above. The following primary antibodies were used for DPC detection: anti-histone H3 (Cell Signaling Technology, 9715; rabbit; 1:3000), anti-Ku80 (Cell Signaling Technology, 2753; rabbit; 1:1000), anti-PARP1 (Cell Signaling Technology, 9532; rabbit; 1:1000), anti-TOP1 (Santa Cruz, sc-271285; mouse; 1:1000), anti-DNMT1 (Cell Signaling Technology, 5032; rabbit; 1:1000), anti-TOP2A (Abcam, ab52934; rabbit; 1:1000), anti-POLR3A (Cell Signaling Technology, 12825; rabbit; 1:1000), and anti-MCM2 (Cell Signaling Technology, 3619; rabbit; 1:1000). HRP-conjugated anti-rabbit secondary antibody (Sigma-Aldrich, A0545; 1:100000) was used for rabbit primary antibodies, whereas HRP-conjugated anti-mouse secondary antibody (Sigma-Aldrich, A9044; 1:100000) was used for mouse primary antibody (anti-TOP1).

To verify the accuracy of DNA quantification and normalization of DPC samples, 2 ng of DNA from each proteinase K-treated aliquot was analyzed as a dsDNA loading control by dot blot. For this purpose, each DNA sample was diluted in 200 µL TBST, and applied to a nylon membrane, which was used because of its high affinity for DNA. Before loading, the membrane was pre-wetted in TBST for 1 min, mounted in the dot blot apparatus, and the wells were washed with 200 µL TBST under vacuum. Subsequently, 200 µL of each diluted sample was loaded per well and drawn through the membrane by vacuum-assisted aspiration, followed by one additional wash with 200 µL TBST. The membrane regions containing the samples were then excised, air-dried for 15 min, and exposed to UV light (312 nm) for 5 min to crosslink DNA to the membrane. After blocking, the membrane was incubated overnight at 4 °C with anti-dsDNA antibody (Abcam, ab27156; mouse; 1:9000). Immunodetection was then performed using the same conditions as described for protein dot blot analysis.

2.12. Imaging

Zebrafish embryos were photographed using a Samsung Galaxy A54 smartphone camera mounted to the ocular of a Motic SMZ-171 stereomicroscope.

2.13. Data quantification and statistical analysis

Quantification of silver-stained gels, western blots, and dot blots was performed using ImageJ (Schneider et al., 2012). Graphs were prepared and statistical analyses were carried out using GraphPad Prism (v9.0.0, GraphPad Software). Data are presented as mean ± SD. Depending on the experimental design, differences between groups were evaluated using an unpaired two-tailed Student's t-test or one-way ANOVA. Differences were considered statistically significant at $p < 0.05$ (ns, $p > 0.05$; * $p < 0.05$; ** $p < 0.01$; *** $p < 0.001$; **** $p < 0.0001$).

3. RESULTS

3.1. Role of Acrc in DPC repair in zebrafish

3.1.1. Mutations in the SprT domain of Acrc cause early embryonic lethality in zebrafish

To examine DPC repair *in vivo*, two zebrafish *acrc* mutant lines targeting the SprT domain were generated using the CRISPR/Cas9 system. In one line, an in-frame deletion of 12 nucleotides within the predicted catalytic site removed the catalytic glutamate E451 together with the next three amino acids of the protease core, including the zinc-coordinating histidine H454 (ΔEMCH) (Figure 9). This mutant allele was named *rbi5* (Ruđer Bošković Institute 5) according to the nomenclature guidelines of ZFIN (The Zebrafish Information Network, zfin.org). The second mutant line carried mutations in exon 12 that introduced frameshifts and premature stop codons at amino acid positions 477 and 472 (Figure 9). These alleles were designated *rbi8* and *rbi9* (Ruđer Bošković Institute 8 and 9).

Both mutant lines exhibited maternal-zygotic embryonic lethality, with embryos dying before 24 hpf (Figure 9). Notably, lethality in the line carrying the catalytic-core mutation (*rbi5*, ΔEMCH) indicates that the phenotype most likely results from loss of Acrc proteolytic activity. The maternal-zygotic nature of this phenotype was supported by the early lethality of heterozygous embryos obtained from crosses between WT males and homozygous mutant females. This phenotype was rescued by injection of *in vitro* transcribed Acrc-WT mRNA into embryos at the 1-cell stage (Figure 11). By contrast, homozygous mutant embryos derived from heterozygous parents showed no obvious morphological abnormalities (Figure 9), indicating that maternal deposition of functional Acrc protein and/or Acrc mRNA into the oocyte is required for normal embryonic development.

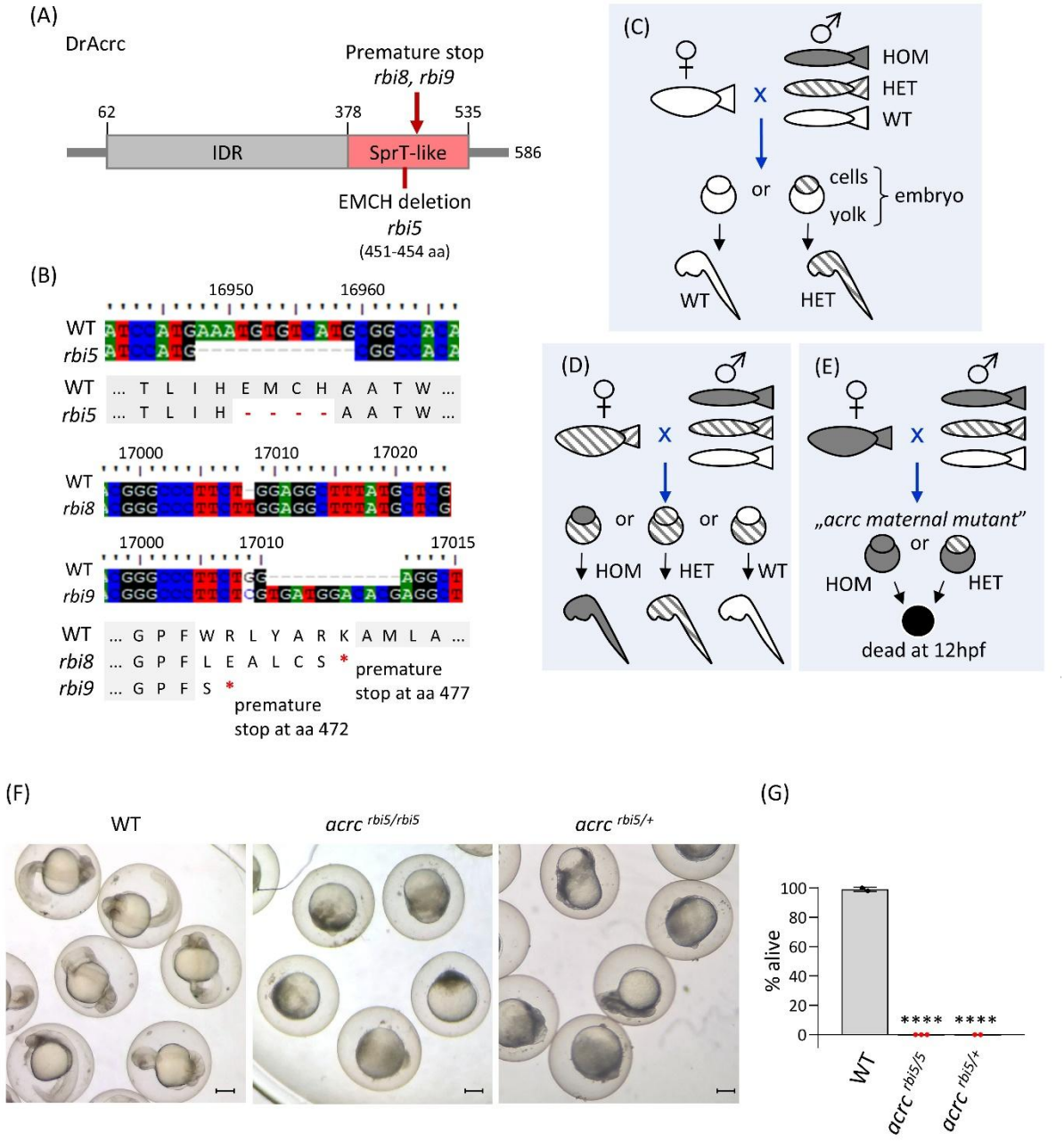

Figure 9. Creation of *acrc* mutant zebrafish lines. (A, B) Scheme of the Acrc protein showing the sequences and positions of the 4 amino-acids deletion (ΔEMCH, 451 – 454 aa) in the enzymatic core of the SprT domain in the *rbi5* allele, and of the premature stop codons resulting from the *rbi8* and *rbi9* alleles. **(C – E)** Schemes representing genotype-phenotype correlations upon loss of one or both *acrc* wild type (WT) alleles: (C) – crossing a WT female with any male (WT: white, heterozygote: stripes, or mutant: grey) always leads to viable fish, (D) – crossing a heterozygous female with any male (WT, heterozygote or mutant) always leads to viable fish, and (E) – crossing an *acrc* mutant female with any male (WT, heterozygote or mutant) always results in embryos with an early lethal phenotype (black yolk). **(F)** Representative images of WT, mutant and heterozygous (from homozygous females crossed with WT males) zebrafish embryos at 24 hpf. Scale bars: 250 µm. **(G)** Quantification of embryo survival at 24 hpf. Data are shown as the percentage of live embryos from at least 2 independent experiments with at least 15 embryos each (mean ± SD; one-way ANOVA, **** $p < 0.0001$). hpf – hours post-fertilization. Figure was prepared by Cecile Otten (Otten et al., 2025).

Acrc protein was detected in adult ovaries from both mutant lines, *acrc*$^{rbi5/rbi5}$ (ΔEMCH) and *acrc*$^{rbi8/rbi9}$, at levels similar to those observed in wild-type (WT) fish (Figure 10). On SDS-PAGE, Acrc migrated with an apparent molecular weight of approximately 100 kDa rather than the predicted 65 kDa, most likely because of its high hydrophobicity, intrinsically disordered nature, large hydrodynamic radius, clusters of acidic residues, and high proline content. These are typical features of intrinsically disordered proteins and often lead to 1.2 – 1.8-fold slower migration on SDS-PAGE due to reduced SDS binding and a more extended protein conformation, a phenomenon referred to as gel shifting (Shi et al., 2012; Tiwari et al., 2019; Tompa, 2002). As expected, the truncated Acrc protein in *acrc*$^{rbi8/rbi9}$ mutants (predicted molecular weight 53 kDa) migrated slightly faster than the WT protein on SDS-PAGE (Figure 10). Together, these results indicate that the ΔEMCH deletion does not cause detectable protein degradation and is unlikely to result in major protein misfolding *in vivo*, since comparable protein levels and the expected electrophoretic mobility were observed experimentally (Figure 10). In *acrc*$^{rbi8/rbi9}$ mutants, premature termination occurred shortly after the third zinc-coordinating histidine (H467) (Figure 9), thereby altering the SprT domain. However, the truncated Acrc protein was still present at levels comparable to those of WT Acrc (Figure 10).

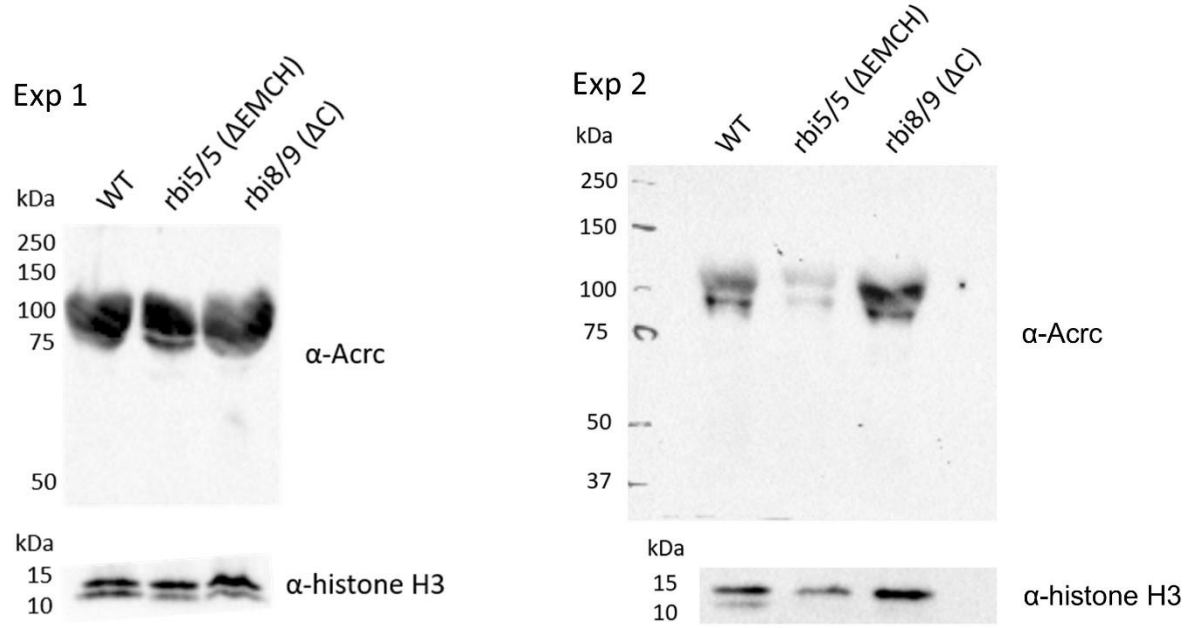

Figure 10. Western blot analysis of adult ovary lysates showing Acrc protein in wild-type (WT) fish and in both mutant lines, *acrc*$^{rbi5/rbi5}$ (ΔEMCH) and *acrc*$^{rbi8/rbi9}$. The predicted molecular masses of WT Acrc, the ΔEMCH mutant protein, and the truncated Acrc protein in *acrc*$^{rbi8/rbi9}$ mutants are 65.43, 64.94, and 52.56 kDa, respectively. WT and ΔEMCH Acrc migrate at an apparent molecular weight of ~100 kDa on SDS-PAGE, likely

because of gel shifting associated with the intrinsically disordered and acidic nature of the protein, whereas the truncated protein from *acrc*$^{rbi8/rbi9}$ line migrates slightly faster.

3.1.2. The putative catalytic core of the SprT domain is essential for Acrc function during early embryonic development

To verify that the catalytic mutation underlies the lethal phenotype and to examine the contribution of other Acrc domains, *in vitro* transcribed and capped mRNAs encoding either WT or mutant Acrc variants (Figure 11) were injected into *acrc*$^{rbi5/rbi5}$ mutant embryos at the 1-cell stage, and their capacity to restore Acrc function and rescue the early lethal phenotype was evaluated. Each mRNA was injected into WT and *acrc* mutant embryos, and embryo viability was scored at 24 hpf as either "alive" or "dead" (Figure 11). This analysis included *acrc*$^{rbi5/rbi5}$ and *acrc*$^{rbi8/rbi9}$ mutants, with WT embryos serving as controls (Figure 11). As an initial control, injection of Acrc-WT mRNA into mutant embryos resulted in clear rescue of the lethal phenotype (Figure 11). At 24 hpf, 70.2% of *acrc*$^{rbi5/rbi5}$ mutant embryos and 95.1% of *acrc*$^{rbi8/rbi9}$ mutant embryos injected with Acrc-WT mRNA were alive (Figure 11). The rescue was sufficiently efficient that most injected embryos (> 50%) developed normally not only to adulthood (3 months of age) but also to older age (1.5 years).

Secondly, the catalytic glutamate E451 within the putative protease core proved essential for embryonic development, as injection of Acrc-E451A mRNA did not rescue the lethal phenotype (Figure 11). At 24 hpf, no *acrc*$^{rbi5/rbi5}$ mutant embryos injected with Acrc-E451A mRNA were alive (Figure 11), indicating that E451 in the protease core is required for Acrc function during early embryonic development. Next, the role of other Acrc domains in the lethality phenotype was assessed. To this end, constructs encoding the isolated SprT domain (Acrc-SprT), Acrc without the SprT domain (Acrc-ΔSprT), and a truncated Acrc variant lacking the C-terminal tail (Acrc-ΔC) were examined. Acrc-SprT, a shortened Acrc variant lacking the entire IDR and consisting mainly of the SprT domain, was injected into *acrc*$^{rbi8/rbi9}$ mutants (Figure 11). This construct significantly rescued the lethal phenotype, with 50.9 ± 17.6% of embryos remaining alive at 24 hpf (Figure 11). However, the extent of rescue was lower than that obtained with the Acrc-WT construct (95.1 ± 5.4%) (Figure 11). In contrast, the Acrc variant consisting predominantly of the IDR region (Acrc-ΔSprT) did not rescue the lethal phenotype (Figure 11). The construct carrying a short C-terminal truncation while retaining intact SprT and IDR domains (Acrc-ΔC) rescued the lethal phenotype to a similar degree as

Acrc-WT (Figure 11). Following injection of Acrc-ΔC mRNA, 71.7 ± 30.6% of *acrc*$^{rbi5/rbi5}$ maternal mutant embryos were alive at 24 hpf (Figure 11).

Because Sprtn, like Acrc, contains a SprT domain (Figures 3, 4) and shares a highly similar protease core, its ability to compensate for Acrc loss during early embryonic development was examined. Since endogenous Sprtn expression was not sufficient to rescue Acrc deficiency in the mutants, Sprtn overexpression was tested by mRNA injection. However, injection of zebrafish Sprtn mRNA into *acrc*$^{rbi5/rbi5}$ mutant embryos did not rescue the early lethal phenotype, and no viable embryos were detected at 24 hpf (Figure 11). To further assess whether the proteolytic function of Acrc is required for early development, mouse Acrc, which lacks a SprT domain (Figure 11), was also tested for its ability to rescue the early embryonic lethality of *acrc* mutant zebrafish. For this purpose, mouse Acrc mRNA was injected into *acrc*$^{rbi5/rbi5}$ mutant embryos (Figure 11), and no injected embryos were alive at 24 hpf (Figure 11).

Overall, the rescue experiments showed that an intact Acrc protease core is essential for survival during early embryonic development. Notably, embryos from both *acrc* mutant lines (*rbi5/rbi5* and *rbi8/rbi9*) that were injected with full-length Acrc-WT mRNA survived to adulthood and remained fertile, which enabled propagation and maintenance of the mutant lines.

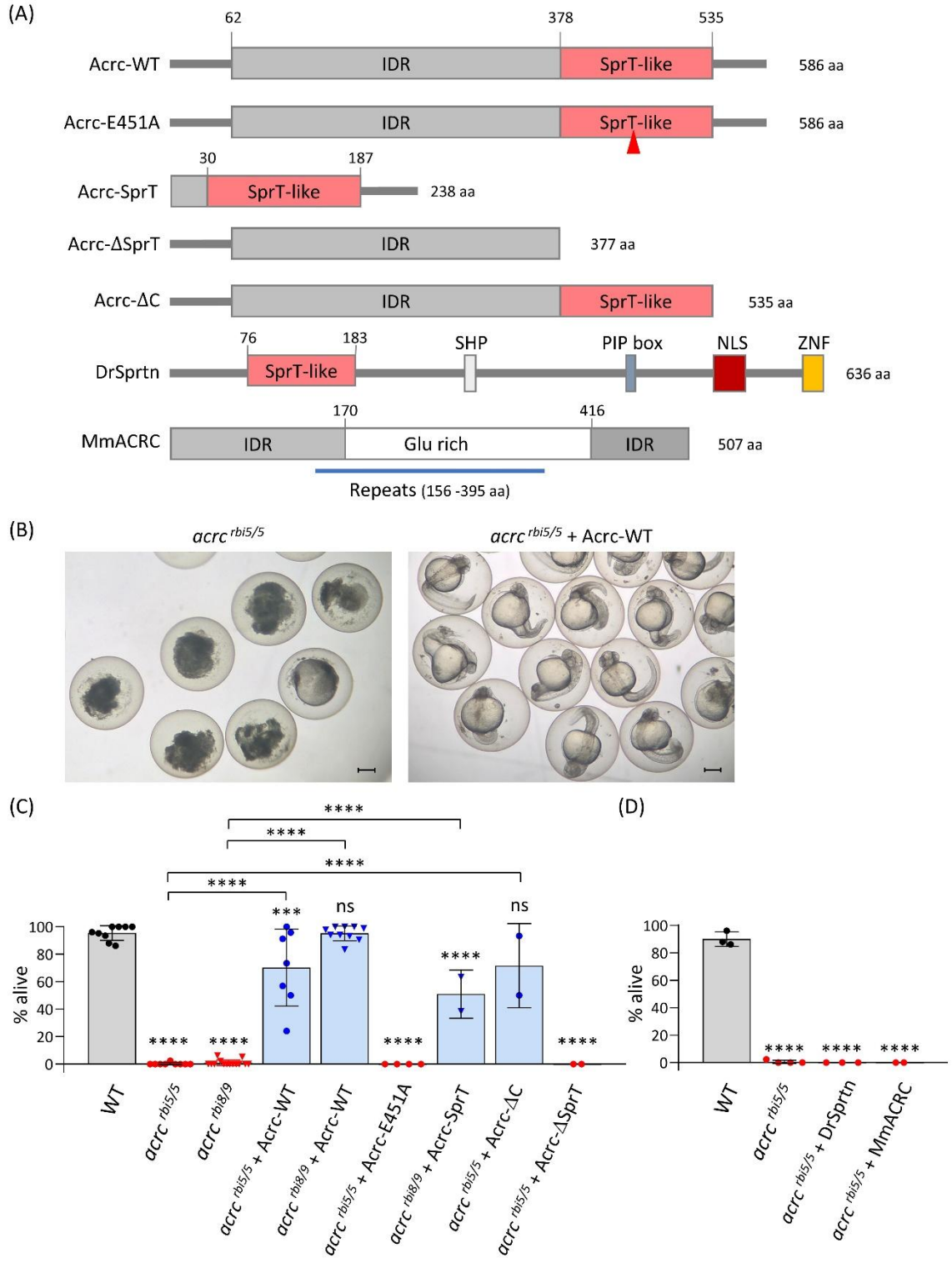

Figure 11. Injection of Acrc-WT mRNA rescues the *acrc* mutant phenotype, while injection of Acrc-E451A, DrSprtn and MmAcrc mRNA does not. (A) Schemes of the injected rescue constructs: Acrc-WT, Acrc-E451A, Acrc-SprT, Acrc-ΔSprT (IDR), Acrc-ΔC, DrSprtn and MmACRC. Mm – *Mus musculus*, Dr – *Danio rerio*. **(B)** Representative pictures of 24 hpf *acrc*$^{rbi5/rbi5}$ mutant embryos and *acrc*$^{rbi5/rbi5}$ mutant embryos injected with Acrc-WT mRNA at the one-cell stage. Scale bars: 250 µm. **(C, D)** Quantification of *acrc* mutant embryo survival at 24 hpf after injection with the rescue constructs shown in (A). Data are presented as

the percentage of live embryos from at least 2 independent experiments with at least 15 embryos each (mean ± SD). Each condition was compared with WT, and conditions with rescued embryos were compared with the respective uninjected *acrc*$^{rbi5/rbi5}$ or *acrc*$^{rbi8/rbi9}$ mutants; one-way ANOVA and Dunnett's test (**** $p < 0.0001$, *** $p < 0.001$, ns: not significant). Figure was prepared by Cecile Otten (Otten et al., 2025).

3.1.3. Acrc mutants accumulate DPCs before the onset of lethality

After establishing that an intact Acrc protease core is required for embryonic development, it was next examined whether the observed embryonic lethality could result from defective DNA-protein crosslink repair. To address this, DPCs were isolated from 6 hpf mutant embryos, that is, before the onset of lethality, at a stage when the mutants were morphologically indistinguishable from WT embryos. For DPC isolation, a modified RADAR protocol previously adapted for zebrafish embryos was used (Anticevic et al., 2023). In *acrc*$^{rbi5/rbi5}$ mutants, total cellular DPC levels were significantly elevated relative to WT embryos (1.45 ± 0.14-fold) (Figure 12). To assess which DPC classes were most affected by Acrc deficiency, DPCs were grouped into three classes based on the apparent size of the crosslinked protein: high molecular weight (HMW, > 151 kDa), medium molecular weight (MMW, 41 – 150 kDa), and low molecular weight (LMW, 5 – 40 kDa) (Anticevic et al., 2023). Although this classification has certain limitations, analyzing DPC size may still provide insight into Acrc function in DPC repair, since the contribution of individual repair factors can depend on the size of the crosslinked protein. Compared with WT embryos, Acrc-deficient embryos showed significantly increased cellular DPC levels in all three classes. The strongest accumulation was observed for HMW-DPCs (2.16 ± 0.34-fold), followed by MMW-DPCs (1.75 ± 0.08-fold), whereas LMW-DPCs showed only a modest increase (1.35 ± 0.07-fold) (Figure 12).

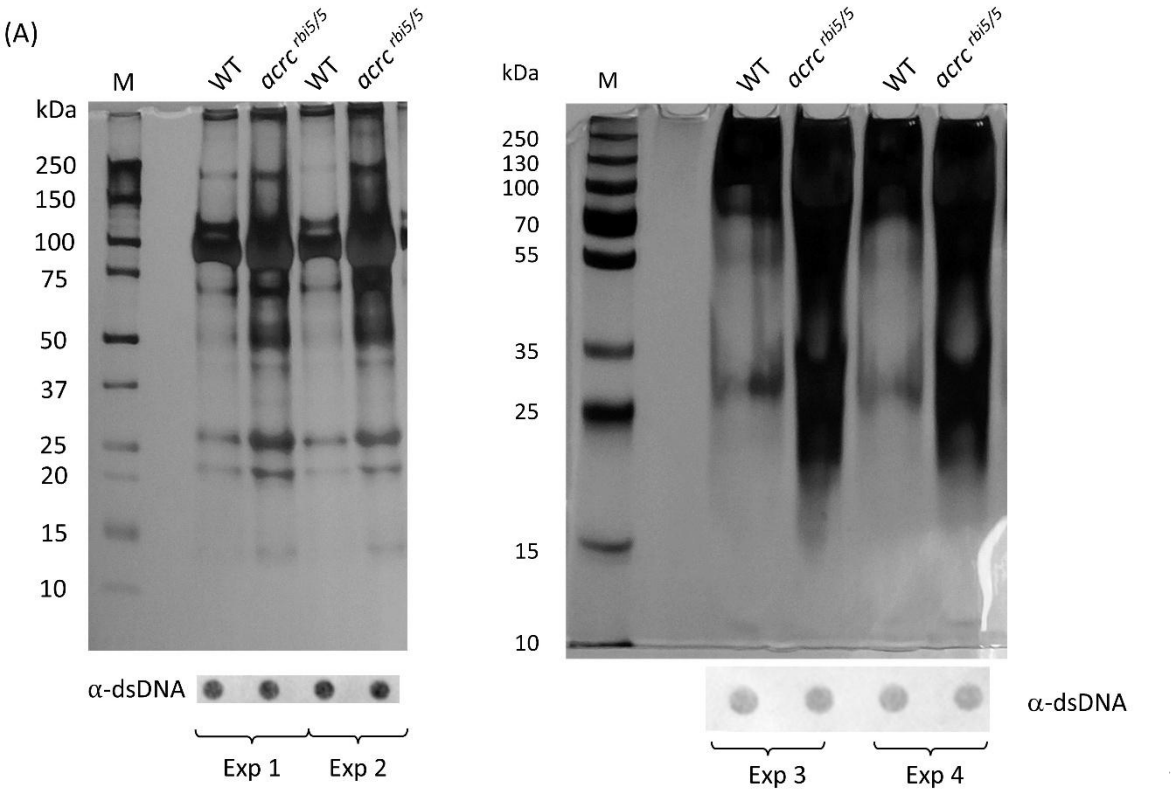

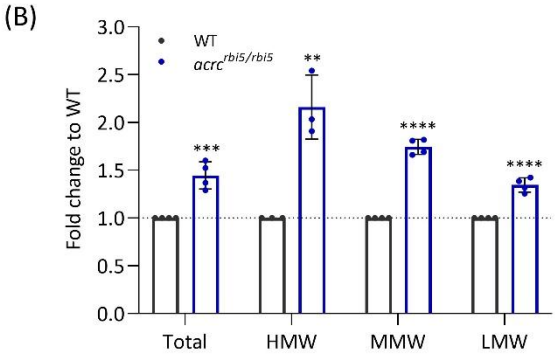

Figure 12. DNA-protein crosslinks accumulate in *acrc* mutant embryos. (A) Total cellular DPCs in WT and *acrc* mutant embryos, resolved on SDS-PAGE gel and stained with silver. DPCs were isolated using modified RADAR method from 50 WT and *acrc*$^{rbi5/rbi5}$ embryos (6 hpf). A DPC equivalent of 25 ng total DNA was loaded per well. Dot blots showing DNA loading controls for DPC analysis are shown below (2 ng of total DNA were loaded per well). M, molecular weight marker. **(B)** Quantification of (A) using ImageJ based on data shown here (biological replicates). Quantification of total, HMW-DPCs (high molecular weight DPCs, Mr > 151 kDa), MMW-DPCs (medium molecular weight DPCs, Mr = 41 – 150 kDa), and LMW-DPCs (low molecular weight DPCs, Mr < 40 kDa) from (A). Data are shown as mean ± SD (n = 3 – 4), and statistically significant differences compared with WT embryos are indicated; Student's t-test (**** $p < 0.0001$, *** $p < 0.001$, ** $p < 0.01$).

3.1.4. The catalytic mutation in Acrc leads to accumulation of Dnmt1-, Top1-, Top2-, histone H3-, Parp1-, Polr3a-, and Mcm2-DPCs

For quantification of specific DPC species, a modified RADAR method was applied, as this approach allows isolation of intact crosslinked proteins and thereby subsequent identification of the protein component. It was first tested whether two previously proposed Acrc substrates, DNA methyltransferase 1 (Dnmt1) and topoisomerase 2 (Top2) (Borgermann et al., 2019; Dokshin et al., 2020), accumulate in crosslinked form in *acrc*$^{rbi5/rbi5}$ mutant embryos at 6 hpf, a stage at which the embryos still exhibited normal WT-like morphology. In addition, because histones represent the most abundant class of cellular DPCs (Kiianitsa & Maizels, 2020), it was examined whether core histones could also be Acrc substrates, using histone H3 as a representative. The possible role of Acrc in the removal of other abundant cellular DPCs previously identified by mass spectrometry in human cells was also assessed (Kiianitsa & Maizels, 2020), including Top1 (DNA topoisomerase 1), Parp1 (poly(ADP-ribose) polymerase 1), Polr3a (DNA-directed RNA polymerase III subunit RPC1), and Mcm2 (minichromosome maintenance complex component 2).

Compared with WT embryos at 6 hpf, *acrc*$^{rbi5/rbi5}$ mutants showed marked accumulation of Top1-DPCs (8.54 ± 1.35-fold), Top2-DPCs (9.65 ± 0.45-fold), and Parp1-DPCs (9.40 ± 0.98-fold) (Figure 13). Histone H3-DPCs were likewise significantly elevated, with a 4.39 ± 0.26-fold increase relative to WT embryos (Figure 13). Significant increases were also observed for Polr3a-DPCs (2.18 ± 0.93-fold), Dnmt1-DPCs (2.00 ± 0.63-fold), and Mcm2-DPCs (1.93 ± 0.54-fold) in *acrc*$^{rbi5/rbi5}$ mutants (Figure 13).

To evaluate the specificity of these findings, which indicate that Acrc contributes to the repair of multiple cellular DPCs, DPCs were also isolated and quantified after injection of Acrc-WT mRNA into *acrc*$^{rbi8/rbi9}$ mutants. Complementation with Acrc-WT significantly lowered Top1-, Top2-, and Dnmt1-DPC levels in *acrc*$^{rbi8/rbi9}$ mutant embryos at 6 hpf, reducing them from 10.40 ± 0.55-fold, 15.26 ± 1.37-fold, and 17.50 ± 0.65-fold, respectively, to 1.36 ± 0.30-fold, 1.11 ± 0.01-fold, and 2.48 ± 0.24-fold. Top1- and Top2-DPC levels were restored to near-WT values, whereas Dnmt1-DPC levels were strongly reduced but remained above those in WT embryos (Figure 14).

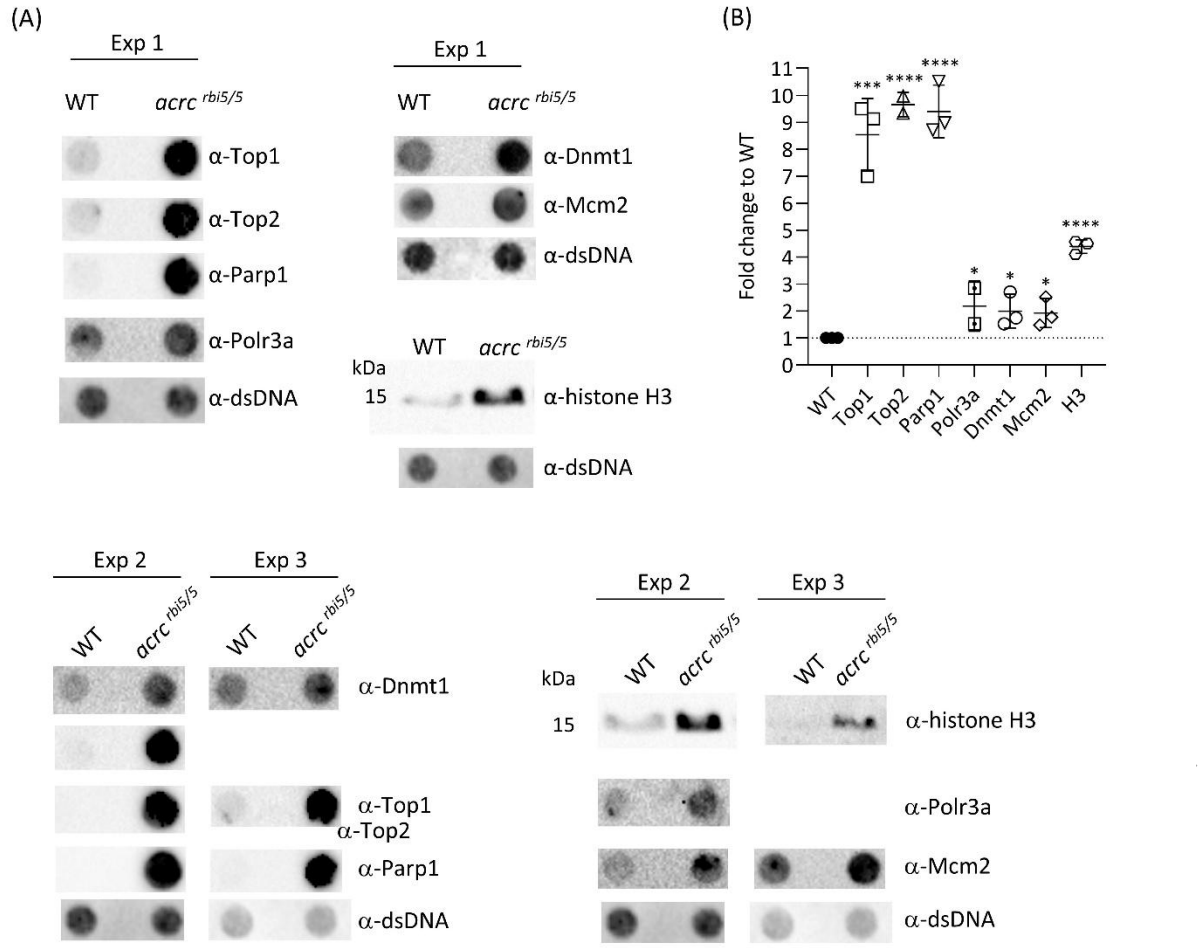

Figure 13. Acrc is involved in the repair of multiple cellular DPCs. (A) Top1-, Top2-, Parp1-, Polr3a-, Dnmt1-, Mcm2-, and histone H3-DPCs accumulate in *acrc*$^{rbi5/rbi5}$ mutant embryos. DPCs were isolated using modified RADAR method from 50 WT and *acrc*$^{rbi5/rbi5}$ embryos (6 hpf) and visualized using dot blotting or western blotting with specific antibodies. A DPC equivalent of 25 ng total DNA was loaded per well. Dot blots showing DNA loading controls for DPC analysis are shown below (2 ng of total DNA were loaded per well). **(B)** Quantification of (A) using ImageJ based on data shown here (biological replicates). Data are shown as mean ± SD (n = 2 – 3), and statistically significant differences compared with WT embryos are indicated; Student's t-test (**** $p < 0.0001$, *** $p < 0.001$, * $p < 0.05$).

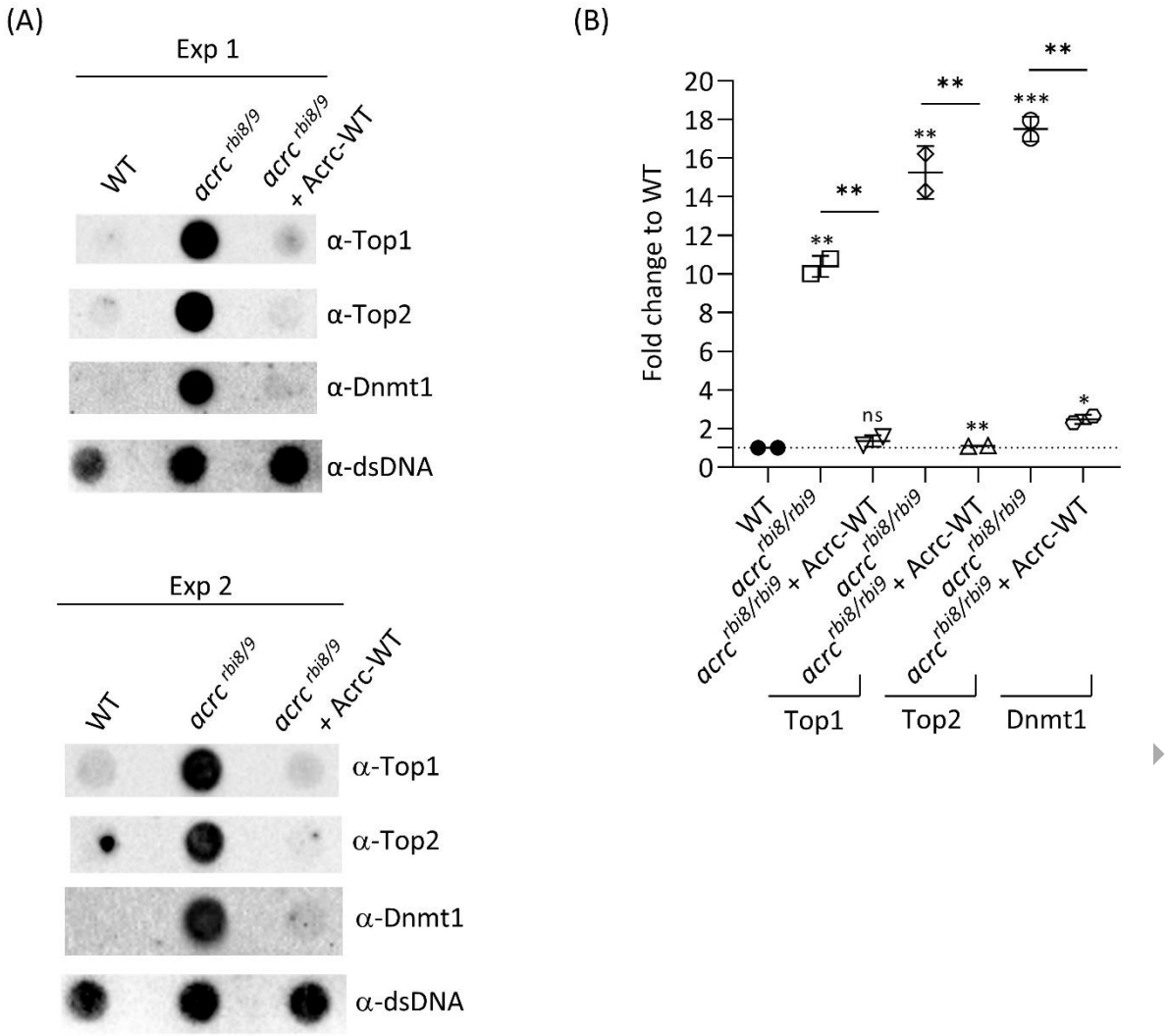

Figure 14. Acrc-WT complementation reduces DPC levels in *acrc* mutants. (A) Top1-, Top2- and Dnmt1-DPC levels in *acrc* mutants are similar to WT embryos after injection of Acrc-WT mRNA in *acrc*$^{rbi8/rbi9}$ mutants. DPCs were isolated using modified RADAR method from 50 embryos (6 hpf) and visualized using dot blotting with specific antibodies. A DPC equivalent of 25 ng total DNA was loaded per well. Dot blots showing DNA loading controls for DPC analysis are shown below (2 ng of total DNA were loaded per well). **(B)** Quantification of (A) using ImageJ, based on data shown here (biological replicates). Data are shown as mean ± SD (n = 2), and statistically significant differences compared with WT embryos are indicated; Student's t-test (*** $p < 0.001$, ** $p < 0.01$, * $p < 0.05$, ns: not significant).

3.2. Role of p97 in DPC repair in human cells and zebrafish

3.2.1. Inhibition of p97 causes accumulation of multiple cellular DPCs in HeLa cells

To examine the contribution of the p97 unfoldase/segregase to DPC repair in human cells, HeLa cells were first treated with the p97 inhibitors NMS-873 and CB-5083 and analyzed by MTT assay to exclude overt cytotoxicity under the conditions intended for DPC analysis. NMS-873 is a selective small-molecule p97 inhibitor that acts allosterically by blocking the conformational changes required for p97 activity (Nandi et al., 2024). CB-5083 is a highly selective first-generation p97 inhibitor that competitively targets the D2 ATPase site of p97 (Nandi et al., 2024). No detectable cytotoxicity was observed after 6 h treatment with either inhibitor at 5 or 10 µM, either without recovery or after 20 h recovery (Figure 15), indicating that these conditions were suitable for subsequent DPC experiments. DMSO was used at a final concentration of 0.02% as the vehicle control because the p97 inhibitors were dissolved in DMSO, and under these conditions DMSO showed no detectable cytotoxicity in the MTT assay (Figure 15). Based on these results and previous literature, treatment with 10 µM NMS-873 or 5 µM CB-5083 for 6 h was selected for subsequent exposure experiments.

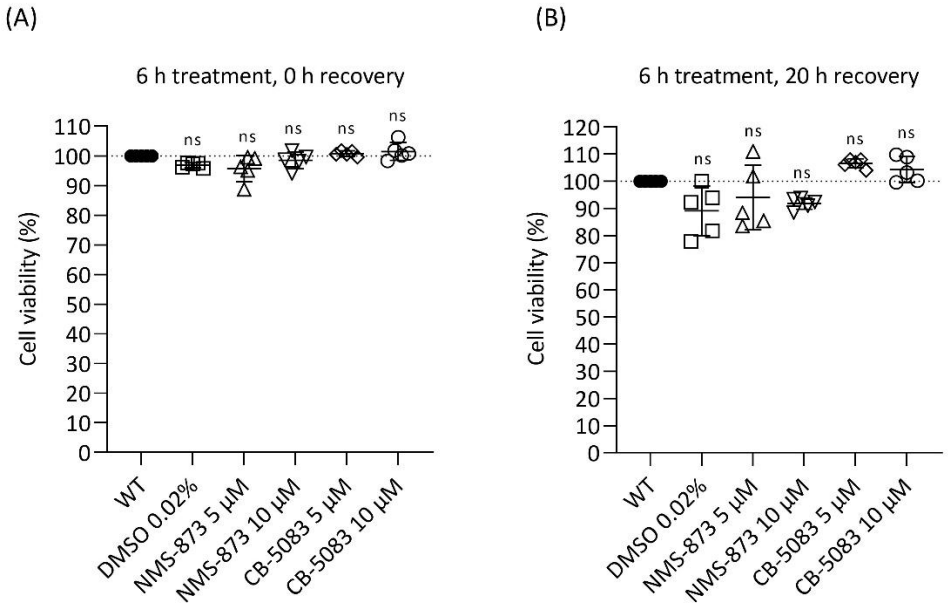

Figure 15. MTT assays show that the p97 inhibitors (p97i) NMS-873 and CB-5083 do not cause detectable cytotoxicity in HeLa cells at the concentrations used for DNA-protein crosslink analyses. (A) MTT assay in HeLa cells after 6 h p97i treatment without recovery. **(B)** MTT assay in HeLa cells after 6 h p97i treatment followed by 20 h recovery. NMS-873 and CB-5083 were used at 5 and 10 µM. DMSO was used at a final concentration of 0.02% as the

vehicle control. Data are shown as mean ± SD (n = 5), and statistically significant differences compared with untreated HeLa WT cells are indicated; one-way ANOVA with Tukey's multiple-comparisons test (ns: not significant). MTT, 3-(4,5-dimethylthiazol-2-yl)-2,5-diphenyltetrazolium bromide; DMSO, dimethyl sulfoxide.

Total cellular DPCs were isolated from HeLa cells after 6 h inhibitor treatment using the modified RADAR method and quantified after separation into total DPCs and into three size-based DPC classes according to the apparent molecular weight of the crosslinked protein: high molecular weight (HMW, > 151 kDa), medium molecular weight (MMW, 41 – 150 kDa), and low molecular weight (LMW, 5 – 40 kDa). These classes were quantified separately because the contribution of DPC repair factor may depend on the size of the crosslinked protein. Inhibition of p97 with either NMS-873 or CB-5083 caused a strong and statistically significant accumulation of total cellular DPCs compared with untreated HeLa cells, reaching 1.57 ± 0.24-fold and 1.42 ± 0.11-fold, respectively (Figure 16). Analysis of size-defined DPC classes showed that both inhibitors significantly increased HMW-DPCs and MMW-DPCs, with NMS-873 producing a somewhat stronger effect than CB-5083 in these fractions (HMW-DPCs: 1.77 ± 0.15-fold vs. 1.48 ± 0.08-fold; MMW-DPCs: 1.71 ± 0.18-fold vs. 1.58 ± 0.23-fold) (Figure 16). LMW-DPCs were also significantly elevated after both treatments, but in this class the effect was more pronounced after CB-5083 treatment than after NMS-873 treatment (2.29 ± 0.51-fold vs. 1.47 ± 0.17-fold) (Figure 16). Together, these data indicate that pharmacological inhibition of p97 leads to accumulation of DPCs across multiple size classes in HeLa cells.

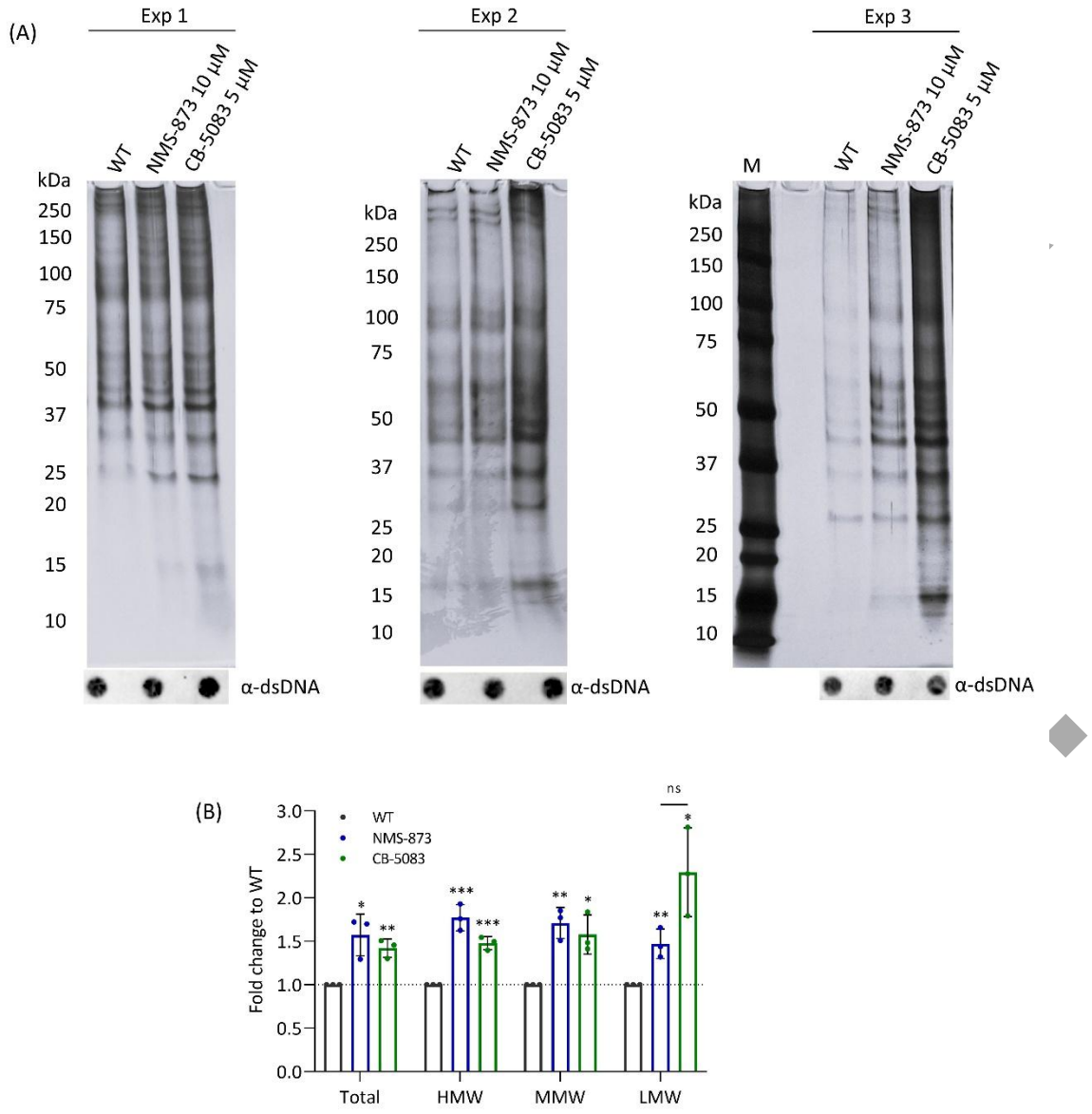

Figure 16. Total cellular DNA-protein crosslink levels in HeLa cells treated with p97 inhibitors (p97i) NMS-873 (10 µM) or CB-5083 (5 µM) for 6 h. (A) Total cellular DPCs in HeLa cells after 6 h p97i treatment, resolved on SDS-PAGE gel and stained with silver. DPCs were isolated using modified RADAR method from HeLa cells. A DPC equivalent of 200 ng total DNA was loaded per well. Dot blots showing DNA loading controls for DPC analysis are shown below (2 ng of total DNA were loaded per well). M, molecular weight marker. **(B)** Quantification of (A) using ImageJ based on data shown here (biological replicates). Quantification of total, HMW-DPCs (high molecular weight DPCs, Mr > 151 kDa), MMW-DPCs (medium molecular weight DPCs, Mr = 41 – 150 kDa), and LMW-DPCs (low molecular weight DPCs, Mr < 40 kDa) from (A). Data are shown as mean ± SD (n = 3), and statistically significant differences compared with untreated HeLa WT cells are indicated; Student's t-test (*** $p < 0.001$, ** $p < 0.01$, * $p < 0.05$, ns: not significant).

After quantification of total cellular DPCs, the same RADAR isolates were used for a more detailed analysis of selected DPC species. We focused on histone H3 because histones

represent the most abundant class of cellular DPCs (Kiianitsa & Maizels, 2020); on Ku80 as a representative structural, non-enzymatic DNA-binding protein; on PARP1 as an abundant chromatin-associated DNA repair factor; on TOP1 and TOP2 as enzymatic DPCs formed through covalent topoisomerase-DNA intermediates; and on DNMT1 as a chromatin-associated enzyme that can also form DPCs. This set of targets was selected to examine whether p97 inhibition affects multiple mechanistically distinct classes of endogenous DPCs. All analyzed DPC species were significantly increased after treatment with either NMS-873 or CB-5083 compared with untreated HeLa cells (Figure 17). The strongest increases were observed for TOP2-DPCs, which reached 6.53 ± 1.60-fold after NMS-873 treatment and 6.46 ± 1.18-fold after CB-5083 treatment, and for TOP1-DPCs, which increased 2.43 ± 0.98-fold after NMS-873 and 6.29 ± 2.29-fold after CB-5083 treatment (Figure 17). DNMT1-DPCs were also strongly elevated with both inhibitors, reaching 5.08 ± 2.71-fold and 4.97 ± 2.67-fold after NMS-873 and CB-5083 treatment, respectively (Figure 17). Histone H3-DPCs showed a marked increase as well, to 4.27 ± 1.34-fold after NMS-873 and 3.58 ± 0.77-fold after CB-5083 treatment (Figure 17). Ku80-DPCs and PARP1-DPCs were likewise significantly increased, with Ku80-DPCs reaching 2.62 ± 1.00-fold after NMS-873 and 3.68 ± 0.95-fold after CB-5083, and PARP1-DPCs reaching 2.22 ± 0.34-fold and 3.52 ± 0.37-fold, respectively (Figure 17). Together, these findings indicate that p97 inhibition leads to accumulation of multiple endogenous DPC species in HeLa cells, including both structural and enzymatic DPCs, consistent with a broad role of p97 in DPC repair.

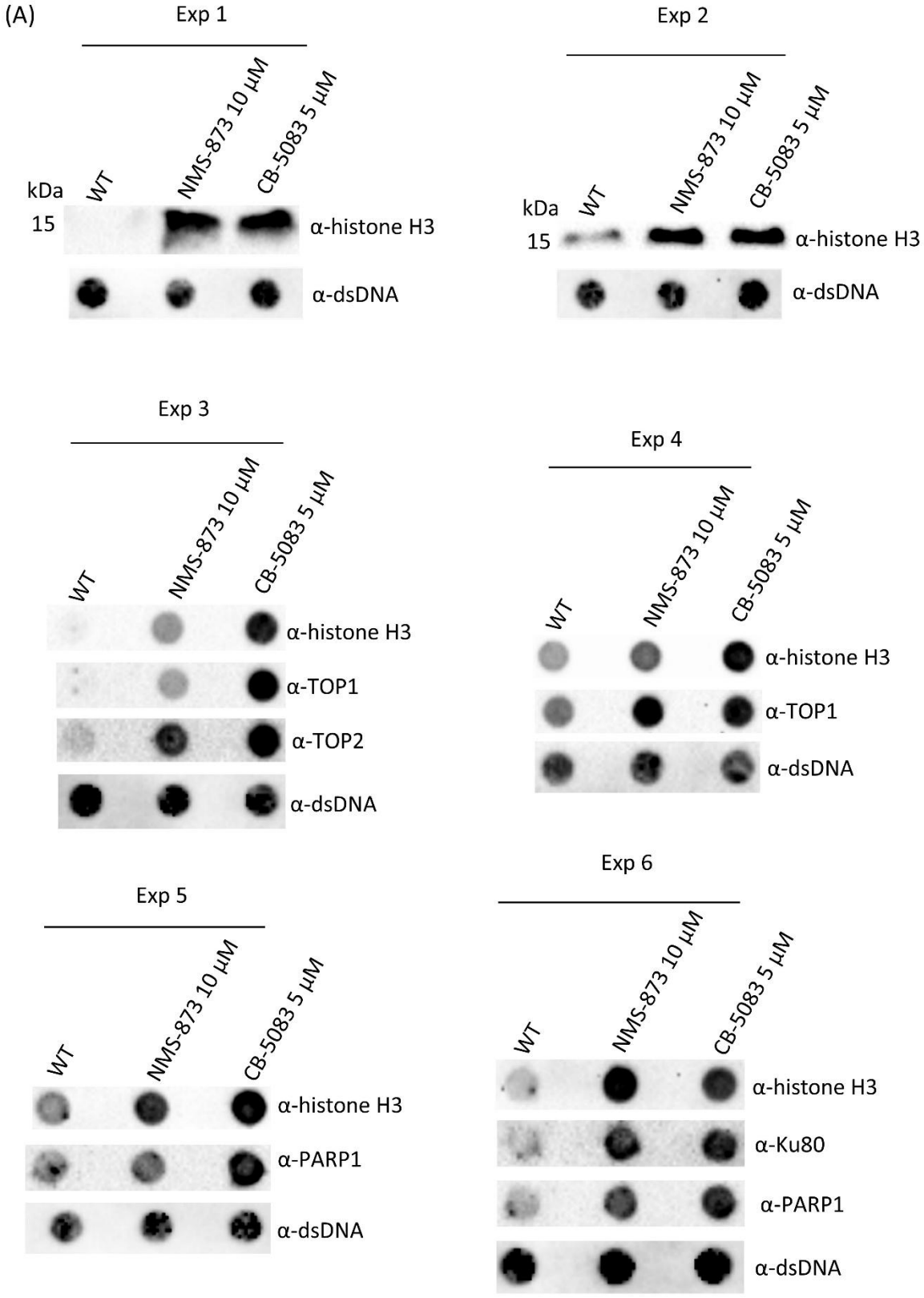
(A)
Exp 1
kDa
WT
NMS-873 10 μM
CB-5083 5 μM
15
α-histone H3
α-dsDNA
Exp 2
kDa
WT
NMS-873 10 μM
CB-5083 5 μM
15
α-histone H3
α-dsDNA
Exp 3
WT
NMS-873 10 μM
CB-5083 5 μM
α-histone H3
α-TOP1
α-TOP2
α-dsDNA
Exp 4
WT
NMS-873 10 μM
CB-5083 5 μM
α-histone H3
α-TOP1
α-dsDNA
Exp 5
WT
NMS-873 10 μM
CB-5083 5 μM
α-histone H3
α-PARP1
α-dsDNA
Exp 6
WT
NMS-873 10 μM
CB-5083 5 μM
α-histone H3
α-Ku80
α-PARP1
α-dsDNA

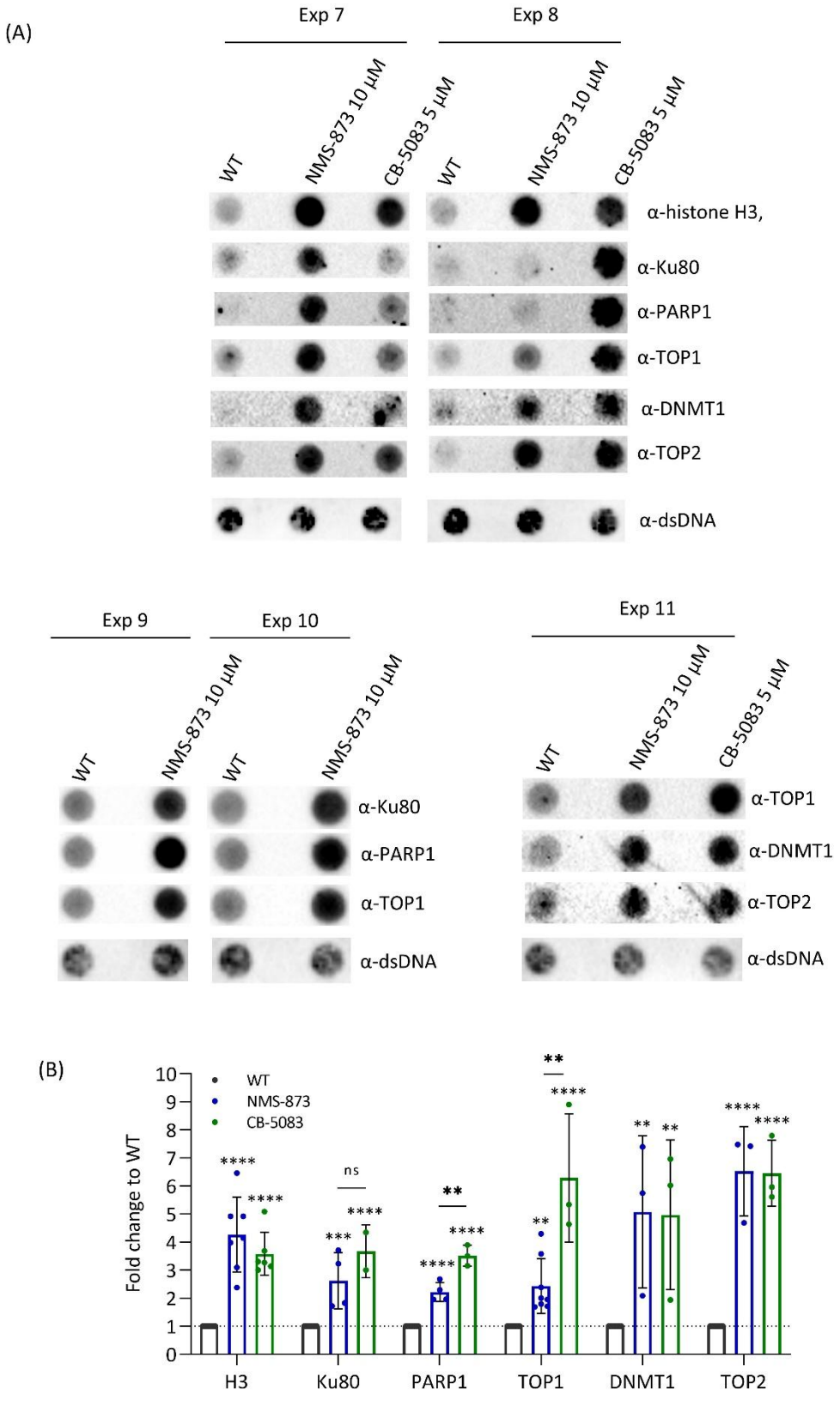

Figure 17. Specific cellular DNA-protein crosslinks in HeLa cells treated with p97 inhibitors (p97i) NMS-873 (10 µM) or CB-5083 (5 µM) for 6 h. (A) Histone H3-, Ku80-, PARP1-, TOP1-, DNMT1-, and TOP2-DPC levels in HeLa cells after 6 h p97i treatment. DPCs were isolated using modified RADAR method from HeLa cells and visualized using western

blotting or dot blotting with specific antibodies. A DPC equivalent of 200 ng (histone H3) or 500 ng (Ku80, PARP1, TOP1, DNMT1, TOP2) total DNA was loaded per well. Dot blots showing DNA loading controls for DPC analysis are shown below (2 ng of total DNA were loaded per well). **(B)** Quantification of (A) using ImageJ based on data shown here (biological replicates). Data are shown as mean ± SD (n = 2 – 8), and statistically significant differences compared with untreated HeLa WT cells are indicated; Student's t-test (**** $p < 0.0001$, *** $p < 0.001$, ** $p < 0.01$, ns: not significant).

3.2.2. Inhibition of p97 causes dose-dependent morphological defects and DPC accumulation in zebrafish embryos

To examine whether acute pharmacological inhibition of p97 also affects DPC levels *in vivo*, titration experiments were performed in wild-type zebrafish embryos. Embryos were treated at 24 hpf for 6 h with increasing concentrations of NMS-873 or CB-5083, and both morphology and specific DPC species were assessed. The DPC analysis was designed to test *in vivo* whether p97 inhibition in embryos, similarly to HeLa cells, is associated with accumulation of multiple endogenous DPCs. A clear dose-dependent phenotypic response was observed with both inhibitors. NMS-873 treatment (5, 10, and 20 μM) produced the more severe morphological phenotype, characterized by reduced or absent pigmentation, abnormal body curvature, impaired heart development, a shortened and thickened yolk extension, and overall developmental delay (Figure 18). By contrast, CB-5083 treatment (5, 10, 20, 40, and 60 μM) caused a milder phenotype, characterized mainly by dose-dependent dorsal curvature of the tail tip (Figure 19).

RADAR isolation followed by dot blotting with specific antibodies showed that these morphological changes were accompanied by dose-dependent accumulation of selected DPC species. After NMS-873 treatment, histone H3-DPC levels increased with dose, from 1.84-fold at 5 μM to 2.44-fold at 10 μM and 3.66-fold at 20 μM, whereas Top2-DPC levels increased from 0.60-fold to 1.04-fold and 1.98-fold, respectively (Figure 18). CB-5083 treatment likewise caused dose-dependent accumulation of Parp1- and Top2-DPCs, with Parp1-DPC levels increasing from 1.09-fold at 5 μM to 1.23-fold at 10 μM and 2.00-fold at 20 μM, and Top2-DPC levels increasing from 1.52-fold to 1.87-fold and 4.07-fold, respectively (Figure 19).

Thus, although NMS-873 and CB-5083 induced distinct morphological phenotypes, both produced similar overall biochemical outcome, namely accumulation of DPCs in zebrafish embryos. Because the effects of these two p97 inhibitors had not previously been characterized in zebrafish embryos, these titration experiments also provided an essential basis for selecting

the conditions used in subsequent DPC analyses. Importantly, embryos treated with 20 μM NMS-873 or 20 μM CB-5083 were still alive at the time of collection after 6 h exposure, whereas 24 h treatment with either inhibitor resulted in embryo death. Based on these results, 20 μM NMS-873 and 20 μM CB-5083 were selected for further DPC experiments in zebrafish embryos.

(A)

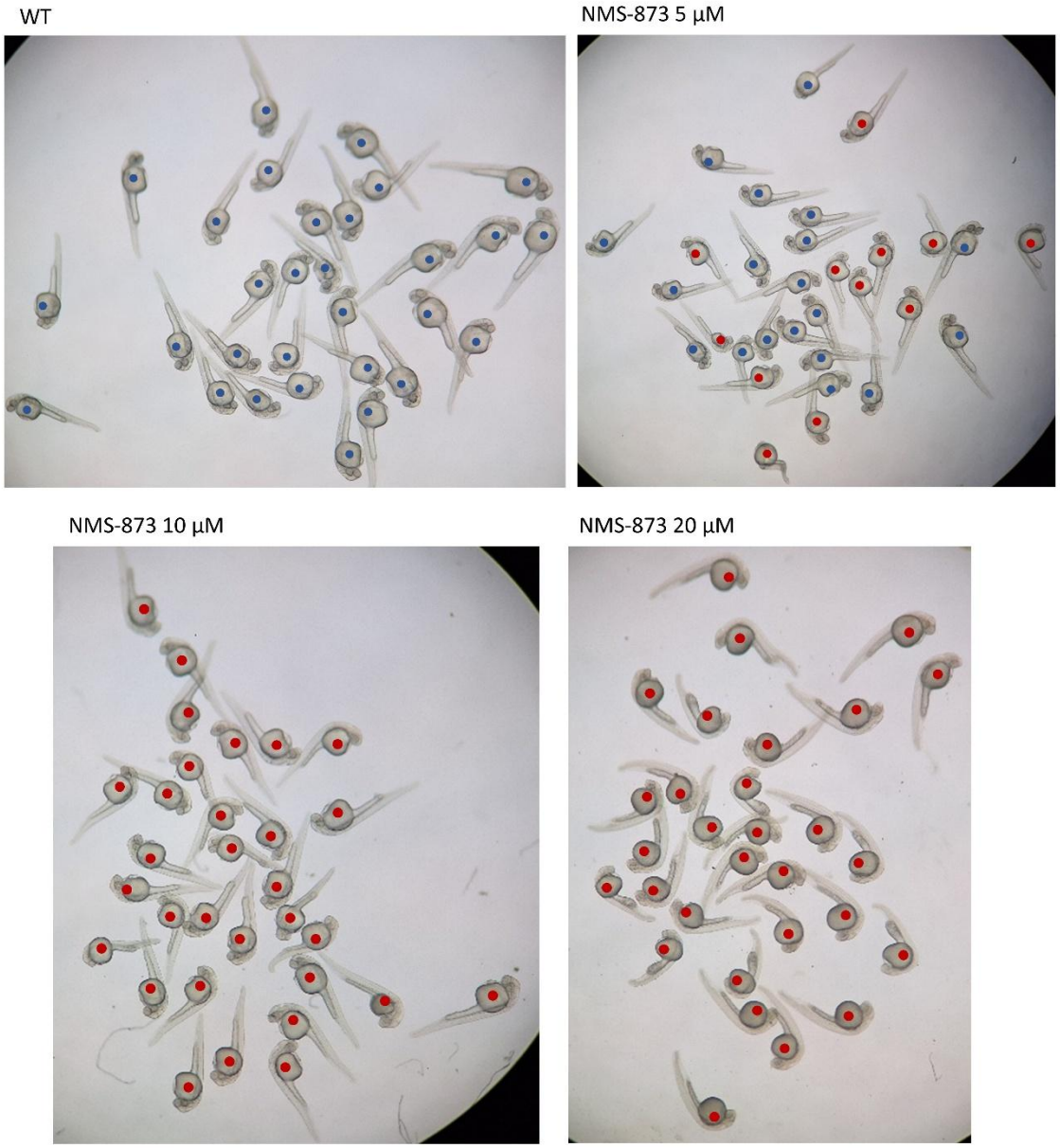
WT
NMS-873 5 µM
NMS-873 10 µM
NMS-873 20 µM

(B)

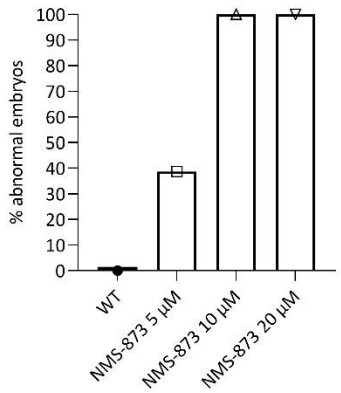
% abnormal embryos
100
90
80
70
60
50
40
30
20
10
0
WT
NMS-873 5 µM
NMS-873 10 µM
NMS-873 20 µM

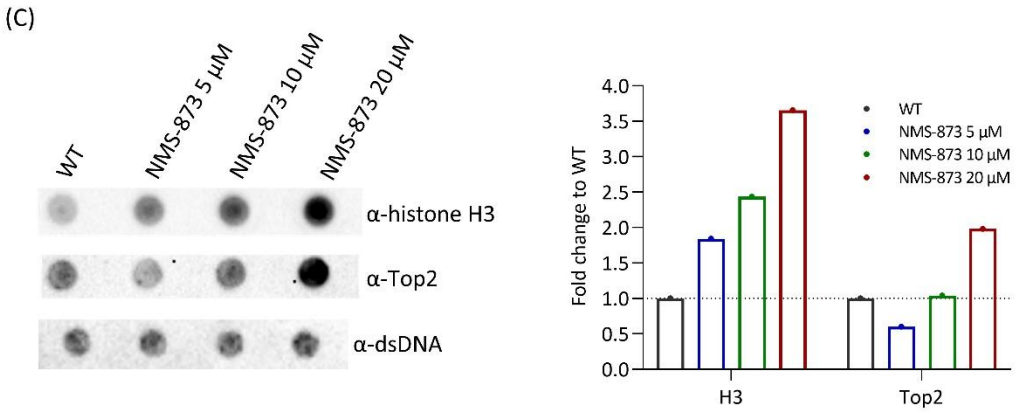

Figure 18. Treatment of zebrafish embryos with the p97 inhibitor (p97i) NMS-873 for 6 h. **(A)** Representative images of wild-type zebrafish embryos at 30 hpf following 6 h treatment with NMS-873 at 5, 10, and 20 µM. Embryos with a WT-like phenotype are indicated by blue dots, whereas embryos with an abnormal phenotype are indicated by red dots. **(B)** Quantification of the data shown in (A), presented as the percentage of embryos with an abnormal phenotype after 6 h treatment with NMS-873. **(C)** Histone H3- and Top2-DPC levels in embryos shown in (A) after 6 h treatment with NMS-873. DPCs were isolated using modified RADAR method from 25 embryos (30 hpf) and visualized using dot blotting with specific antibodies. A DPC equivalent of 200 ng (histone H3) or 500 ng (Top2) total DNA was loaded per well. Dot blots showing DNA loading controls for DPC analysis are shown below (2 ng of total DNA were loaded per well). The right panel shows ImageJ-based quantification of histone H3- and Top2-DPC levels detected in the dot blots shown in the left panel.

(A)

WT

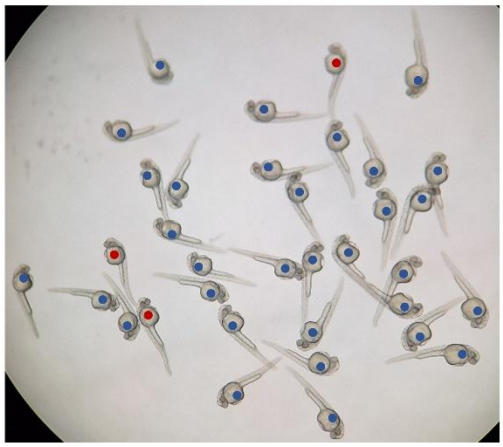

CB-5083 5 µM

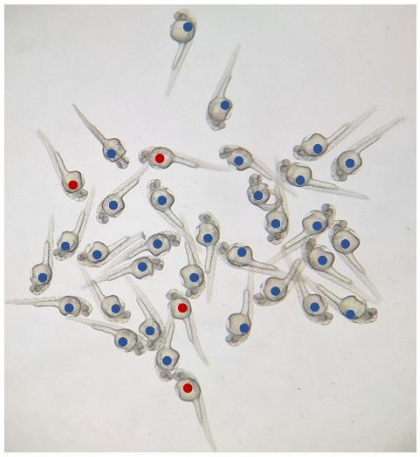

CB-5083 10 µM

CB-5083 20 µM

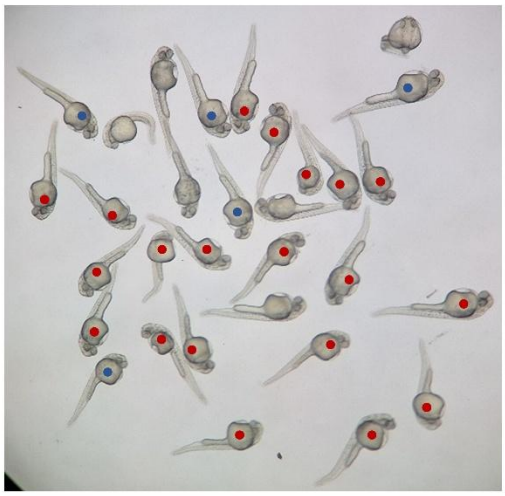

CB-5083 40 µM

CB-5083 60 µM

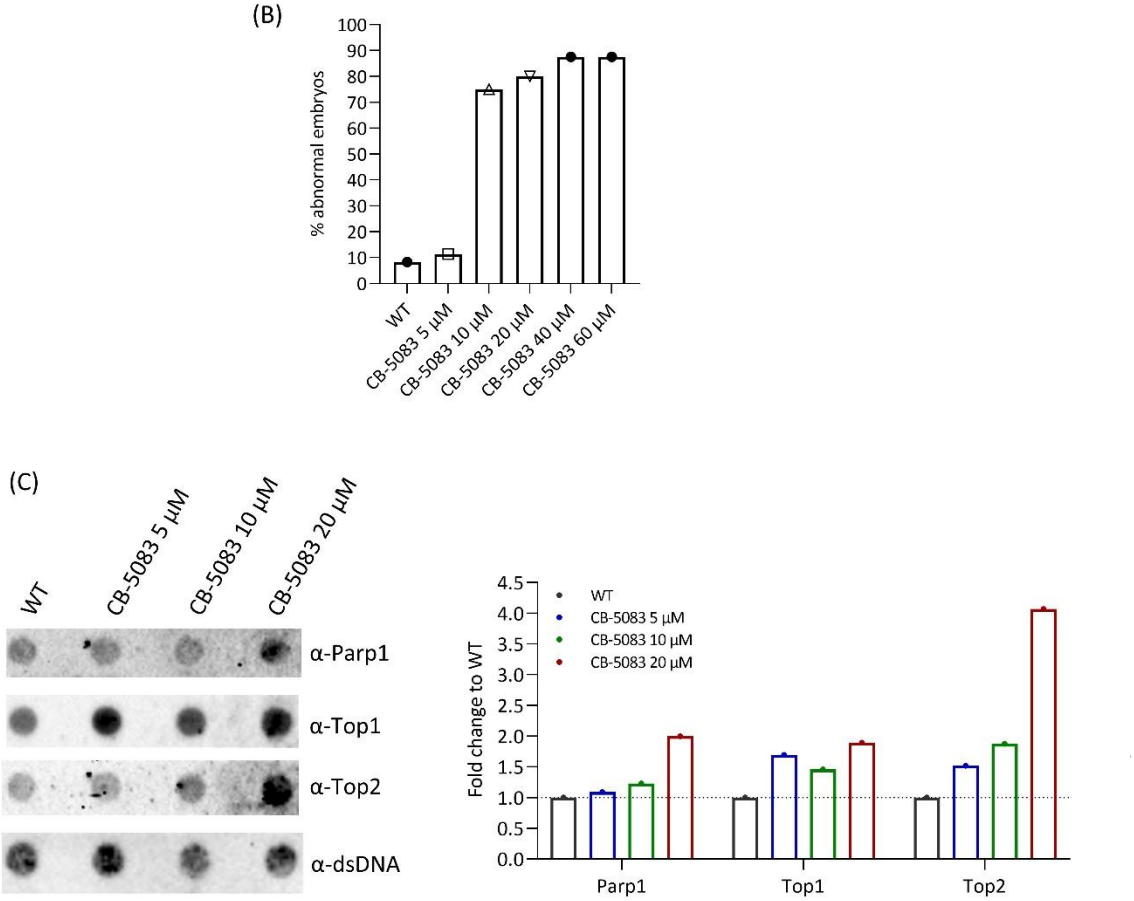

Figure 19. Treatment of zebrafish embryos with the p97 inhibitor (p97i) CB-5083 for 6 h. **(A)** Representative images of wild-type zebrafish embryos at 30 hpf after 6 h treatment with different concentrations of CB-5083 (5, 10, 20, 40, and 60 µM). Embryos with a WT-like phenotype are indicated by blue dots, whereas embryos with an abnormal phenotype are indicated by red dots. **(B)** Quantification of (A), shown as the percentage of embryos with an abnormal phenotype after 6 h treatment with CB-5083. **(C)** Parp1-, Top1-, and Top2-DPC levels in embryos shown in (A) after 6 h treatment with CB-5083. DPCs were isolated using modified RADAR method from 25 embryos (30 hpf) and visualized using dot blotting with specific antibodies. A DPC equivalent of 500 ng total DNA was loaded per well. Dot blots showing DNA loading controls for DPC analysis are shown below (2 ng of total DNA were loaded per well). The right panel shows ImageJ-based quantification of Parp1-, Top1-, and Top2-DPC levels detected in the dot blots shown in the left panel.

3.2.3. Inhibition of p97 causes accumulation of multiple cellular DPCs in zebrafish embryos

To further examine the contribution of p97 to DPC repair *in vivo*, wild-type zebrafish embryos were treated at 24 hpf with NMS-873 (20 µM) or CB-5083 (20 µM) for 6 h and analyzed at 30 hpf. Specific DPC species were then quantified after RADAR isolation by dot

blotting with specific antibodies. Inhibition of p97 with either NMS-873 or CB-5083 caused statistically significant accumulation of all analyzed DPC species compared with untreated WT embryos (Figure 20). After NMS-873 treatment, the strongest increase was observed for Ku80-DPCs (6.62 ± 0.86-fold), followed by Parp1-DPCs (4.98 ± 1.10-fold), Dnmt1-DPCs (4.70 ± 0.41-fold), Top2-DPCs (4.21 ± 1.93-fold), Top1-DPCs (3.92 ± 0.27-fold), and histone H3-DPCs (2.60 ± 0.97-fold) (Figure 20). After CB-5083 treatment, histone H3-DPCs showed the greatest increase (3.10 ± 1.25-fold), followed by Top2-DPCs (2.76 ± 1.25-fold), Parp1-DPCs (2.67 ± 0.97-fold), Dnmt1-DPCs (2.05 ± 0.08-fold), Top1-DPCs (1.85 ± 0.39-fold), and Ku80-DPCs (1.66 ± 0.31-fold) (Figure 20). Together, these data show that acute pharmacological inhibition of p97 in zebrafish embryos leads to accumulation of multiple endogenous DPC species *in vivo*, consistent with the effects observed in HeLa cells and supporting a prominent role of p97 in DPC repair.

(A)

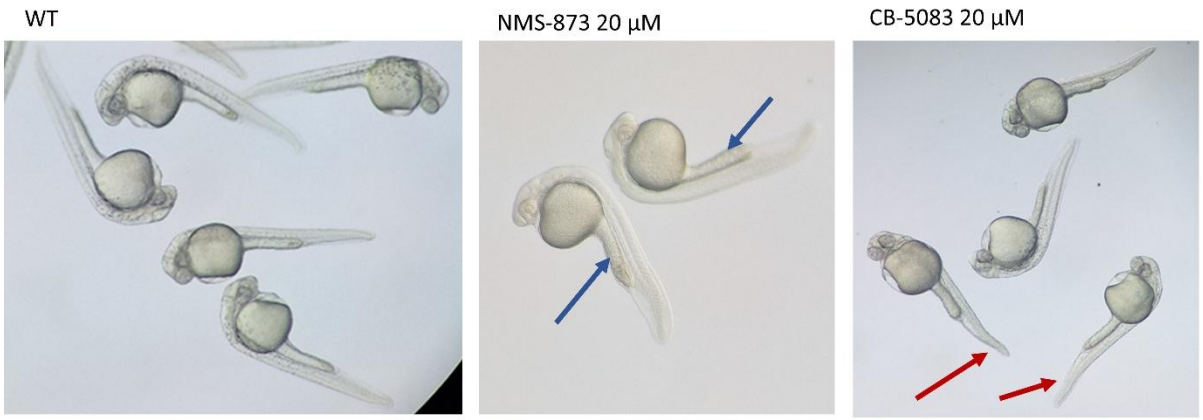
WT
NMS-873 20 μM
CB-5083 20 μM

(B)

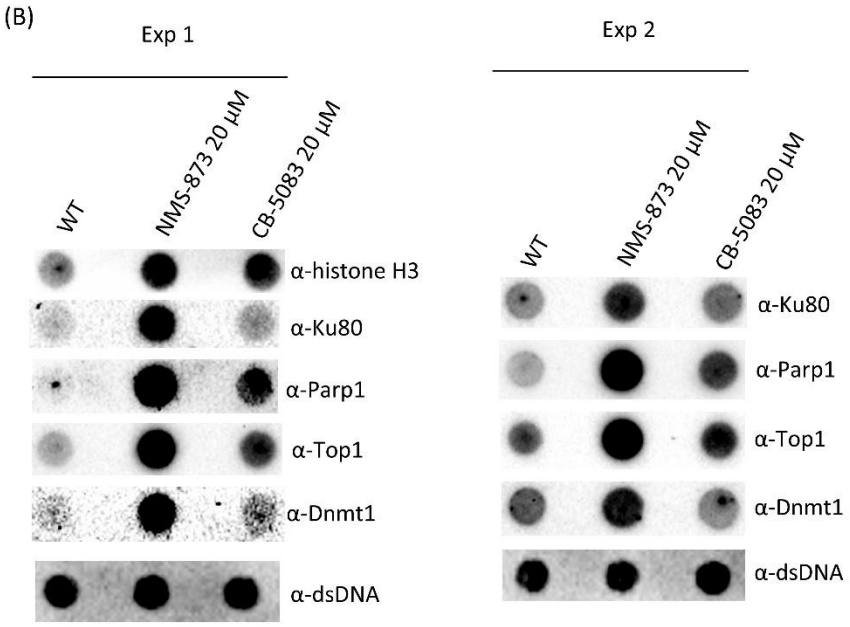
Exp 1
Exp 2
WT
NMS-873 20 μM
CB-5083 20 μM
α-histone H3
α-Ku80
α-Parp1
α-Top1
α-Dnmt1
α-dsDNA

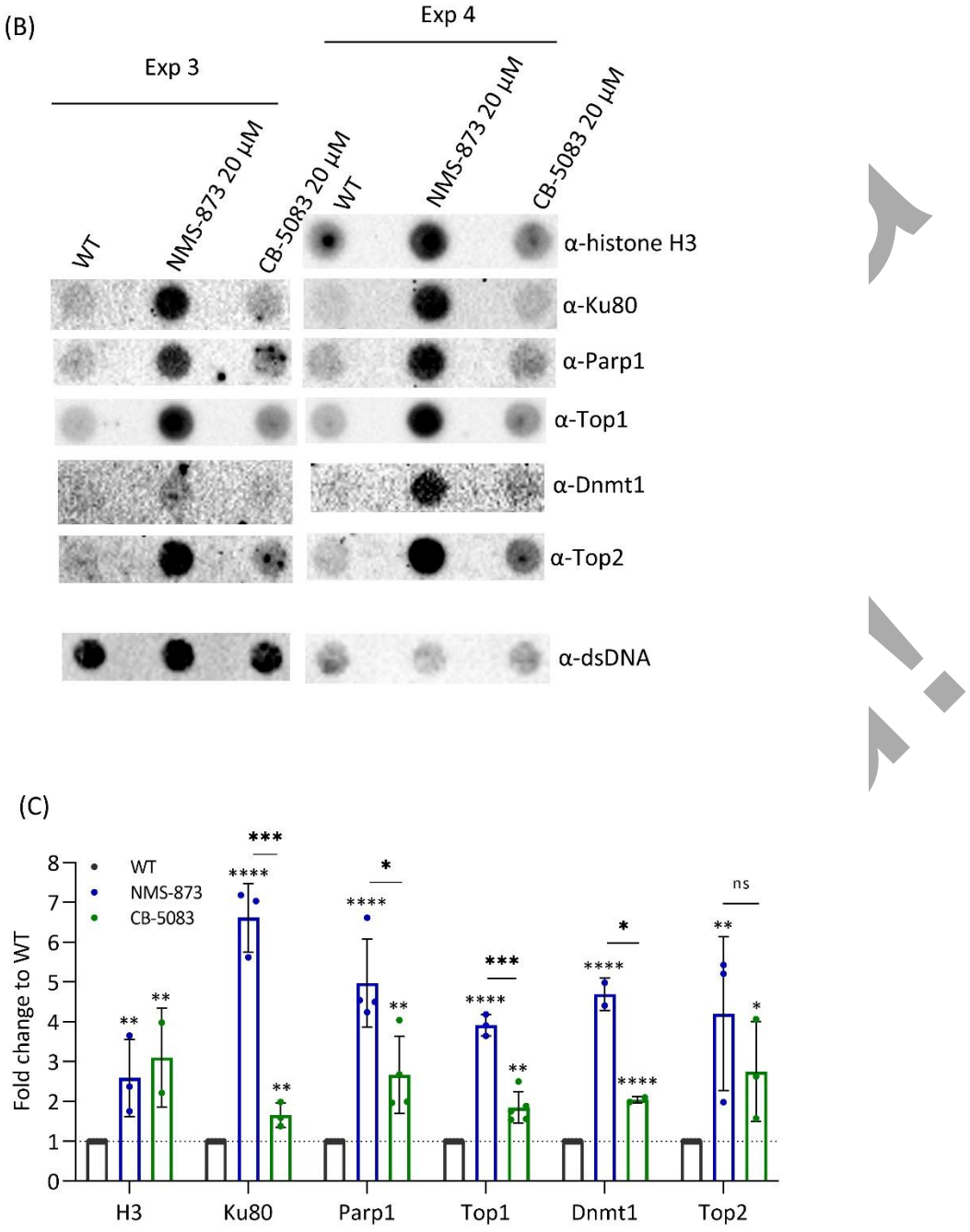

Figure 20. DNA-protein crosslink levels in zebrafish embryos treated with the p97 inhibitors (p97i) NMS-873 (20 µM) or CB-5083 (20 µM) for 6 h. (A) Representative images of wild-type zebrafish embryos at 30 hpf after 6 h treatment with 20 µM NMS-873 or 20 µM CB-5083. The blue arrow indicates a shortened and thickened yolk extension, whereas the red arrow indicates dorsal curvature of the tail tip. **(B)** Histone H3-, Ku80-, Parp1-, Top1-, DNMT1-, and Top2-DPC levels in embryos after 6 h treatment with p97i. DPCs were isolated using modified RADAR method from 25 embryos (30 hpf) and visualized using dot blotting with specific antibodies. A DPC equivalent of 200 ng (histone H3) or 500 ng (Ku80, Parp1, Top1, Dnmt1, Top2) total DNA was loaded per well. Dot blots showing DNA loading controls for DPC analysis are shown below (2 ng of total DNA were loaded per well). **(C)** Quantification of (B) using ImageJ based on data shown here (biological replicates). Data are shown as mean ± SD (n = 2 – 5), and statistically significant differences compared with untreated wild-type

embryos are indicated; Student's t-test (**** $p < 0.0001$, *** $p < 0.001$, ** $p < 0.01$, * $p < 0.05$, ns: not significant).

3.2.4. Silencing of p97 causes accumulation of multiple cellular DPCs in zebrafish embryos

To complement the pharmacological inhibition experiments and further examine the contribution of p97 to DPC repair *in vivo*, a morpholino-based zebrafish embryo system was used. Wild-type embryos were injected with a p97 morpholino at the 1-cell stage and analyzed at 30 hpf. At the time of collection, p97 morpholino-injected embryos showed no overt morphological abnormalities and were visually similar to WT embryos (Figure 21), in contrast to the clear developmental defects observed after 6 h treatment with NMS-873 or CB-5083 (Figure 21). Silencing of p97 was confirmed at the RNA level by RT-PCR. Consistent with the use of a splice-blocking morpholino, p97 morpholino-injected embryos showed loss of the WT p97 RT-PCR product together with the appearance of a larger product corresponding to an aberrantly spliced p97 transcript (Figure 21).

Specific DPC species were then quantified after RADAR isolation by dot blotting with specific antibodies. Reduction of p97 levels was associated with increased levels of several endogenous DPC species compared with WT embryos. The strongest increase was observed for Top1-DPCs (1.90-fold), followed by Ku80-DPCs (1.48 ± 0.05-fold), Top2-DPCs (1.42 ± 0.09-fold), and Parp1-DPCs (1.30 ± 0.14-fold) (Figure 21). The increases in Ku80- and Top2-DPC levels were statistically significant, whereas Parp1- and Top1-DPCs showed a similar upward trend (Figure 21). Thus, consistent with the results obtained with NMS-873 and CB-5083 treatment, morpholino-mediated p97 knockdown was also associated with accumulation of multiple cellular DPCs in zebrafish embryos, providing additional evidence that p97 contributes to DPC repair *in vivo*.

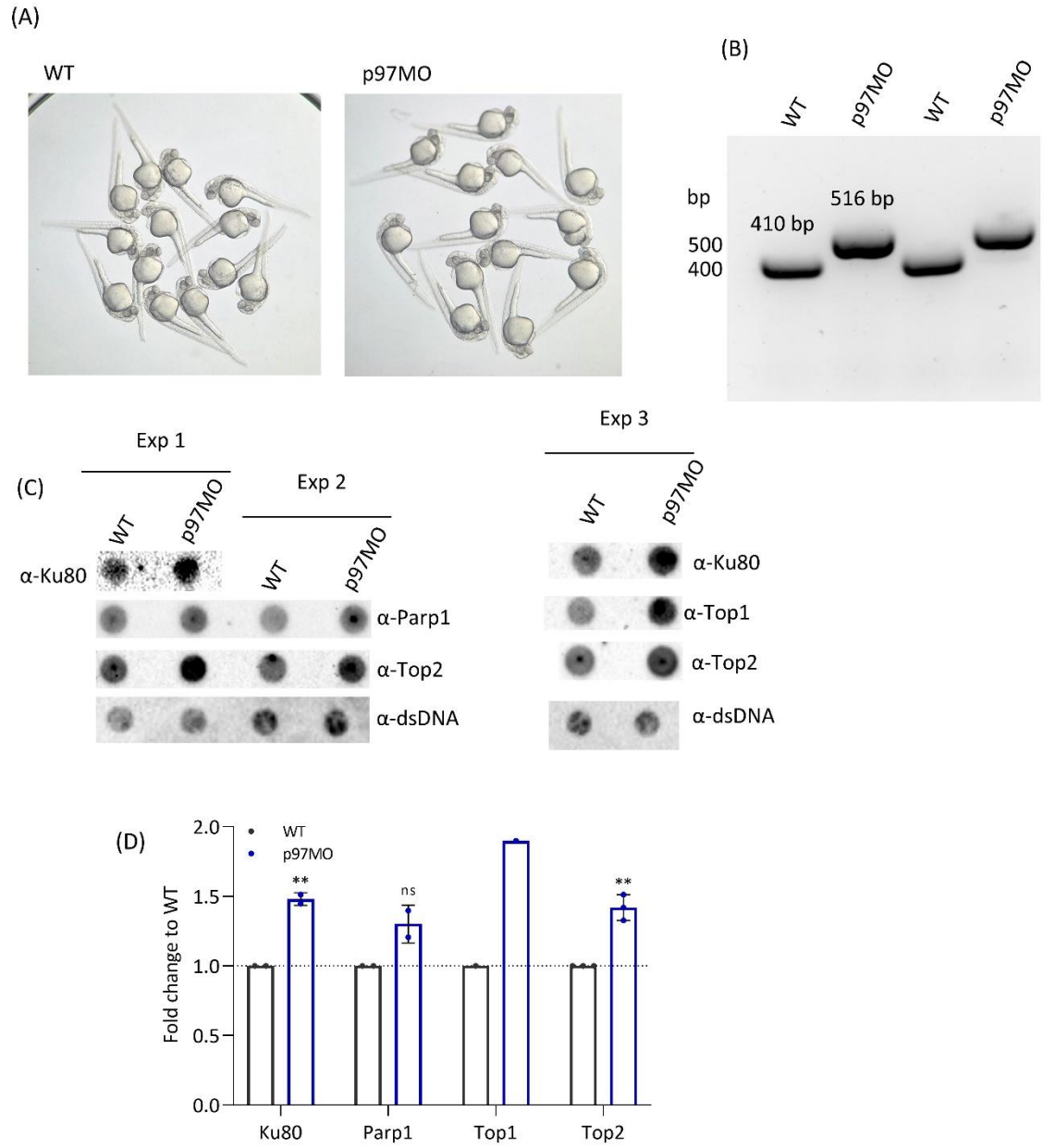

Figure 21. DNA-protein crosslink levels in zebrafish embryos after p97 silencing using a p97 morpholino. (A) Representative images of WT and p97MO embryos showing that morpholino-mediated p97 silencing did not produce an overt morphological phenotype and that p97MO embryos were morphologically similar to WT embryos. **(B)** p97 silencing was confirmed at the RNA level by RT-PCR. Because a splice-blocking morpholino was used, retention of intron 5 generated a larger PCR product. **(C)** Ku80-, Parp1-, Top1-, and Top2-DPC levels in embryos at 30 hpf after p97 silencing with a p97 morpholino. DPCs were isolated using modified RADAR method from 25 embryos (30 hpf) and visualized using dot blotting with specific antibodies. A DPC equivalent of 500 ng total DNA was loaded per well. Dot blots showing DNA loading controls for DPC analysis are shown below (2 ng of total DNA were loaded per well). **(D)** Quantification of (C) using ImageJ based on data shown here (biological replicates). Data are shown as mean ± SD (n = 1 – 3), and statistically significant differences compared with wild-type embryos are indicated; Student's t-test (** $p < 0.01$, ns: not significant). MO – morpholino.

3.3. Role of SPRTN-p97 interaction in DPC repair in human cells and zebrafish

3.3.1. Silencing of endogenous SPRTN increases cellular DPC levels in HEK293T cells

To examine the contribution of SPRTN and its p97-interacting SHP motif to DPC repair in human cells, a rescue system was established in HEK293T cells in which endogenous SPRTN was silenced with siSPRTN, while SPRTN-WT, SPRTN-SHPmut, or SPRTN-E112A was overexpressed from transfected plasmids. Silencing of endogenous SPRTN reduced SPRTN mRNA levels by 74.3% (Figure 22). Overexpression of all three constructs was confirmed at the mRNA level, reaching 22.5 ± 0.22-fold for SPRTN-WT, 29.10 ± 0.60-fold for SPRTN-SHPmut, and 27.38 ± 0.50-fold for SPRTN-E112A relative to WT cells (Figure 22).

Total cellular DPCs were then isolated using the modified RADAR method and quantified as total, HMW-, MMW-, and LMW-DPC classes. Silencing of endogenous SPRTN was associated with increased DPC levels across all classes compared with WT cells, indicating that SPRTN broadly contributes to DPC repair in this system. Total DPC levels increased 2.78-fold, while HMW-, MMW-, and LMW-DPC levels increased 1.35-fold, 2.16-fold, and 7.40-fold, respectively (Figure 22). Overexpression of SPRTN-WT, SPRTN-SHPmut, and SPRTN-E112A in the SPRTN-silenced background reduced DPC levels relative to siSPRTN-treated cells, with all three constructs lowering DPC levels to below WT levels across all classes (Figure 22).

However, interpretation of this assay proved problematic. Although reduction of DPC levels by SPRTN-WT was expected, the catalytically inactive control SPRTN-E112A also reduced the induced DPC levels in this system, contrary to the expected behaviour of a protease-dead SPRTN mutant (Vaz et al., 2016). Because the negative control did not behave as anticipated, this HEK293T rescue system was not considered suitable for further functional analysis of the SHP motif. Since resolving this issue would require substantial additional optimization, subsequent experiments were performed in an alternative SPRTN-deficient system (next chapter).

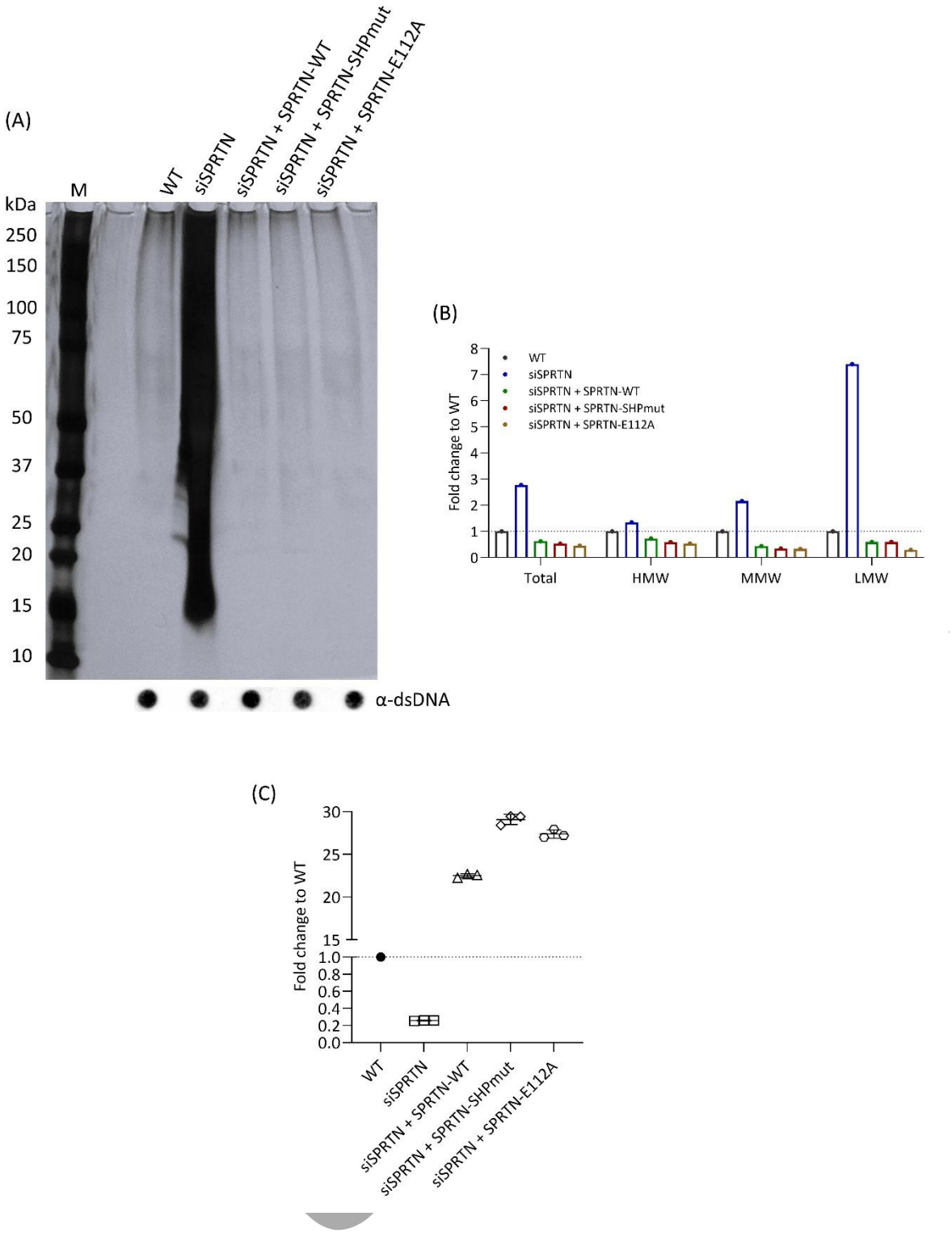

Figure 22. DNA-protein crosslink levels in HEK293T cells with overexpressed SPRTN-WT, SPRTN-SHPmut, or SPRTN-E112A in the background of silenced endogenous SPRTN. (A) Total cellular DPCs in HEK293T cells with silenced endogenous SPRTN and overexpressed different SPRTN constructs (SPRTN-WT, SPRTN-SHPmut, SPRTN-E112A), resolved on SDS-PAGE gel and stained with silver. DPCs were isolated using modified RADAR method from HEK293T cells. A DPC equivalent of 200 ng total DNA was loaded per well. Dot blots showing DNA loading controls for DPC analysis are shown below (2 ng of total DNA were loaded per well). M, molecular weight marker. **(B)** Quantification of (A) using

ImageJ based on data shown here. Quantification of total, HMW-DPCs (high molecular weight DPCs, Mr > 151 kDa), MMW-DPCs (medium molecular weight DPCs, Mr = 41 – 150 kDa), and LMW-DPCs (low molecular weight DPCs, Mr < 40 kDa) from (A). **(C)** Levels of SPRTN mRNA confirming silencing of endogenous SPRTN and overexpression of different SPRTN constructs in HEK293T cells. Data are shown as mean ± SD (n = 3 technical replicates). siSPRTN = small interfering RNA targeting SPRTN mRNA.

3.3.2. The p97-interacting SHP motif of SPRTN is not crucial for DPC repair in HeLa ΔSPRTN cells under physiological conditions

To examine the contribution of the SPRTN-p97 interaction to DPC repair in human cells, a HeLa ΔSPRTN cell system was used, in which two of the three endogenous *SPRTN* alleles are disrupted (Vaz et al., 2016) and SPRTN-WT, SPRTN-SHPmut, or SPRTN-E112A was overexpressed from transfected plasmid DNA. Because HeLa cells are triploid for chromosome 1, this model represents a partial rather than complete SPRTN knockout, and residual endogenous SPRTN expression was still detectable. Consistent with this, the mean SPRTN qPCR Ct value in HeLa ΔSPRTN cells was 22.8, which was similar to that measured in the HeLa WT cells used in our laboratory (Ct 22.5), indicating that this system was not a true SPRTN-null background. Importantly, the parental HeLa WT cells from which the HeLa ΔSPRTN cells were originally derived were not available as a control in these experiments. Overexpression of all three SPRTN constructs was confirmed at the mRNA level in all three experiments. Relative to HeLa ΔSPRTN cells, SPRTN-WT was overexpressed 31.99 ± 0.78-fold, 45.28 ± 0.40-fold, and 71.70 ± 5.11-fold; SPRTN-SHPmut 19.33 ± 0.07-fold, 76.36 ± 8.39-fold, and 90.56 ± 2.54-fold; and SPRTN-E112A 33.75 ± 3.03-fold, 71.10 ± 6.52-fold, and 91.73 ± 8.49-fold (Figure 23).

Total cellular DPCs were isolated using the modified RADAR method and quantified as total, HMW-, MMW-, and LMW-DPC classes. Compared with HeLa ΔSPRTN cells, overexpression of SPRTN-WT and SPRTN-SHPmut significantly reduced total DPC levels to 0.70 ± 0.13-fold and 0.67 ± 0.13-fold, respectively (Figure 23). Significant reductions were also observed for MMW-DPCs, which decreased to 0.51 ± 0.17-fold and 0.54 ± 0.20-fold, and for LMW-DPCs, which decreased to 0.59 ± 0.16-fold and 0.53 ± 0.22-fold, respectively (Figure 23). HMW-DPCs showed a similar downward trend, reaching 0.84 ± 0.26-fold after SPRTN-WT overexpression and 0.72 ± 0.21-fold after SPRTN-SHPmut overexpression (Figure 23). In contrast, the catalytically inactive SPRTN-E112A construct did not significantly reduce total, HMW-, MMW-, or LMW-DPC levels (although a downward trend was observed), which

remained at 0.80 ± 0.18-fold, 0.83 ± 0.29-fold, 0.74 ± 0.27-fold, and 0.57 ± 0.29-fold relative to HeLa ΔSPRTN cells, respectively (Figure 23). Thus, unlike in the HEK293T cells, SPRTN-E112A behaved to some extent as an appropriate negative control in this system (it failed to rescue total DPC levels in two of the three experiments), making the HeLa ΔSPRTN model more informative for subsequent analysis of the SHP motif.

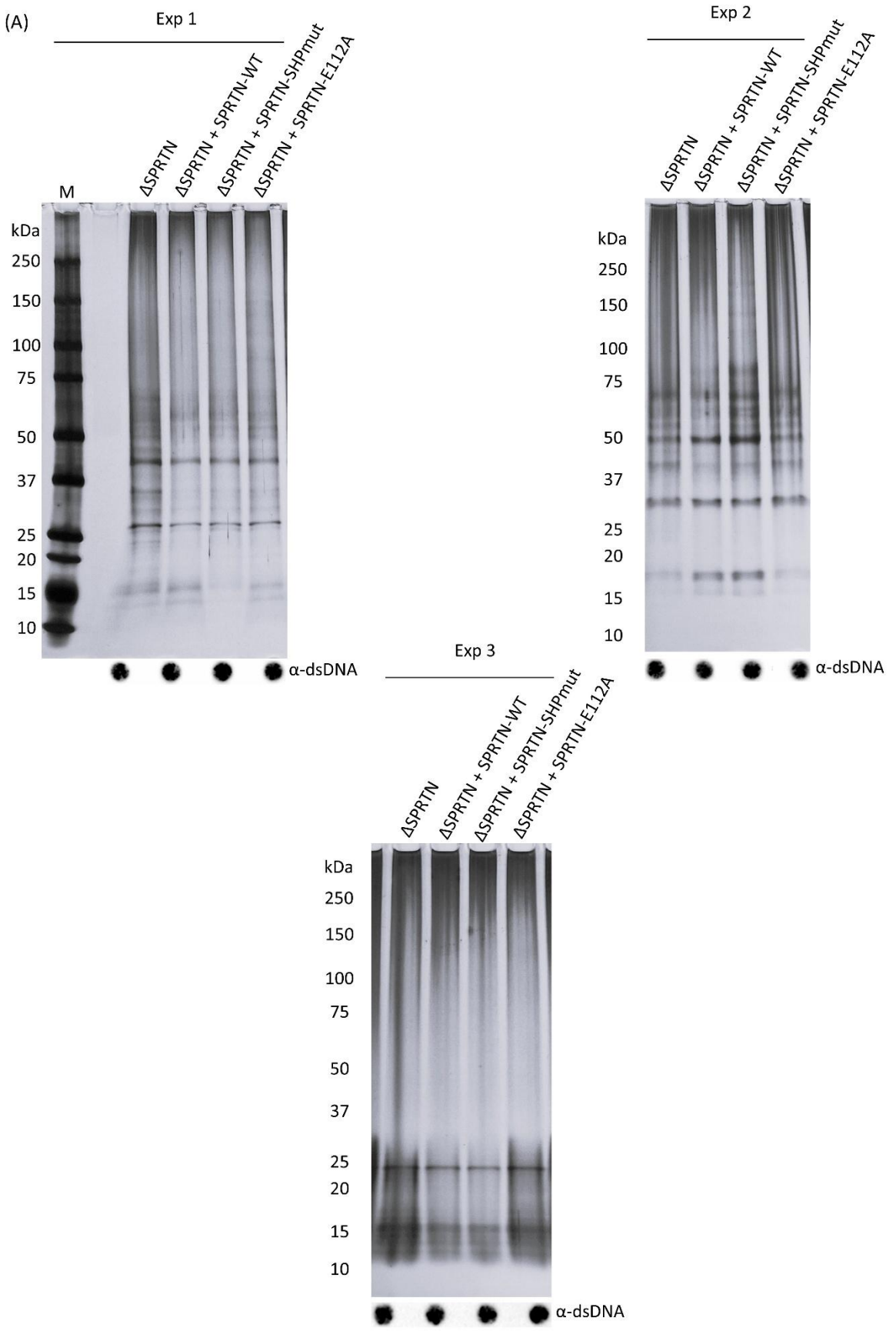
(A)
Exp 1
M
ΔSPRTN
ΔSPRTN + SPRTN-WT
ΔSPRTN + SPRTN-SHPmut
ΔSPRTN + SPRTN-E112A
kDa
250
150
100
75
50
37
25
20
15
10
α-dsDNA
Exp 2
ΔSPRTN
ΔSPRTN + SPRTN-WT
ΔSPRTN + SPRTN-SHPmut
ΔSPRTN + SPRTN-E112A
kDa
250
150
100
75
50
37
25
20
15
10
α-dsDNA
Exp 3
ΔSPRTN
ΔSPRTN + SPRTN-WT
ΔSPRTN + SPRTN-SHPmut
ΔSPRTN + SPRTN-E112A
kDa
250
150
100
75
50
37
25
20
15
10
α-dsDNA

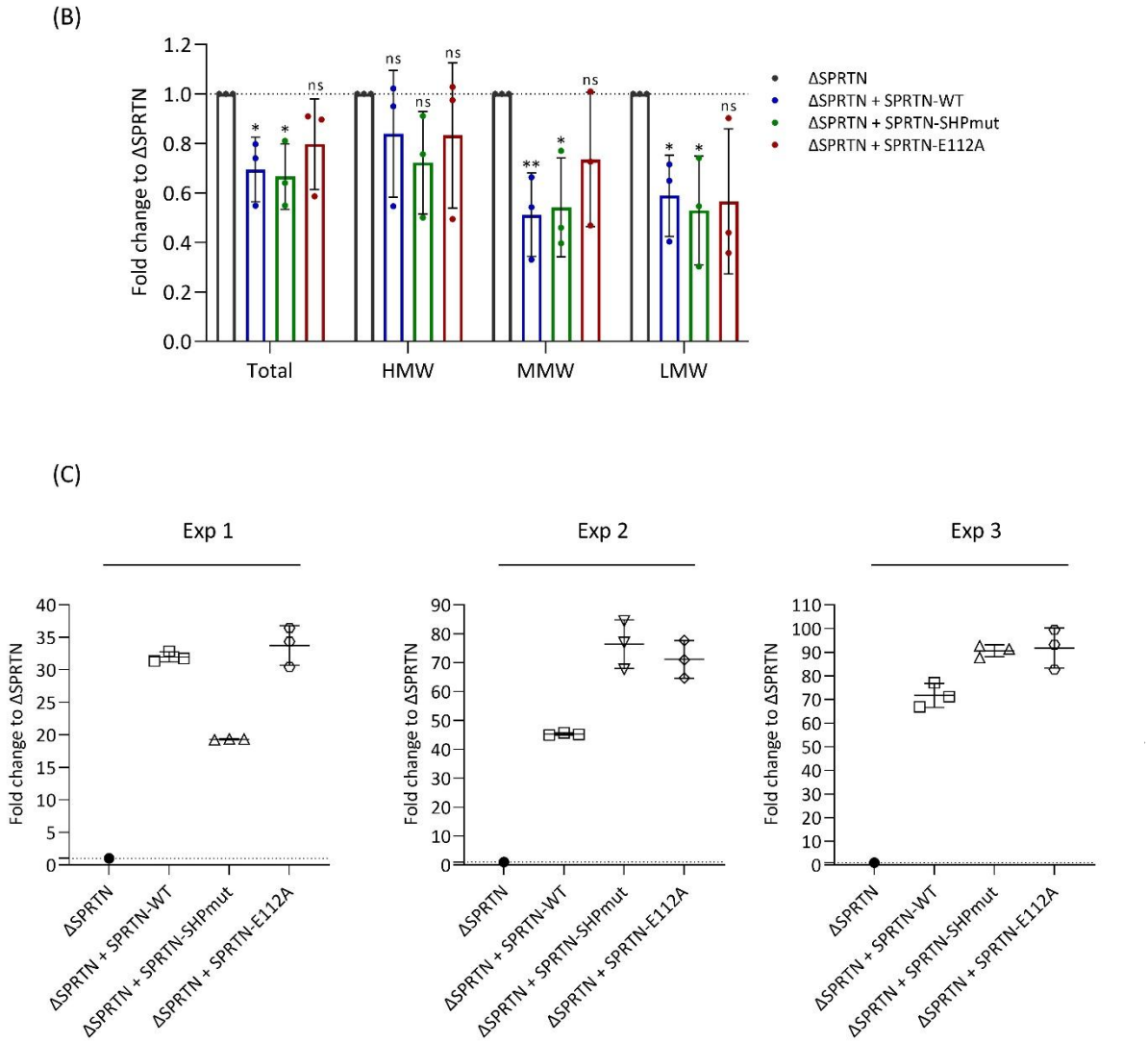

Figure 23. Total cellular DNA-protein crosslink levels in HeLa ΔSPRTN cells with overexpressed SPRTN-WT, SPRTN-SHPmut, or SPRTN-E112A. (A) Total cellular DPCs in HeLa ΔSPRTN cells with overexpressed different SPRTN constructs (SPRTN-WT, SPRTN-SHPmut, SPRTN-E112A), resolved on SDS-PAGE gel and stained with silver. DPCs were isolated using modified RADAR method from HeLa ΔSPRTN cells. A DPC equivalent of 200 ng total DNA was loaded per well. Dot blots showing DNA loading controls for DPC analysis are shown below (2 ng of total DNA were loaded per well). M, molecular weight marker. **(B)** Quantification of (A) using ImageJ based on data shown here (biological replicates). Quantification of total, HMW-DPCs (high molecular weight DPCs, Mr > 151 kDa), MMW-DPCs (medium molecular weight DPCs, Mr = 41 – 150 kDa), and LMW-DPCs (low molecular weight DPCs, Mr < 40 kDa) from (A). Data are shown as mean ± SD (n = 3), and statistically significant differences compared with HeLa ΔSPRTN cells are indicated; Student's t-test (** $p < 0.01$, * $p < 0.05$, ns: not significant). **(C)** Levels of SPRTN mRNA confirming overexpression of different SPRTN constructs in HeLa ΔSPRTN cells. Data are shown as mean ± SD (n = 3 technical replicates).

Because the catalytically inactive control behaved partly as expected in this assay, selected specific DPC species were analyzed next, starting with histone H3. Histone H3-DPC

levels were significantly reduced by both SPRTN-WT and SPRTN-SHPmut, to 0.44 ± 0.17-fold and 0.47 ± 0.01-fold, respectively, relative to HeLa ΔSPRTN cells, whereas SPRTN-E112A had a much weaker effect and histone H3-DPC levels remained close to those in HeLa ΔSPRTN cells (0.89 ± 0.02-fold) (Figure 24). A similar overall pattern was observed in single experiments for Ku80-, PARP1-, TOP1-, DNMT1-, TOP2-, POLR3A-, and MCM2-DPCs. Relative to HeLa ΔSPRTN cells, these DPC levels decreased to 0.69-, 0.27-, 0.61-, 0.44-, 0.29-, 0.36-, and 0.07-fold after SPRTN-WT overexpression, and to 0.51-, 0.08-, 0.39-, 0.69-, 0.31-, 0.44-, and 0.09-fold after SPRTN-SHPmut overexpression, whereas SPRTN-E112A showed little or no reduction in these DPC levels, with values of 1.11-, 0.66-, 0.90-, 1.11-, 0.95-, 1.05-, and 0.66-fold, respectively (Figure 24). However, these additional analyses were performed only once and, given the observed interexperimental variability in this system, they should be interpreted cautiously. Taken together, these findings suggest that, in this partial HeLa ΔSPRTN background and under physiological conditions, the p97-interacting SHP motif is not crucial for repair of the majority of endogenous DPCs, although the residual endogenous SPRTN expression in this system limits firmer conclusions.

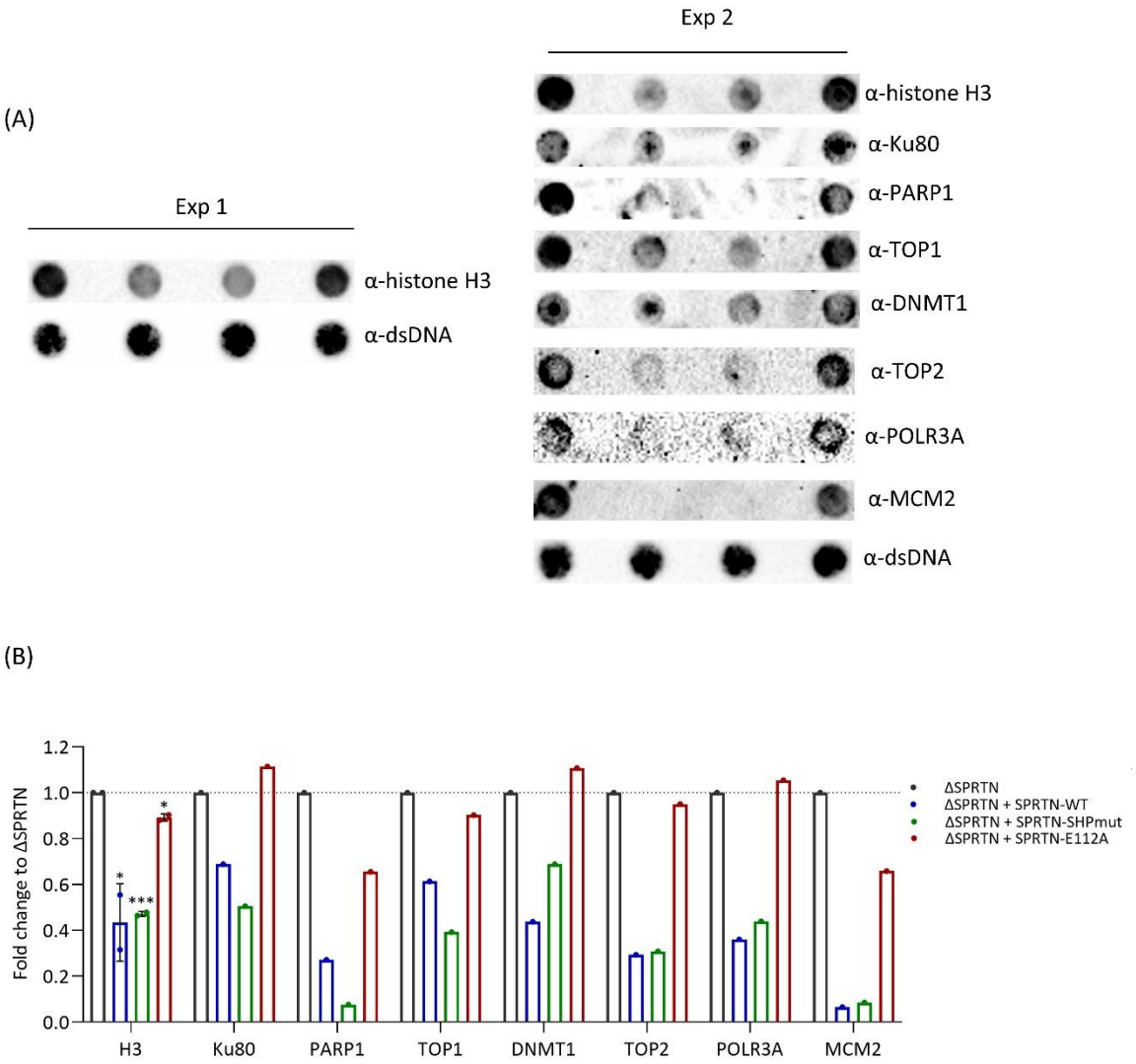

Figure 24. Specific cellular DNA-protein crosslinks in HeLa ΔSPRTN cells with overexpressed SPRTN-WT, SPRTN-SHPmut, or SPRTN-E112A. (A) Histone H3-, Ku80-, PARP1-, TOP1-, DNMT1-, TOP2-, POLR3A-, and MCM2-DPC levels in HeLa ΔSPRTN cells with overexpressed different SPRTN constructs (SPRTN-WT, SPRTN-SHPmut, SPRTN-E112A). DPCs were isolated using modified RADAR method from HeLa ΔSPRTN cells and visualized using dot blotting with specific antibodies. A DPC equivalent of 200 ng (histone H3) or 500 ng (Ku80, PARP1, TOP1, DNMT1, TOP2, POLR3A, MCM2) total DNA was loaded per well. Dot blots showing DNA loading controls for DPC analysis are shown below (2 ng of total DNA were loaded per well). **(B)** Quantification of (A) using ImageJ based on data shown here (biological replicates for histone H3). For histone H3, data are shown as mean ± SD (n = 2), and statistically significant differences compared with HeLa ΔSPRTN cells are indicated; Student's t-test (*** $p < 0.001$, * $p < 0.05$).

3.3.3. The SPRTN-p97 interaction might be important for the repair of certain endogenous DPCs in zebrafish embryos

To examine the contribution of the SPRTN-p97 interaction to DPC repair *in vivo*, a zebrafish embryo rescue system analogous to the HEK293T cell approach was used. Wild-type embryos were injected at the 1-cell stage with Sprtn morpholinos to reduce endogenous Sprtn levels, together with *in vitro* synthesized mRNA encoding Sprtn-WT, Sprtn-SHPmut, or Sprtn-L147A, and were analyzed at 30 hpf. Specific DPC species were then quantified after RADAR isolation by dot blotting with specific antibodies. All injected embryos showed a grossly WT-like morphology at the time of collection. Sprtn-L147A was included as a reduced-activity comparison construct based on the analogous residue in the RJALS-associated human SPRTN variant (Vaz et al., 2016), although the extent to which this zebrafish mutant reproduces the functional defect of the human variant remains uncertain. In addition, the degree of morpholino-mediated Sprtn silencing and the mRNA levels of the injected constructs varied between experiments, indicating interexperimental variability in this system.

Knockdown of endogenous Sprtn caused statistically significant accumulation of multiple endogenous DPC species relative to WT embryos. The strongest increase was observed for Top1-DPCs (2.92 ± 0.67-fold), followed by Parp1-DPCs (2.35 ± 1.03-fold), Dnmt1-DPCs (1.83 ± 0.32-fold), and Ku80-DPCs (1.54 ± 0.13-fold) (Figure 25). Co-injection of Sprtn-WT reduced DPC levels overall, with Dnmt1-, Ku80-, and Parp1-DPCs decreasing to near-WT levels (1.13 ± 0.27-fold, 1.21 ± 0.21-fold, and 1.21 ± 0.45-fold, respectively), whereas Top1-DPCs remained elevated (2.37 ± 0.68-fold) but showed a downward trend relative to Sprtn morpholino alone (Figure 25). These findings indicate that the morpholino phenotype is specific and support a role for Sprtn in the repair of several endogenous DPC species during early embryogenesis.

In contrast, co-injection of Sprtn-SHPmut did not restore most analyzed DPCs to near-WT levels. Under these conditions, Parp1-DPCs showed the highest accumulation (3.35 ± 1.36-fold), followed by Top1-DPCs (2.82 ± 1.13-fold), Ku80-DPCs (1.55 ± 0.48-fold), and Dnmt1-DPCs (1.34 ± 0.19-fold) (Figure 25). Parp1-, Top1-, and Dnmt1-DPCs remained significantly elevated relative to WT embryos, whereas Ku80-DPCs were not significantly increased but still showed an upward trend (Figure 25). After injection of Sprtn-L147A, all analyzed DPC species remained significantly elevated compared with WT embryos, with Top1-DPCs again showing the highest level (2.44 ± 0.33-fold), followed by Parp1-DPCs (2.00 ± 0.63-fold), Ku80-DPCs

(1.73 ± 0.32-fold), and Dnmt1-DPCs (1.20 ± 0.002-fold) (Figure 25). However, because some rescue of selected DPCs by Sprtn-L147A was observed in individual experiments, and because the overall response varied between experiments, the behavior of this construct should be interpreted cautiously. Taken together, these results suggest that interaction of Sprtn with p97 through the SHP motif may contribute to repair of at least a subset of endogenous DPCs in zebrafish embryos, particularly Parp1-, Top1-, and Dnmt1-DPCs, although additional experiments will be required for firmer conclusions.

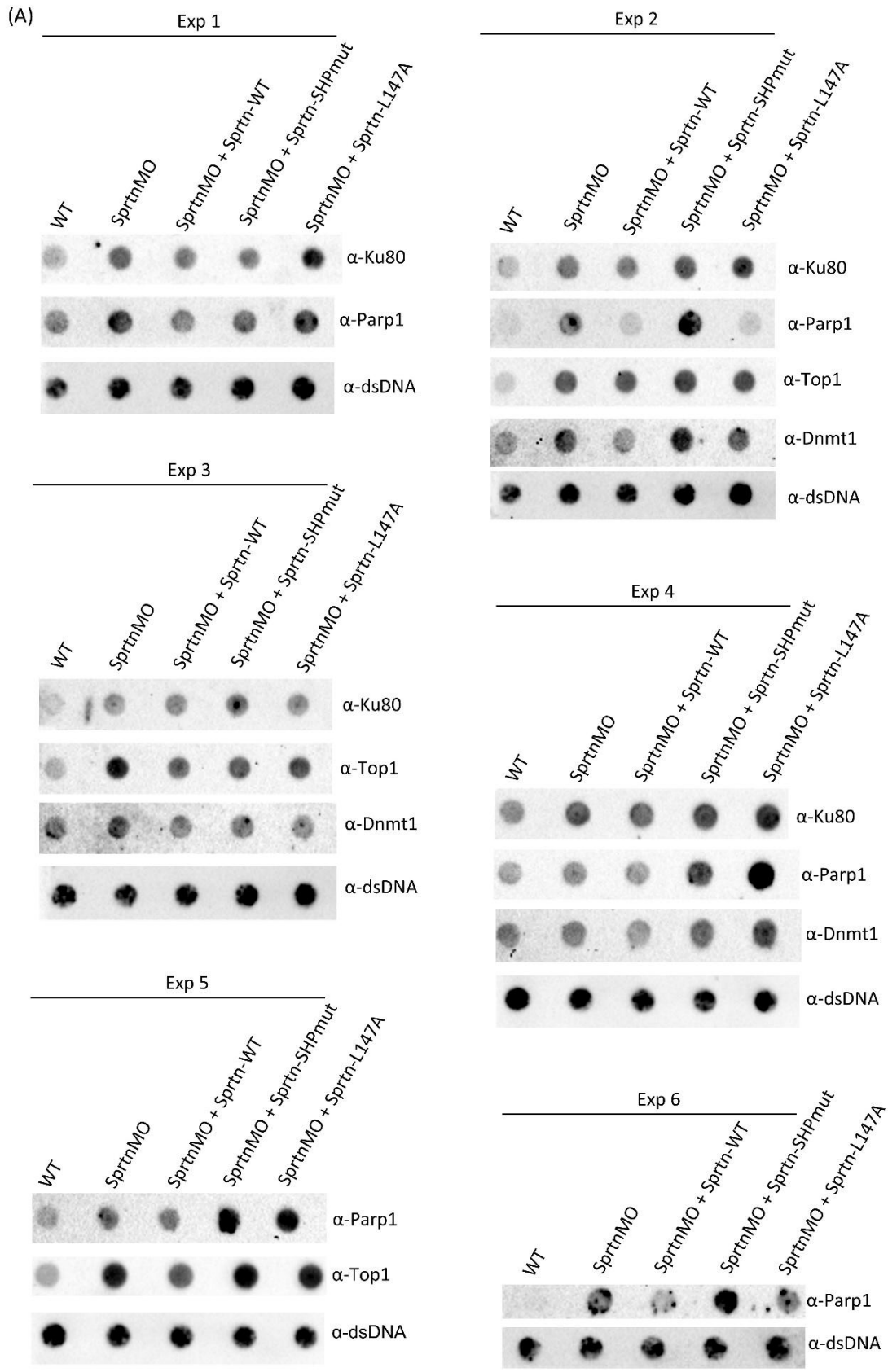
(A)
Exp 1
WT
SprtnMO
SprtnMO + Sprtn-WT
SprtnMO + Sprtn-SHPmut
SprtnMO + Sprtn-L147A
α-Ku80
α-Parp1
α-dsDNA
Exp 2
WT
SprtnMO
SprtnMO + Sprtn-WT
SprtnMO + Sprtn-SHPmut
SprtnMO + Sprtn-L147A
α-Ku80
α-Parp1
α-Top1
α-Dnmt1
α-dsDNA
Exp 3
WT
SprtnMO
SprtnMO + Sprtn-WT
SprtnMO + Sprtn-SHPmut
SprtnMO + Sprtn-L147A
α-Ku80
α-Top1
α-Dnmt1
α-dsDNA
Exp 4
WT
SprtnMO
SprtnMO + Sprtn-WT
SprtnMO + Sprtn-SHPmut
SprtnMO + Sprtn-L147A
α-Ku80
α-Parp1
α-Dnmt1
α-dsDNA
Exp 5
WT
SprtnMO
SprtnMO + Sprtn-WT
SprtnMO + Sprtn-SHPmut
SprtnMO + Sprtn-L147A
α-Parp1
α-Top1
α-dsDNA
Exp 6
WT
SprtnMO
SprtnMO + Sprtn-WT
SprtnMO + Sprtn-SHPmut
SprtnMO + Sprtn-L147A
α-Parp1
α-dsDNA

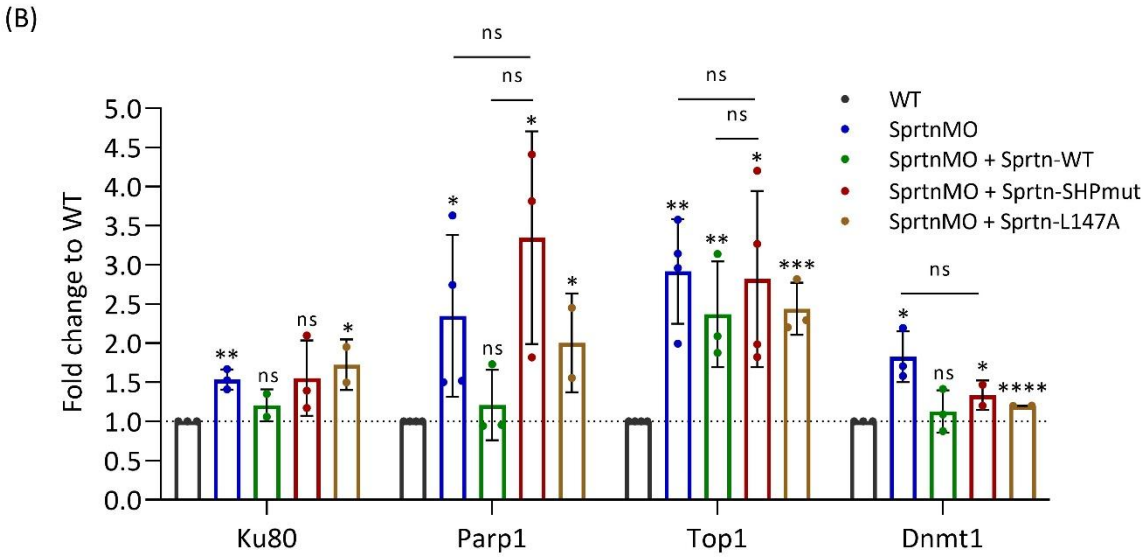

Figure 25. Specific cellular DNA-protein crosslinks in zebrafish embryos with overexpressed Sprtn-WT, Sprtn-SHPmut, or Sprtn-L147A in the background of silenced endogenous Sprtn by Sprtn morpholinos. (A) Ku80-, Parp1-, Top1-, and Dnmt1-DPC levels in zebrafish embryos at 30 hpf after silencing of endogenous Sprtn with Sprtn morpholinos and overexpression of different Sprtn constructs (Sprtn-WT, Sprtn-SHPmut, and Sprtn-L147A). DPCs were isolated using modified RADAR method from 25 embryos (30 hpf) and visualized using dot blotting with specific antibodies. A DPC equivalent of 500 ng total DNA was loaded per well. Dot blots showing DNA loading controls for DPC analysis are shown below (2 ng of total DNA were loaded per well). **(B)** Quantification of (A) using ImageJ based on data shown here (biological replicates). Data are shown as mean ± SD (n = 2 – 4), and statistically significant differences compared with wild-type embryos are indicated; Student's t-test (**** $p < 0.0001$, *** $p < 0.001$, ** $p < 0.01$, * $p < 0.05$, ns: not significant). MO – morpholino.

4. DISCUSSION

4.1. Role of Acrc in DPC repair in zebrafish

In this study, Acrc emerged as an essential factor for zebrafish embryonic development. This is consistent with earlier work placing ACRC mainly in germ cells and early embryonic contexts, and with previous genetic studies showing severe germline or early-embryo phenotypes, including maternal-effect embryonic lethality in zebrafish after *acrc* disruption (Bhargava et al., 2020; Borgermann et al., 2019; Carmell et al., 2016; Dokshin et al., 2020). Earlier zebrafish work further showed modest accumulation of total DPCs in *acrc* mutants, but the critical functional domain and the affected endogenous DPC species remained unresolved (Bhargava et al., 2020). In our study, Acrc activity, and consequently embryo viability, depended on an intact SprT domain, with the catalytic glutamate being particularly important, indicating that the proteolytic function of Acrc is essential for development. Our data also extend previous links between ACRC and endogenous DPC repair by showing that zebrafish Acrc participates in the repair of several endogenous cellular DPCs, including Dnmt1-, topoisomerase 1- and 2-, histone H3-, Parp1-, Polr3a-, and Mcm2-DPCs.

Considering that ACRC is required during vertebrate embryogenesis, its strong evolutionary conservation is not unexpected and is consistent with earlier evolutionary analyses showing that ACRC is an ancient eukaryotic protein family that arose before the major eukaryotic lineages diverged and is generally represented by a single ortholog in most animal species (Carmell et al., 2016; Fielden et al., 2018). In line with the functional data, the C-terminal SprT domain of ACRC is highly conserved from invertebrates to humans, whereas the N-terminal half is largely intrinsically disordered and much more variable between species. Because mouse Acrc lacks a SprT domain (Carmell et al., 2016), rodent orthologs were examined in more detail and we saw that the majority of rodent species retain this domain (Otten et al., 2025). It remains of interest to determine why the SprT domain was lost in only some rodent species, including *Rattus norvegicus*, *Neotoma lepida*, *Arvicanthis niloticus*, *Mus caroli*, *Mus musculus*, and *Mus pahari*, and what functional consequences this had in those species. In addition, the predicted three-dimensional structures of the human and zebrafish ACRC SprT domains are almost identical, further supporting zebrafish as a suitable model for studies of ACRC-mediated DPC proteolysis (Otten et al., 2025).

ACRC was first characterized mainly as a protein associated with germ cells and with early embryonic or otherwise highly proliferative settings (Bhargava et al., 2020; Borgermann et al., 2019; Carmell et al., 2016; Dokshin et al., 2020). However, analysis of zebrafish *acrc* mRNA expression in adult tissues showed a broader pattern (Otten et al., 2025; Supina Pavić, 2023). As expected, expression was very high in ovaries and testes, consistent with previous work linking ACRC to germline functions. At the same time, *acrc* transcripts were also detected in all other tissues examined, including brain, liver, kidney, intestine, eye, gills, and muscle. In contrast, mouse *Acrc* expression appears to be largely confined to the testis, which again emphasizes the divergence between mouse Acrc, lacking a SprT domain, and vertebrate orthologs such as zebrafish Acrc (Otten et al., 2025). Given the substantial expression of *acrc* in adult zebrafish somatic tissues, it is reasonable to consider that Acrc may also have functions beyond DPC repair during germline meiosis. Previous work had mainly linked ACRC to germline meiosis and early embryonic contexts (Bhargava et al., 2020; Carmell et al., 2016; Dokshin et al., 2020). During embryogenesis, both *acrc* and *sprtn* were highly expressed at the earliest stages, peaking at 1 hpf, consistent with strong maternal mRNA contribution, and then dropped markedly by 6 hpf (Otten et al., 2025; Supina Pavić, 2023). Importantly, *acrc* expression remained at least threefold higher than *sprtn* expression up to 48 hpf, raising the possibility that Acrc is the dominant DPC protease during this developmental interval.

The results further showed that the integrity of the Acrc protease core is crucial for embryo survival. The mutant line carrying deletion of the catalytic glutamate E451 together with the following three residues (*rbi5* allele; Figure 9) displayed embryonic lethality (Figure 9). Earlier work had shown that early frameshift disruption of *acrc* causes maternal-effect embryonic lethality in zebrafish (Bhargava et al., 2020), but the relevant functional domain had remained undefined. Because the lethality phenotype could be rescued by injection of Acrc-WT mRNA at the one-cell stage (Figure 11), and these rescued mutants later developed into adults without obvious abnormalities, the data suggest that Acrc is specifically required to repair critical DPC lesions during early embryogenesis. Under physiological conditions at this stage, other DPC proteases and nucleolytic DPC repair pathways appeared unable to compensate for disruption of the Acrc protease core strongly enough to prevent embryonic death. In contrast, Acrc did not seem to be required for adult viability or gross morphology under standard laboratory conditions, since rescued *acrc* mutants appeared similar to WT fish.

A flexible, non-genetic rescue approach was then used to evaluate constructs encoding altered or truncated Acrc proteins in zebrafish. All constructs were expressed from injected

mRNAs, and translation of the corresponding Myc-tagged proteins was confirmed by anti-Myc immunostaining (Otten et al., 2025). This confirmed the importance of the catalytic activity itself, because injection of Acrc-E451A mRNA did not rescue embryonic lethality (Figure 11). A related strategy had previously been used in *Drosophila*, where a catalytically impaired HE>AA Gcna/Acrc transgene failed to suppress excessive DNA damage in mutant germ cells, yet partially alleviated maternal-effect embryonic semi-lethality, suggesting that in flies the IDR may contribute to chromosome stability during early development even without full SprT-domain activity (Bhargava et al., 2020). In zebrafish, however, the SprT domain proved to be indispensable: a construct composed mainly of the SprT domain rescued the lethality phenotype, whereas an IDR-only construct did not (Figure 11). Thus, the SprT domain is required for Acrc function during development, whereas the IDR alone is insufficient. This conclusion was further supported by the finding that mouse Acrc mRNA, encoding a largely IDR-containing protein without the SprT domain (Figure 11), also failed to rescue embryonic lethality in *acrc* mutants (Figure 11). In contrast, an *Acrc* conditional knockout mouse model showed severe male infertility (Carmell et al., 2016), and later work described premature chromatin condensation, persistent DNA-damage markers, crossover defects, and phenotypes compatible with impaired TOP2-linked genome maintenance during spermatogenesis (Dokshin et al., 2020). Still, a direct role of mouse Acrc in DPC repair has not been demonstrated. Instead, mouse Acrc has been proposed to preserve genome integrity through protease-independent IDR-mediated functions, including SUMO-interaction motif-dependent protein interactions during meiotic genome maintenance (Dokshin et al., 2020) and histone-chaperone activity during DNA replication in undifferentiated spermatogonia (Ribeiro & Crossan, 2023).

The results further showed that Sprtn and Acrc are not functionally redundant during early zebrafish development. Although endogenous *sprtn* expression was high in *acrc* mutants at 6 hpf (Otten et al., 2025), this was not sufficient to prevent lethality, and additional Sprtn provided by Sprtn-WT mRNA injection also failed to rescue the phenotype (Figure 11). These findings provide direct functional evidence that Sprtn cannot substitute for loss of Acrc protease-core activity during this developmental stage. Their lack of redundancy may reflect, at least in part, differences in cell-cycle regulation. SPRTN is mainly present in S phase, G2, and early M phase, because APC/C-Cdh1-dependent proteolysis limits its abundance from mitotic exit through G1 (Mosbech et al., 2012). By contrast, ACRC levels are lowest in G1, increase during S phase, remain high in G2/M, and the protein localizes to condensed chromosomes, including meiotic chromosomes in mouse spermatocytes and mitotic

chromosomes in *C. elegans* embryos (Dokshin et al., 2020). Recent work showed that SPRTN also contributes to mitotic DPC repair, indicating that its function is not restricted to S phase (Tomaskovic et al., 2026).

Because mutation of the Acrc protease core caused early embryonic lethality, it was important to determine whether DPC accumulation occurs before overt developmental failure. Indeed, endogenous DPC levels were already significantly elevated in *acrc* mutant embryos at 6 hpf, when no obvious abnormalities were yet visible and the embryos still appeared similar to WT embryos (Figures 12, 13), indicating that DPC accumulation precedes the onset of lethality. Increased DPC levels were observed in all three molecular-weight classes, with the strongest effect seen in HMW-DPCs, followed by MMW-DPCs, whereas the increase in LMW-DPCs was more modest (Figure 12). Among individual lesions, Top1-, Top2-, and Parp1-DPCs accumulated most prominently, histone H3-DPCs also increased substantially, and Dnmt1-, Polr3a-, and Mcm2-DPCs showed more moderate accumulation (Figure 13). These proteins all have essential cellular functions: TOP1, TOP2, and MCM2 are involved in DNA replication and chromosome dynamics; PARP1 is central to DNA damage signaling and repair; POLR3A is the catalytic subunit of RNA polymerase III and is needed for transcription of small non-coding RNAs; DNMT1 maintains DNA methylation patterns after replication; and histone H3 is a core nucleosomal component required for genome organization and stability (Alberts et al., 2022).

Taken together, the strong accumulation of the aforementioned and likely other DPCs in Acrc-deficient embryos, combined with the apparent inability of Sprtn, the proteasome, and nucleolytic repair pathways to compensate, supports the view that ACRC is an essential DPC protease during early vertebrate development, when rapid cell-cycle progression and frequent mitotic divisions make genome maintenance particularly critical. This interpretation is consistent with the development of the early zebrafish embryo. In the first hours after fertilization, development depends largely on maternally deposited RNAs and proteins until the maternal-to-zygotic transition (MZT), while the main wave of zygotic genome activation begins around 3 hpf. During these cleavage stages, cell cycles are extremely rapid, the genome is replicated in less than 15 minutes, and divisions occur without gap phases (Akdogan-Ozdilek et al., 2020). DNA replication, chromatin reorganization, and onset of zygotic transcription are therefore compressed into a very narrow developmental window. Under such conditions, the embryonic genome is likely particularly sensitive to DPC formation, making efficient repair of

these lesions essential for uninterrupted cleavage divisions and embryo survival, with ACRC likely playing a central role in this process.

4.2. Role of p97 in DPC repair in human cells and zebrafish

4.2.1. Role of p97 in DPC repair in human cells

In this study, we showed that p97 contributes to the repair of multiple cellular DPCs in human cells. Acute pharmacological inhibition of p97 in HeLa cells caused significant accumulation of total cellular DPCs, as well as of high-, medium-, and low-molecular-weight DPC classes (Figure 16). In parallel, several specific DPC species were increased, including histone H3-, Ku80-, PARP1-, TOP1-, DNMT1-, and TOP2-DPCs (Figure 17). Previous studies showed that p97 acts as a chromatin-associated segregase that can extract some chromatin-bound protein obstacles, such as lesion-stalled RNA polymerase II (Zhu et al., 2024), sterically trapped Ku70/Ku80 rings (van den Boom et al., 2016), and Aurora B kinase (Ramadan et al., 2007), and that it also removes trapped PARP1 from chromatin (Krastev et al., 2022). Our data extend this framework by providing the first evidence that p97 contributes broadly to cellular defense against endogenous DPCs.

The interpretation of these findings is strengthened by the experimental design. DPC accumulation was assessed after only 6 h of treatment with the p97 inhibitors NMS-873 (10 μM) or CB-5083 (5 μM), and under these conditions no detectable cytotoxicity was observed in the MTT assay, either immediately after treatment or after a recovery period (Figure 15). This is important because it argues that the observed increase in DPC levels is unlikely to be explained simply by nonspecific secondary consequences of massive cell death or overt collapse of cellular metabolism. Instead, the data are more consistent with a relatively direct requirement for p97 activity in limiting DPC accumulation under basal growth conditions. The fact that similar DPC accumulation was observed with two structurally and mechanistically distinct, widely used p97 inhibitors further supports the interpretation that the DPC induction reflects loss of p97 function rather than an off-target effect of a single compound. Although some context-specific off-target effects have been reported for these inhibitors (Bouwer et al., 2021; Leinonen et al., 2021), they are unlikely to be relevant in the present system. These results fit well with the general molecular role of p97. p97 is a highly abundant AAA+ ATPase that functions as an ATP-driven segregase/unfoldase in many protein quality-control and genome-maintenance pathways (Costantini et al., 2021; Noireterre & Stutz, 2024; Pontifex et al., 2024). Through ATP hydrolysis and the action of cofactors such as UFD1-NPL4, p97 can remodel substrates and extract ubiquitylated proteins from chromatin or other stable assemblies, thereby promoting their degradation, recycling, or relocalization (Bodnar & Rapoport, 2017; Costantini

et al., 2021; Noireterre & Stutz, 2024). In the context of DPC repair, such an activity is appealing because DPCs are bulky protein-DNA adducts that may first need to be unfolded, loosened from chromatin, or otherwise remodeled before proteolysis or downstream excision steps can proceed efficiently (Kröning et al., 2022). The present results are therefore compatible with a model in which p97 acts upstream of, or in parallel with, dedicated DPC proteases and other repair factors by helping to process the proteinaceous component of the lesion (Fielden et al., 2020; Kröning et al., 2022; Noireterre & Stutz, 2024).

Important aspect of our results is that p97 inhibition increased DPC levels across all molecular-weight classes (Figure 16). This suggests that the role of p97 is probably not restricted to unusually large protein adducts. Rather, the broad increase in high-, medium-, and low-molecular-weight DPCs indicates that p97 likely acts at a step that influences the efficiency of DPC processing across multiple repair pathways.

The accumulation of **TOP1-DPCs** upon p97 inhibition (Figure 17) is especially informative because it is consistent with previous mechanistic work implicating p97 in TOP1-DPC processing. Earlier studies showed that p97 ATPase activity is required to limit endogenous TOP1cc accumulation in human cells, and that TEX264 (a p97 cofactor/adaptor protein) can recruit p97 and SPRTN to camptothecin-induced TOP1-DPCs, thereby promoting their proteolytic processing (Fielden et al., 2020). More recently, TEX264 was also shown to mediate a distinct p97-dependent, SPRTN-independent pathway that delivers low-dose camptothecin-induced TOP1-DPCs to lysosomes by selective nucleophagy (Lascaux et al., 2024). Our data extend that concept by showing that acute p97 inhibition in HeLa cells is sufficient to increase endogenous TOP1-DPC levels even in the absence of topoisomerase poisons such as camptothecin. This suggests that p97 contributes not only under conditions of exogenous challenge, but also to the clearance of endogenous TOP1-DPCs arising during replication and transcription (Ashour et al., 2015; Pommier, 2009).

Vertebrates have two TOP2 isoforms, TOP2α and TOP2β. Both help resolve topological stress during replication and transcription, but TOP2α is the dominant isoform in proliferating cells and is particularly important for replication-associated chromosome dynamics, chromosome condensation, and sister-chromatid segregation, whereas TOP2β has been more linked to transcription-associated functions (Nitiss, 2009; Wendorff et al., 2012). Trapped TOP2-DNA adducts are highly toxic lesions (Dokshin et al., 2020; Nitiss, 2009). Previous work showed that p97 inhibition causes persistence of etoposide-induced TOP2-DPCs and increases levels of ubiquitylated TOP2-DPCs (Swan et al., 2021). The observed increase in **TOP2-DPCs**

after p97 inhibition (Figure 17) is therefore consistent with the idea that p97 contributes to TOP2-DPC processing. Taken together, these findings support a role for p97 in the repair of mechanistically distinct enzymatic DPCs.

The observed increase in **DNMT1-DPCs** (Figure 17) is in line with earlier observations that p97 activity contributes to the repair of DNMT1-DPCs induced by 5-aza-2'-deoxycytidine (5-aza-dC, decitabine), a cytidine analogue and DNA methylation inhibitor (Weickert et al., 2023). DNMT1 is the maintenance DNA methyltransferase that acts on newly replicated hemimethylated DNA, and upon incorporation of 5-aza-dC into DNA it can become covalently trapped, forming DNMT1-DPCs (Maslov et al., 2012; Santi et al., 1984). In Weickert et al. (2023), p97 inhibition with 5 μM CB-5083 impaired removal of 5-aza-dC-induced DNMT1-DPCs in synchronized HeLa cells, as assessed after a 2 h chase by PxP (purification of x-linked proteins) followed by western blotting, whereas our results extend this observation by showing that p97 inhibition also increases endogenous DNMT1-DPC levels in HeLa cells. The accumulation of DNMT1-DPCs under p97 inhibition therefore further supports that p97 participates in the handling of enzymatic DPCs linked to normal DNA metabolism. In recent years, trapped PARP1 has emerged as a clinically relevant chromatin obstacle, especially in the context of PARP inhibitor treatment, and p97 has been implicated in its removal from chromatin after SUMOylation and ubiquitylation (Krastev et al., 2022). In Krastev et al. (2022), p97 involvement was demonstrated in a PARP-trapping system, in which MMS plus talazoparib-induced chromatin-trapped PARP1 persisted when p97 was inhibited with 10 μM CB-5083, as assessed by chromatin fractionation and western blotting. The increased **PARP1-DPC** accumulation observed here (Figure 17) suggests that p97 also limits accumulation of endogenously occurring PARP1-DPCs. These findings support the idea that p97 acts at the interface between protein quality control and DNA repair by contributing to the repair of DPCs.

Histones are among the most abundant chromatin proteins and are thought to constitute a major fraction of total cellular DPCs, particularly after exposure to nonspecific crosslinking agents such as formaldehyde (Kiianitsa & Maizels, 2020). Accumulation of **histone H3-DPCs** (Figure 17) after p97 inhibition suggests that p97 contributes not only to the repair of enzymatic DPCs. Ku proteins are best known for binding DNA ends during double-strand break repair and can become sterically trapped on DNA. p97 has already been shown to extract trapped Ku70/Ku80 rings from DNA (van den Boom et al., 2016). The observed accumulation of **Ku80-DPCs** (Figure 17) is therefore consistent with the broader view that p97 contributes to the

processing of diverse chromatin-associated proteins that become covalently crosslinked to DNA under physiological conditions.

Taken together, the variety of substrates identified here indicates that p97 functions as an important factor in DPC repair. p97 contributes to the repair of both non-enzymatic (structural) DPCs, such as histone H3-DPCs and Ku80-DPCs, and several classes of enzymatic DPCs, including TOP1-, TOP2-, DNMT1-, and PARP1-DPCs. A plausible model is that p97 acts as a chromatin-associated segregase or remodeler that helps channel distinct DPC lesions into the appropriate downstream processing route. Three modes of action can be envisaged. First, p97 may promote direct extraction of the crosslinked protein from chromatin, as it has been shown to do for several other chromatin-associated substrates, including lesion-stalled RNA polymerase II (Zhu et al., 2024), sterically trapped Ku70/Ku80 rings during DNA double-strand break repair (van den Boom et al., 2016), the DNA polymerase α/primase complex during unperturbed DNA replication (Rodríguez-Acebes et al., 2025), and ubiquitylated Aurora B during mitotic exit (Ramadan et al., 2007). Second, p97 may unfold or remodel DPC substrates to facilitate their proteolytic processing, for example by SPRTN, as proposed for TOP1-DPC repair in the TEX264-p97-SPRTN pathway (Fielden et al., 2020). Third, p97-driven remodeling may facilitate nucleolytic processing and subsequent lesion handover into alternative pathways, such as TEX264-dependent nucleophagy, which requires MRE11 nuclease activity (Lascaux et al., 2024). Although the data presented here do not, on their own, resolve the precise mechanistic position of p97 in the pathway, they clearly demonstrate that p97 contributes to the repair of various cellular DPCs. Together with previous reports, our findings establish p97 as an important factor in DPC repair in human cells. Because impaired DPC processing is linked to genome instability, cancer, and aging (Lessel et al., 2014; Maskey et al., 2017; Tomaskovic et al., 2026), a better understanding of p97-dependent DPC repair may also prove relevant for therapeutic strategies that exploit DPC-inducing agents or target p97 itself. CB-5083, a first-generation p97 inhibitor, entered Phase I trials for advanced solid tumors and for lymphoid hematologic malignancies including multiple myeloma (NCT02243917; NCT02223598), but development was stopped because of ocular adverse effects. CB-5339, a second-generation p97 inhibitor, was then advanced into Phase I testing for relapsed/refractory AML (acute myeloid leukemia), intermediate- or higher-risk MDS (myelodysplastic syndromes), related myeloid neoplasms, and multiple myeloma (NCT04402541). However, because p97 supports many essential cellular functions beyond DPC repair, broad p97 inhibition is likely to be a relatively

blunt therapeutic approach, highlighting the potential value of more selective strategies targeting specialized DPC factors, such as SPRTN or adaptors such as TEX264.

4.2.2. Role of p97 in DPC repair in zebrafish embryos

The zebrafish experiments extended the findings obtained in human cells and provided evidence that p97 contributes to the repair of endogenous DNA-protein crosslinks *in vivo*. Because the effects of NMS-873 and CB-5083 had not previously been characterized in zebrafish embryos, titration experiments were an essential first step. Zebrafish is well suited to this type of analysis because embryos develop externally, are transparent, and permit direct observation of developmental changes after experimental manipulation (Bozkurt, 2020; Lantz-McPeak et al., 2015). Zebrafish p97 is an ortholog of human p97. Ensembl also identifies *zgc:136908* (ENSDARG00000011983) as a paralog of the zebrafish *vcp* gene, indicating that zebrafish contains a related *VCP/p97*-family gene, although this gene remains poorly characterized and is not currently annotated in ZFIN as a second canonical *vcp* gene. Embryos were treated at 24 hpf for 6 h with increasing concentrations of the p97 inhibitors NMS-873 or CB-5083, and both phenotype and selected DPC species were evaluated (Figures 18, 19). This design was appropriate because it allowed assessment of whether acute p97 inhibition was sufficient to produce measurable developmental consequences and whether these consequences paralleled changes in DPC levels. In both cases, a clear dose-response relationship was observed. Thus, even before more detailed DPC analyses were performed, the titration experiments already indicated that zebrafish embryos are highly sensitive to perturbation of p97 activity and that the chosen assay window is suitable for detecting both morphological and biochemical consequences of p97 inhibition *in vivo*.

An important observation was that the two inhibitors did not produce identical phenotypes, although both caused progressively more severe defects as their concentration increased. NMS-873 treatment produced the more severe overall morphological phenotype, characterized by reduced or absent pigmentation, abnormal body curvature, impaired heart development, a shortened and thickened yolk extension, and developmental delay; these defects were already apparent at the lowest concentration tested and became more pronounced at higher doses (Figure 18). By contrast, CB-5083 treatment caused a milder phenotype, characterized mainly by dose-dependent dorsal curvature of the tail tip (Figure 19). Both inhibitors reproducibly perturbed embryonic development and the extent of perturbation correlated with dose. This strongly supports the conclusion that normal p97 activity is required during this

developmental period. The more severe effect of NMS-873 may reflect differences in effective exposure of embryonic tissues to the two compounds. In zebrafish chemical-treatment experiments, the concentration in exposure solution is not identical to the intracellular concentration ultimately achieved in embryonic cells. Small molecules must first cross the embryonic epidermis (because the embryos were dechorionized before collection) and then the cell membranes of different embryonic tissues before they can distribute within the embryo. Two chemically distinct p97 inhibitors may differ substantially in uptake, retention, or efflux, even if both are applied at 20 μM in the medium. A further layer of complexity is metabolism. Developing zebrafish embryos express xenobiotic-metabolizing CYP enzymes, and both the expression of these enzymes and their metabolic activity vary across developmental stages (Nawaji et al., 2020). This means that NMS-873 and CB-5083 could also differ in the rate at which they are biotransformed in embryos, potentially altering their effective half-life or generating metabolites with lower or higher biological activity. Although the present study does not directly address pharmacokinetics in zebrafish embryos, such factors provide a possible explanation for why two p97 inhibitors can produce distinct phenotypes *in vivo*.

The dose-dependent morphological phenotypes were accompanied by dose-dependent increases in specific DPC species (Figures 18, 19). After NMS-873 treatment, histone H3- and Top2-DPC levels increased in a dose-dependent manner compared with untreated WT embryos (Figure 18), whereas CB-5083 caused a dose-dependent increase in Parp1- and Top2-DPC levels (Figure 19) (the same DPC species were not assessed for both inhibitors because of technical limitations of the experiments). Thus, both inhibitors converged on the same general biochemical consequence: accumulation of DPCs in zebrafish embryos. The titration experiments were also valuable because they identified concentrations suitable for subsequent DPC experiments. The choice of 20 μM NMS-873 and 20 μM CB-5083 was justified because both produced robust and readily detectable morphological phenotypes together with clear DPC induction within the 6 h treatment window, and the embryos remained alive at the time of collection.

When the selected concentrations from the titration experiments were used for in depth DPC analysis, inhibition of p97 with either NMS-873 or CB-5083 caused significant accumulation of multiple cellular DPC species in zebrafish embryos, including histone H3-, Ku80-, Parp1-, Top1-, Dnmt1-, and Top2-DPCs (Figure 20). Thus, similarly to the results obtained in HeLa cells (Figure 17), acute pharmacological inhibition of p97 *in vivo* produced a

broad DPC accumulation phenotype. This strongly supports the conclusion that p97 contributes to the repair of multiple endogenous DPCs *in vivo*.

These findings are particularly important because they move the interpretation beyond morphology alone. After 6 h of p97i treatment almost all embryos already displayed an abnormal phenotype (Figures 18, 19, 20), whereas prolonged treatment for 24 h was lethal. However, because p97 is a highly pleiotropic ATPase that functions in multiple pathways, including protein quality control, chromatin-associated turnover, DNA replication, cell-cycle progression, and DNA damage responses (Costantini et al., 2021), the resulting embryonic morphological phenotype cannot be attributed exclusively to defective DPC repair. Rather, the most plausible interpretation is that DPC accumulation represents one important component of a broader collapse of p97-dependent proteostasis and genome-maintenance functions during a developmentally sensitive window. In other words, the embryo phenotype is likely composite: impaired DPC repair probably contributes to it, but is unlikely to be the sole underlying cause.

p97 has already been implicated in the processing of several chromatin-bound DPC or DPC-like substrates in human cells, including TOP1- (Fielden et al., 2020), TOP2- (Swan et al., 2021), and DNMT1-associated lesions (Weickert et al., 2023), as well as trapped PARP1 (Krastev et al., 2022). The zebrafish data are consistent with that framework and this is the first study to demonstrate the role of p97 in DPC repair *in vivo*. In particular, the accumulation of Top1-, Top2-, Dnmt1-, and Parp1-DPCs in embryos (Figure 20) suggests that the spectrum of p97-relevant substrates is not restricted to cultured human cells, but extends to an *in vivo* vertebrate context. At the same time, the observed increase in histone H3- and Ku80-DPCs (Figure 20) indicates that p97 is also relevant for structurally distinct DNA-protein adducts and not only for enzymatic DPCs. Taken together, this broad substrate range suggests that p97 functions as an important general factor in DPC repair *in vivo*.

An important point in the zebrafish experiments is that NMS-873 and CB-5083 did not produce identical outcomes. Although both inhibitors caused a dose-dependent phenotype and both led to DPC accumulation, NMS-873 consistently produced a more severe morphological phenotype (Figure 20). In the broader DPC analysis performed at 20 μM, DPC induction was also generally stronger after NMS-873 treatment than after CB-5083 treatment for most analyzed substrates (approaching or exceeding a twofold stronger induction), with histone H3-DPC representing the only exception (Figure 20). Thus, the biochemical data mostly paralleled the morphological findings: the inhibitor that produced the more severe developmental phenotype also tended to cause the stronger DPC accumulation. Even so, the overall

interpretation remains clear. The fact that both inhibitors caused abnormal embryonic development, that prolonged exposure to either inhibitor led to embryo death, and that both induced accumulation of multiple DPC species strongly supports the conclusion that p97 activity is required during this stage of zebrafish development, as expected given that p97 is an essential cellular factor with broad functions. p97 inhibition resulted in accumulation of multiple endogenous DPCs in HeLa cells and in zebrafish embryos, suggesting that p97 plays a conserved and relatively broad role in DPC homeostasis. In embryos, the functional consequences of p97 inhibition appear especially severe, likely because the rapid pace of development makes the organism highly dependent on uninterrupted protein quality control, chromatin dynamics, and genome maintenance. Under such conditions, even a short period of impaired p97 activity may be sufficient to trigger developmental derailment. Thus, the zebrafish results support a model in which p97 contributes to the repair of multiple endogenous DPCs *in vivo*, but also indicate, as expected, that the developmental consequences of p97 inhibition extend beyond DPC accumulation alone.

An important extension of the zebrafish embryo experiments was the use of morpholino-mediated p97 knockdown as an independent approach to perturb p97 function *in vivo*. This was particularly relevant because the experiments with NMS-873 and CB-5083 could in principle still be influenced by compound-specific properties. By contrast, reduction of p97 levels by injection of a p97 morpholino at the one-cell stage provided a conceptually distinct way to test the same biological question. When p97 morphants were analyzed at 30 hpf, Ku80- and Top2-DPC levels were significantly increased compared with WT embryos, whereas Parp1- and Top1-DPCs showed a similar upward trend (Figure 21). Thus, the morpholino experiments reproduced similar overall effect as the inhibitor experiments, namely accumulation of multiple cellular DPCs upon p97 silencing, and therefore provide an additional line of evidence that p97 contributes to DPC repair in zebrafish embryos. At the same time, the morpholino effect was clearly milder than the effect observed after acute pharmacological inhibition of p97. Unlike embryos treated with NMS-873 or CB-5083, which were already morphologically abnormal after 6 h of treatment (Figure 20) and died upon longer exposure, p97 morphants at 30 hpf did not show obvious phenotypic abnormalities and appeared grossly WT-like (Figure 21). In parallel, the increase in specific DPC species was lower than that seen after inhibitor treatment (Figure 21). This difference is biologically plausible because the splice-blocking morpholino abolished the WT p97 transcript and generated an aberrantly spliced product (Figure 21), indicating efficient disruption of p97 mRNA processing, but does not exclude persistence of

residual p97 protein in the embryos. By contrast, small-molecule inhibitors act directly on the existing p97 protein pool and can therefore suppress p97 function more rapidly and more completely. Residual p97 protein in p97 morphants may thus have been sufficient to maintain normal embryonic morphology, while still permitting measurable accumulation of DPCs.

Another important point is that the morpholino experiments help address the question of specificity of the inhibitor phenotype. In zebrafish embryos, NMS-873 and CB-5083 produced somewhat different morphological outputs and somewhat different relative magnitudes of DPC induction, which most likely reflect differences in mechanism of inhibition, effective intracellular exposure, uptake, retention, efflux, or metabolism. Nevertheless, both compounds converged on the same central biochemical outcome: accumulation of multiple DPC species. The fact that morpholino-mediated reduction of p97 levels also caused DPC accumulation in embryos strongly supports that this shared biochemical phenotype is indeed linked to p97 loss of function.

4.3. Role of SPRTN-p97 interaction in DPC repair in human cells and zebrafish

4.3.1. Role of SPRTN-p97 interaction in DPC repair in human cells

After establishing that p97 contributes broadly to DPC repair, the next relevant question was whether part of this role depends on its functional cooperation with the DPC protease SPRTN. This possibility is biologically plausible, because SPRTN contains a conserved SHP box motif that mediates binding to the N-terminal domain of p97, and previous studies have shown that SPRTN and p97 can cooperate in at least some chromatin-associated repair processes (Kröning et al., 2022; Mosbech et al., 2012). Mosbech et al. (2012) linked the SPRTN-p97 interaction to replication-stress responses by showing that SPRTN recruits p97 to stalled replication forks and facilitates p97-dependent removal of Pol η from UV-induced foci. Kröning et al. (2022) then demonstrated direct biochemical cooperation *in vitro*, where p97-UFD1-NPL4 unfolded a tightly folded Eos-DPC substrate and thereby enabled its proteolysis by SPRTN. It was therefore reasonable to test whether the p97-interacting SHP motif is generally important for SPRTN-dependent repair of endogenous cellular DPCs.

To address this question, an initial rescue system was established in HEK293T cells. Endogenous SPRTN was silenced by siRNA, while cells were transfected with plasmids encoding one of three SPRTN constructs: SPRTN-WT, representing the functional wild-type protein; SPRTN-SHPmut, carrying mutations in the SHP motif and therefore expected to be defective in p97 binding (Mosbech et al., 2012); and SPRTN-E112A, a catalytically inactive active-site mutant used as a negative control for SPRTN protease function (Vaz et al., 2016). This design was intended to provide a rapid assay in which the consequences of SPRTN depletion could be compared with rescue by either the wild-type protein, a p97-binding-defective variant, or a catalytically inactive variant. In this system, silencing of endogenous SPRTN led to the increase of total cellular DPCs, and this increase was observed across all molecular-weight classes (Figure 22). This was consistent with the general conclusion already supported by the literature, namely that SPRTN contributes broadly to DPC repair. This finding also fits well with previous work showing that SPRTN deficiency causes accumulation of endogenous and induced DPCs in proliferating human cells and that SPRTN functions as a general DPC protease during genome maintenance (Maskey et al., 2017; Stingele et al., 2016; Vaz et al., 2016; Weickert et al., 2023).

However, the interpretation of the rescue experiments proved problematic. Overexpression of SPRTN-WT reduced DPC levels relative to SPRTN-silenced cells, which was expected (Figure 22) (Vaz et al., 2016). At first glance, the observation that SPRTN-SHPmut also reduced DPC levels (Figure 22) might have suggested that the interaction with p97 is not essential for DPC repair in this system. The critical problem was that SPRTN-E112A, which should lack proteolytic activity, also reduced DPC levels in the same assay (Figure 22). Because a catalytically inactive SPRTN mutant is not expected to restore SPRTN-dependent DPC proteolysis (Vaz et al., 2016), this result made the system unsuitable for drawing conclusions about the role of the SHP motif. Because the negative control did not behave as expected, the rescue data from this system cannot be used to determine whether the SHP motif is important for DPC repair, and the findings therefore warrant further investigation.

After the HEK293T rescue approach proved inconclusive, a second human-cell system was tested in a more genetically defined SPRTN-deficient background. This model was based on HeLa ΔSPRTN cells originally generated by Vaz et al. (2016), in which two of the three endogenous SPRTN alleles are disrupted (Vaz et al., 2016). Thus, these cells represent a partial rather than complete SPRTN knockout, because one endogenous SPRTN allele remains intact and residual SPRTN expression is still present. Because one endogenous SPRTN allele remains, it cannot be regarded as a true null background, and long-term propagation of this established cell line may also have introduced adaptive changes that influence DPC homeostasis. In addition, the original parental HeLa WT cells from which HeLa ΔSPRTN cells were derived were not available in the present study, meaning that the main comparison had to be made against the ΔSPRTN background itself rather than against a matched WT control. These caveats should be kept in mind when interpreting the rescue experiments in this system. Despite these limitations, the HeLa ΔSPRTN system was more informative than the HEK293T system because the catalytically inactive SPRTN-E112A construct behaved largely as expected and did not efficiently rescue the DPC phenotype. Overexpression of SPRTN-WT and SPRTN-SHPmut reduced total, HMW-, MMW-, and LMW-DPC levels relative to HeLa ΔSPRTN cells (Figure 23). By contrast, SPRTN-E112A produced only a weaker, nonsignificant trend toward reduction in all classes (Figure 23). Thus, unlike in the HEK293T system, the negative control failed to rescue the phenotype, making this assay more suitable for mechanistic interpretation. In this setting, the similar behaviour of SPRTN-WT and SPRTN-SHPmut suggests that the p97-interacting SHP motif is not crucial for bulk repair of endogenous DPCs under basal conditions, at least not to an extent detectable in this assay. Analysis of individual DPC species generally

supported the same conclusion. The strongest evidence was obtained for histone H3-DPCs, which were significantly reduced by both SPRTN-WT and SPRTN-SHPmut compared with HeLa ΔSPRTN cells, whereas rescue by SPRTN-E112A was much weaker (Figure 24). This indicates that SPRTN catalytic activity is required for efficient H3-DPC processing in this system, whereas mutation of the SHP motif does not impair this function. Mostly similar downward trends were observed for Ku80-, PARP1-, TOP1-, DNMT1-, TOP2-, POLR3A-, and MCM2-DPCs (Figure 24), but these analyses were performed only once and therefore should be interpreted cautiously. Among the analyzed proteins, histone-, TOP1-, TOP2- (Vaz et al., 2016), and DNMT1-DPCs (Dürauer et al., 2025; Weickert et al., 2023) have already been linked to SPRTN-dependent processing in human cells. By contrast, Ku80, PARP1, POLR3A, and MCM2 are still not validated SPRTN substrates and, based on the present preliminary data, could be regarded as candidate SPRTN-associated DPC substrates that require further validation.

Taken together, these findings would suggest that direct SPRTN-p97 binding through the SHP motif is not essential for repair of the majority of endogenous DPCs in HeLa ΔSPRTN cells under physiological conditions. However, in this assay, several factors may also have masked a more subtle requirement for p97 binding, including residual endogenous SPRTN from the remaining intact allele, consistent with the finding that the mean *SPRTN* qPCR Ct value in HeLa ΔSPRTN cells (22.8) was similar to that measured in the HeLa WT cells used in our laboratory (22.5), although these were not the parental WT cells from which the mutant line was derived, as discussed above. Nonetheless, the system did not have sufficiently reduced SPRTN activity to allow strong conclusions to be drawn about SPRTN-p97 cooperation in DPC repair. We therefore extended the analysis to zebrafish embryos, where the functional importance of this interaction could be tested *in vivo*.

4.3.2. Role of Sprtn-p97 interaction in DPC repair in zebrafish embryos

In the zebrafish embryo rescue assays, the contribution of the SPRTN-p97 interaction became more apparent than in the human-cell systems. In addition to Sprtn-WT and the p97-binding-defective Sprtn-SHPmut variant, the rescue assay included Sprtn-L147A, designed as the zebrafish counterpart of the RJALS-associated human SPRTN-Y117C variant, which was previously shown to have severely reduced proteolytic activity (Vaz et al., 2016). Nevertheless, because the corresponding residue in zebrafish Sprtn is leucine rather than tyrosine and was substituted with alanine rather than cysteine, the extent to which Sprtn-L147A reproduces the

functional defect of the human Y117C patient variant remains uncertain and should be confirmed in the future using an *in vitro* proteolytic assay. Morpholino-mediated knockdown of endogenous Sprtn caused significant accumulation of Ku80-, Parp1-, Top1-, and Dnmt1-DPCs (Figure 25), indicating that Sprtn contributes to the repair of multiple endogenous DPC species during early embryogenesis. Co-injection of Sprtn-WT mRNA reduced Ku80-, Parp1-, and Dnmt1-DPC levels to near-WT levels and partially rescued Top1-DPCs (Figure 25), supporting the specificity of the morpholino phenotype and indicating that Ku80-, Parp1-, Top1-, and Dnmt1-DPCs represent endogenous DPC species whose repair depends on Sprtn *in vivo*. All injected embryos, including those expressing Sprtn-SHPmut, were grossly WT-like at 30 hpf. In embryos expressing Sprtn-SHPmut, Parp1-, Top1-, and Dnmt1-DPCs remained significantly elevated relative to WT embryos (Figure 25), suggesting that SHP motif-mediated binding to p97 contributes to repair of at least a subset of endogenous DPCs *in vivo*. At the same time, because the degree of rescue varied between experiments and expression of the injected constructs was confirmed only at the mRNA level, but not at the protein level at this stage, these results should be considered indicative and will require additional experimental investigations before firmer conclusions can be drawn. Previous work demonstrated that functional cooperation between SPRTN and p97 is required for efficient TOP1-DPC repair in human cells (Fielden et al., 2020), whereas a later study from the same group suggested that SPRTN is dispensable for TEX264-dependent selective nucleophagy of TOP1-DPCs, indicating that p97 can also promote TOP1-DPC processing through a SPRTN-independent route (Lascaux et al., 2024).

In summary, in HEK293T cells, the rescue assay remained inconclusive because the catalytic negative control did not behave as expected. In HeLa ΔSPRTN cells, interpretation was likewise limited by the caveats of this system discussed above, precluding firm conclusions about the importance of the SHP motif for the repair of endogenous DPCs. The embryo experiments added an important *in vivo* perspective by suggesting that direct SPRTN-p97 coupling might be relevant for repair of endogenous Parp1-, Top1-, and Dnmt1-DPCs. Thus, the combined data support a model in which p97 has a broad and prominent role in DPC repair, whereas its direct functional cooperation with SPRTN through the SHP motif requires further investigation.

5. CONCLUSIONS

This study identifies **ACRC** as an essential factor in DNA-protein crosslink repair during early vertebrate development. In zebrafish, embryo survival depended on an intact Acrc SprT domain and, in particular, on its catalytic core, showing that the proteolytic activity of Acrc is crucial. Loss of Acrc function led to early accumulation of multiple endogenous DPC species before overt developmental collapse, and rescue experiments showed that the SprT domain, but not the IDR (intrinsically disordered region) alone, is required for the Acrc function. The data further indicated that Acrc and Sprtn are not functionally redundant at this developmental stage. Our findings establish ACRC as an essential DPC protease in vertebrate embryogenesis and broaden the range of endogenous lesions linked to Acrc to include Dnmt1-, Top1-, Top2-, histone H3-, Parp1-, Polr3a-, and Mcm2-DPCs.

Furthermore, the study shows that **p97** is an important and conserved regulator of DPC homeostasis in vertebrates. In HeLa cells, acute inhibition of p97 with two mechanistically distinct inhibitors (NMS-873 and CB-5083) caused accumulation of total cellular DPCs and of several specific DPC species, including histone H3-, Ku80-, PARP1-, TOP1-, DNMT1-, and TOP2-DPCs, indicating that p97 contributes broadly to the repair of endogenous DNA-protein crosslinks. The zebrafish experiments extended this conclusion *in vivo*: both pharmacological inhibition and morpholino-mediated silencing of p97 increased DPC levels in embryos, while acute inhibitor treatment also caused pronounced developmental abnormalities and lethality upon prolonged exposure. Taken together, these results indicate that p97 contributes to repair of multiple endogenous DPCs at both the cellular and organismal level, although the developmental phenotype in embryos most likely reflects not only defective DPC repair but also broader impairment of essential p97-dependent functions.

Finally, the results suggest that direct functional coupling between **p97 and SPRTN** might contribute to DPC repair in a context-dependent manner. In the human-cell systems, the importance of the SPRTN SHP motif remained unresolved because the rescue assays were limited by the behavior of the controls and by the properties of the available cell models. In contrast, the zebrafish embryo rescue experiments suggested that impaired p97 binding to Sprtn *in vivo* could compromise repair of some endogenous DPCs, specifically Parp1-, Top1-, and Dnmt1-associated lesions. Overall, the combined data support a model in which p97 has a broad role in DPC repair, whereas its direct cooperation with SPRTN warrants further investigation.

6. REFERENCES

Abugable, A. A., Morris, J. L. M., Palminha, N. M., Zaksauskaite, R., Ray, S., & El-Khamisy, S. F. (2019). DNA repair and neurological disease: From molecular understanding to the development of diagnostics and model organisms. *DNA Repair, Cutting-Edge Perspectives in Genomic Maintenance VI*, *81*, 102669. https://doi.org/10.1016/j.dnarep.2019.102669

Akdogan-Ozdilek, B., Duval, K. L., & Goll, M. G. (2020). Chromatin dynamics at the maternal to zygotic transition: Recent advances from the zebrafish model. *F1000Research*, *9*, F1000 Faculty Rev-299. https://doi.org/10.12688/f1000research.21809.1

Alberts, B., Heald, R., Johnson, A., Morgan, D., Raff, M., Roberts, K., & Walter, P. (2022). *Molecular Biology of the Cell (Seventh Edition)*. W. W. Norton, Incorporated.

Aleström, P., D'Angelo, L., Midtlyng, P. J., Schorderet, D. F., Schulte-Merker, S., Sohm, F., & Warner, S. (2020). Zebrafish: Housing and husbandry recommendations. *Laboratory Animals*, *54*(3), 213–224. https://doi.org/10.1177/0023677219869037

Allier, C., Vincent, R., Navarro, F., Menneteau, M., Ghenim, L., Gidrol, X., Bordy, T., Hervé, L., Cioni, O., Bardin, S., Bornens, M., Usson, Y., & Morales, S. (2018). Lens-free Video Microscopy for the Dynamic and Quantitative Analysis of Adherent Cell Culture. *Journal of Visualized Experiments : JoVE*, (132), 56580. https://doi.org/10.3791/56580

Álvarez-Quilón, A., Wojtaszek, J. L., Mathieu, M.-C., Patel, T., Appel, C. D., Hustedt, N., Rossi, S. E., Wallace, B. D., Setiaputra, D., Adam, S., Ohashi, Y., Melo, H., Cho, T., Gervais, C., Muñoz, I. M., Grazzini, E., Young, J. T. F., Rouse, J., Zinda, M., … Durocher, D. (2020). Endogenous DNA 3′ blocks are vulnerabilities for BRCA1 and BRCA2 deficiency and are reversed by the APE2 nuclease. *Molecular Cell*, *78*(6), 1152-1165.e8. https://doi.org/10.1016/j.molcel.2020.05.021

Anderson, D. J., Le Moigne, R., Djakovic, S., Kumar, B., Rice, J., Wong, S., Wang, J., Yao, B., Valle, E., von Soly, S. K., Madriaga, A., Soriano, F., Menon, M.-K., Wu, Z. Y., Kampmann, M., Chen, Y., Weissman, J. S., Aftab, B. T., Yakes, F. M., … Rolfe, M. (2015). Targeting the AAA ATPase p97 as an approach to treat cancer through disruption of protein homeostasis. *Cancer Cell*, *28*(5), 653–665. https://doi.org/10.1016/j.ccell.2015.10.002

Anticevic, I., Otten, C., & Popovic, M. (2024). Tyrosyl-DNA phosphodiesterase 2 (Tdp2) repairs DNA-protein crosslinks and protects against double strand breaks in vivo. *Frontiers in Cell and Developmental Biology*, *12*. https://doi.org/10.3389/fcell.2024.1394531

Anticevic, I., Otten, C., Vinkovic, L., Jukic, L., & Popovic, M. (2023). Tyrosyl-DNA phosphodiesterase 1 (TDP1) and SPRTN protease repair histone 3 and topoisomerase 1 DNA–protein crosslinks in vivo. *Open Biology*, *13*(10), 230113. https://doi.org/10.1098/rsob.230113

Aparicio, T., Baer, R., Gottesman, M., & Gautier, J. (2016). MRN, CtIP, and BRCA1 mediate repair of topoisomerase II–DNA adducts. *The Journal of Cell Biology*, *212*(4), 399–408. https://doi.org/10.1083/jcb.201504005

Ashour, M. E., Atteya, R., & El-Khamisy, S. F. (2015). Topoisomerase-mediated chromosomal break repair: An emerging player in many games. *Nature Reviews Cancer*, *15*(3), 137–151. https://doi.org/10.1038/nrc3892

Bacurio, J. H. T., Yawson, P., Thomforde, J., Zhang, Q., Kumar, H. V., Den Hartog, H., Tretyakova, N. Y., & Basu, A. K. (2024). 5-Formylcytosine mediated DNA-peptide cross-link induces predominantly semi-targeted mutations in both *Escherichia coli* and human cells. *Journal of Biological Chemistry*, *300*(4), 105786. https://doi.org/10.1016/j.jbc.2024.105786

Bard, J. A. M., Goodall, E. A., Greene, E. R., Jonsson, E., Dong, K. C., & Martin, A. (2018). Structure and Function of the 26S Proteasome. *Annual Review of Biochemistry*, *87*, 697–724. https://doi.org/10.1146/annurev-biochem-062917-011931

Berasain, C., & Avila, M. A. (2015). Regulation of hepatocyte identity and quiescence. *Cellular and Molecular Life Sciences: CMLS*, *72*(20), 3831–3851. https://doi.org/10.1007/s00018-015-1970-7

Bhargava, V., Goldstein, C. D., Russell, L., Xu, L., Ahmed, M., Li, W., Casey, A., Servage, K., Kollipara, R., Picciarelli, Z., Kittler, R., Yatsenko, A., Carmell, M., Orth, K., Amatruda, J. F., Yanowitz, J. L., & Buszczak, M. (2020). GCNA Preserves Genome Integrity and Fertility Across Species. *Developmental Cell*, *52*(1), 38—-52.e10. https://doi.org/10.1016/j.devcel.2019.11.007

Bodnar, N., & Rapoport, T. (2017). Toward an understanding of the Cdc48/p97 ATPase. *F1000Research*, *6*, 1318. https://doi.org/10.12688/f1000research.11683.1

Borgermann, N., Ackermann, L., Schwertman, P., Hendriks, I. A., Thijssen, K., Liu, J. C., Lans, H., Nielsen, M. L., & Mailand, N. (2019). SUMO ylation promotes protective responses to DNA -protein crosslinks. *The EMBO Journal*, *38*(8), 1–17. https://doi.org/10.15252/embj.2019101496

Bouwer, M. F., Hamilton, K. E., Jonker, P. B., Kuiper, S. R., Louters, L. L., & Looyenga, B. D. (2021). NMS-873 Functions as a Dual Inhibitor of Mitochondrial Oxidative Phosphorylation. *Biochimie*, *185*, 33–42. https://doi.org/10.1016/j.biochi.2021.03.004

Bozkurt, Y. (2020). Introductory Chapter: Importance of Zebrafish (Danio rerio) as Model Organism in Biomedical Research. In *Zebrafish in Biomedical Research*. IntechOpen. https://doi.org/10.5772/intechopen.91319

Brégeon, D., & Doetsch, P. W. (2011). Transcriptional mutagenesis: Causes and involvement in tumor development. *Nature Reviews. Cancer*, *11*(3), 218–227. https://doi.org/10.1038/nrc3006

Carmell, M. A., Dokshin, G. A., Skaletsky, H., Hu, Y. C., van Wolfswinkel, J. C., Igarashi, K. J., Bellott, D. W., Nefedov, M., Reddien, P. W., Enders, G. C., Uversky, V. N., Mello, C. C., & Page, D. C. (2016). A widely employed germ cell marker is an ancient disordered protein with reproductive functions in diverse eukaryotes. *eLife*, *5*(OCTOBER2016), 1–25. https://doi.org/10.7554/eLife.19993

Carnie, C. J., Acampora, A. C., Bader, A. S., Erdenebat, C., Zhao, S., Bitensky, E., van den Heuvel, D., Parnas, A., Gupta, V., D'Alessandro, G., Sczaniecka-Clift, M., Weickert, P., Aygenli, F., Götz, M. J., Cordes, J., Esain-Garcia, I., Melidis, L., Wondergem, A. P., Lam, S., … Stingele, J. (2024). Transcription-coupled repair of DNA–protein cross-

links depends on CSA and CSB. *Nature Cell Biology*, *26*(5), 797–810. https://doi.org/10.1038/s41556-024-01391-1

Cervera, L., Gutiérrez, S., Gòdia, F., & Segura, M. M. (2011). Optimization of HEK 293 cell growth by addition of non-animal derived components using design of experiments. *BMC Proceedings*, *5*(Suppl 8), P126. https://doi.org/10.1186/1753-6561-5-S8-P126

Chen, J., Potlapalli, R., Quan, H., Chen, L., Xie, Y., Pouriyeh, S., Sakib, N., Liu, L., & Xie, Y. (2024). Exploring DNA Damage and Repair Mechanisms: A Review with Computational Insights. *BioTech*, *13*(1), 3. https://doi.org/10.3390/biotech13010003

Chu, X.-L. (1981). A Preliminary Revision of Fishes of The Genus Danio From China. *Zoological Research*, *2*(2), 145–156. https://www.zoores.ac.cn/en/article/id/1540

Cortez, D. (2019). Replication-coupled DNA Repair. *Molecular Cell*, *74*(5), 866–876. https://doi.org/10.1016/j.molcel.2019.04.027

Costantini, S., Capone, F., Polo, A., Bagnara, P., & Budillon, A. (2021). Valosin-Containing Protein (VCP)/p97: A Prognostic Biomarker and Therapeutic Target in Cancer. *International Journal of Molecular Sciences*, *22*(18), 10177. https://doi.org/10.3390/ijms221810177

Davis, E. J., Lachaud, C., Appleton, P., Macartney, T. J., Näthke, I., & Rouse, J. (2012). DVC1 (C1orf124) recruits the p97 protein segregase to sites of DNA damage. *Nature Structural & Molecular Biology*, *19*(11), 1093–1100. https://doi.org/10.1038/nsmb.2394

Delabaere, L., Orsi, G. A., Sapey-Triomphe, L., Horard, B., Couble, P., & Loppin, B. (2014). The Spartan Ortholog Maternal Haploid Is Required for Paternal Chromosome Integrity in the Drosophila Zygote. *Current Biology*, *24*(19), 2281–2287. https://doi.org/10.1016/j.cub.2014.08.010

Deshpande, R. A., Lee, J.-H., Arora, S., & Paull, T. T. (2016). Nbs1 Converts the Human Mre11/Rad50 Nuclease Complex into an Endo/Exonuclease Machine Specific for Protein-DNA Adducts. *Molecular Cell*, *64*(3), 593–606. https://doi.org/10.1016/j.molcel.2016.10.010

Dirac-Svejstrup, A. B., Walker, J., Faull, P., Encheva, V., Akimov, V., Puglia, M., Perkins, D., Kümper, S., Hunjan, S. S., Blagoev, B., Snijders, A. P., Powell, D. J., & Svejstrup, J. Q. (2020). DDI2 Is a Ubiquitin-Directed Endoprotease Responsible for Cleavage of Transcription Factor NRF1. *Molecular Cell*, *79*(2), 332-341.e7. https://doi.org/10.1016/j.molcel.2020.05.035

Dokshin, G. A., Davis, G. M., Sawle, A. D., Eldridge, M. D., Nicholls, P. K., Gourley, T. E., Romer, K. A., Molesworth, L. W., Tatnell, H. R., Ozturk, A. R., de Rooij, D. G., Hannon, G. J., Page, D. C., Mello, C. C., & Carmell, M. A. (2020). GCNA Interacts with Spartan and Topoisomerase II to Regulate Genome Stability. *Developmental Cell*, *52*(1), 53-68.e6. https://doi.org/10.1016/j.devcel.2019.11.006

Donsbach, M., Dürauer, S., Grünert, F., Nguyen, K. T., Nigam, R., Yaneva, D., Weickert, P., Bezalel-Buch, R., Semlow, D. R., & Stingele, J. (2023). A non-proteolytic release mechanism for HMCES-DNA-protein crosslinks. *The EMBO Journal*, *42*(18), e113360. https://doi.org/10.15252/embj.2022113360

Dürauer, S., Kang, H.-S., Wiebeler, C., Machida, Y., Schnapka, D. S., Yaneva, D., Renz, C., Götz, M. J., Weickert, P., Major, A. C., Rahmanto, A. S., Gutenthaler-Tietze, S. M.,

Daumann, L. J., Beli, P., Ulrich, H. D., Sattler, M., Machida, Y. J., Schwierz, N., & Stingele, J. (2025). Allosteric activation of the SPRTN protease by ubiquitin maintains genome stability. *Nature Communications*, *16*(1), 5422. https://doi.org/10.1038/s41467-025-61224-z

Duxin, J. P., Dewar, J. M., Yardimci, H., & Walter, J. C. (2014). Repair of a DNA-protein crosslink by replication-coupled proteolysis. *Cell*, *159*(2), 346–357. https://doi.org/10.1016/j.cell.2014.09.024

Fábián, Z., Kakulidis, E. S., Hendriks, I. A., Kühbacher, U., Larsen, N. B., Oliva-Santiago, M., Wang, J., Leng, X., Dirac-Svejstrup, A. B., Svejstrup, J. Q., Nielsen, M. L., Caldecott, K., & Duxin, J. P. (2024). PARP1-dependent DNA-protein crosslink repair. *Nature Communications*, *15*, 6641. https://doi.org/10.1038/s41467-024-50912-x

Fielden, J., Ruggiano, A., Popović, M., & Ramadan, K. (2018). DNA protein crosslink proteolysis repair: From yeast to premature ageing and cancer in humans. *DNA Repair*, *71*, 198–204. https://doi.org/10.1016/j.dnarep.2018.08.025

Fielden, J., Wiseman, K., Torrecilla, I., Li, S., Hume, S., Chiang, S.-C., Ruggiano, A., Narayan Singh, A., Freire, R., Hassanieh, S., Domingo, E., Vendrell, I., Fischer, R., Kessler, B. M., Maughan, T. S., El-Khamisy, S. F., & Ramadan, K. (2020). TEX264 coordinates p97- and SPRTN-mediated resolution of topoisomerase 1-DNA adducts. *Nature Communications*, *11*(1), 1274. https://doi.org/10.1038/s41467-020-15000-w

Flinn, L., Bretaud, S., Lo, C., Ingham, P. W., & Bandmann, O. (2008). Zebrafish as a new animal model for movement disorders. *Journal of Neurochemistry*, *106*(5), 1991–1997. https://doi.org/10.1111/j.1471-4159.2008.05463.x

Gaillard, H., García-Muse, T., & Aguilera, A. (2015). Replication stress and cancer. *Nature Reviews Cancer*, *15*(5), 276–289. https://doi.org/10.1038/nrc3916

Gao, R., Schellenberg, M. J., Huang, S. N., Abdelmalak, M., Marchand, C., Nitiss, K. C., Nitiss, J. L., Williams, R. S., & Pommier, Y. (2014). Proteolytic Degradation of Topoisomerase II (Top2) Enables the Processing of Top2·DNA and Top2·RNA Covalent Complexes by Tyrosyl-DNA-Phosphodiesterase 2 (TDP2) ♦. *The Journal of Biological Chemistry*, *289*(26), 17960–17969. https://doi.org/10.1074/jbc.M114.565374

Ghodke, P. P., Gonzalez-Vasquez, G., Wang, H., Johnson, K. M., Sedgeman, C. A., & Guengerich, F. P. (2021). Enzymatic bypass of an N6-deoxyadenosine DNA–ethylene dibromide–peptide cross-link by translesion DNA polymerases. *The Journal of Biological Chemistry*, *296*, 100444. https://doi.org/10.1016/j.jbc.2021.100444

Grisham, J. W. (1962). A Morphologic Study of Deoxyribonucleic Acid Synthesis and Cell Proliferation in Regenerating Rat Liver; Autoradiography with Thymidine-H3*. *Cancer Research*, *22*(7_Part_1), 842–849.

Halder, S., Torrecilla, I., Burkhalter, M. D., Popović, M., Fielden, J., Vaz, B., Oehler, J., Pilger, D., Lessel, D., Wiseman, K., Singh, A. N., Vendrell, I., Fischer, R., Philipp, M., & Ramadan, K. (2019). SPRTN protease and checkpoint kinase 1 cross-activation loop safeguards DNA replication. *Nature Communications*, *10*(1), 3142. https://doi.org/10.1038/s41467-019-11095-y

Hardy, J. J., Wyrwoll, M. J., Mcfadden, W., Malcher, A., Rotte, N., Pollock, N. C., Munyoki, S., Veroli, M. V., Houston, B. J., Xavier, M. J., Kasak, L., Punab, M., Laan, M., Kliesch, S., Schlegel, P., Jaffe, T., Hwang, K., Vukina, J., Brieño-Enríquez, M. A., … Yatsenko,

A. N. (2021). Variants in GCNA, X-linked germ-cell genome integrity gene, identified in men with primary spermatogenic failure. *Human Genetics*, *140*(8), 1169–1182. https://doi.org/10.1007/s00439-021-02287-y

Heck, H. d'A., & Casanova, M. (2004). The implausibility of leukemia induction by formaldehyde: A critical review of the biological evidence on distant-site toxicity. *Regulatory Toxicology and Pharmacology*, *40*(2), 92–106. https://doi.org/10.1016/j.yrtph.2004.05.001

Hill, A. J., Teraoka, H., Heideman, W., & Peterson, R. E. (2005). Zebrafish as a Model Vertebrate for Investigating Chemical Toxicity. *Toxicological Sciences*, *86*(1), 6–19. https://doi.org/10.1093/toxsci/kfi110

Hoa, N. N., Shimizu, T., Zhou, Z. W., Wang, Z.-Q., Deshpande, R. A., Paull, T. T., Akter, S., Tsuda, M., Furuta, R., Tsutsui, K., Takeda, S., & Sasanuma, H. (2016). Mre11 Is Essential for the Removal of Lethal Topoisomerase 2 Covalent Cleavage Complexes. *Molecular Cell*, *64*(3), 580–592. https://doi.org/10.1016/j.molcel.2016.10.011

Hoch, N. C. (2023). Tissue Specificity of DNA Damage and Repair. *Physiology*, *38*(5), 231–241. https://doi.org/10.1152/physiol.00006.2023

Hoffmann, S., Pentakota, S., Mund, A., Haahr, P., Coscia, F., Gallo, M., Mann, M., Taylor, N. M., & Mailand, N. (2020). FAM111 protease activity undermines cellular fitness and is amplified by gain-of-function mutations in human disease. *EMBO Reports*, *21*(10), e50662. https://doi.org/10.15252/embr.202050662

Howe, K., Clark, M. D., Torroja, C. F., Torrance, J., Berthelot, C., Muffato, M., Collins, J. E., Humphray, S., McLaren, K., Matthews, L., McLaren, S., Sealy, I., Caccamo, M., Churcher, C., Scott, C., Barrett, J. C., Koch, R., Rauch, G.-J., White, S., … Stemple, D. L. (2013). The zebrafish reference genome sequence and its relationship to the human genome. *Nature*, *496*(7446), 498–503. https://doi.org/10.1038/nature12111

Hsiang, Y. H., Lihou, M. G., & Liu, L. F. (1989). Arrest of replication forks by drug-stabilized topoisomerase I-DNA cleavable complexes as a mechanism of cell killing by camptothecin. *Cancer Research*, *49*(18), 5077–5082.

Huang, J., Zhou, Q., Gao, M., Nowsheen, S., Zhao, F., Kim, W., Zhu, Q., Kojima, Y., Yin, P., Zhang, Y., Guo, G., Tu, X., Deng, M., Luo, K., Qin, B., Machida, Y., & Lou, Z. (2020). Tandem Deubiquitination and Acetylation of SPRTN Promotes DNA-Protein Crosslink Repair and Protects against Aging. *Molecular Cell*, *79*(5), 824-835.e5. https://doi.org/10.1016/j.molcel.2020.06.027

Ide, H., Nakano, T., Salem, A. M. H., & Shoulkamy, M. I. (2018). DNA–protein cross-links: Formidable challenges to maintaining genome integrity. *DNA Repair, Cutting-Edge Perspectives in Genomic Maintenance V*, *71*, 190–197. https://doi.org/10.1016/j.dnarep.2018.08.024

Isojima, T., Doi, K., Mitsui, J., Oda, Y., Tokuhiro, E., Yasoda, A., Yorifuji, T., Horikawa, R., Yoshimura, J., Ishiura, H., Morishita, S., Tsuji, S., & Kitanaka, S. (2014). A recurrent de novo FAM111A mutation causes kenny–caffey syndrome type 2. *Journal of Bone and Mineral Research*, *29*(4), 992–998. https://doi.org/10.1002/jbmr.2091

Jackson, S. P., & Bartek, J. (2009). The DNA-damage response in human biology and disease. *Nature*, *461*(7267), 1071–1078. https://doi.org/10.1038/nature08467

Kiianitsa, K., & Maizels, N. (2013). A rapid and sensitive assay for DNA–protein covalent complexes in living cells. *Nucleic Acids Research*, *41*(9), e104. https://doi.org/10.1093/nar/gkt171

Kiianitsa, K., & Maizels, N. (2020). The "adductome": A limited repertoire of adducted proteins in human cells. *DNA Repair*, *89*, 102825. https://doi.org/10.1016/j.dnarep.2020.102825

Kojima, Y., Machida, Y., Palani, S., Caulfield, T. R., Radisky, E. S., Kaufmann, S. H., & Machida, Y. J. (2020). FAM111A protects replication forks from protein obstacles via its trypsin-like domain. *Nature Communications*, *11*(1), 1318. https://doi.org/10.1038/s41467-020-15170-7

Krastev, D. B., Li, S., Sun, Y., Wicks, A. J., Hoslett, G., Weekes, D., Badder, L. M., Knight, E. G., Marlow, R., Pardo, M. C., Yu, L., Talele, T. T., Bartek, J., Choudhary, J. S., Pommier, Y., Pettitt, S. J., Tutt, A. N. J., Ramadan, K., & Lord, C. J. (2022). The ubiquitin-dependent ATPase p97 removes cytotoxic trapped PARP1 from chromatin. *Nature Cell Biology*, *24*(1), 62–73. https://doi.org/10.1038/s41556-021-00807-6

Kröning, A., van den Boom, J., Kracht, M., Kueck, A. F., & Meyer, H. (2022). Ubiquitin-directed AAA+ ATPase p97/VCP unfolds stable proteins crosslinked to DNA for proteolysis by SPRTN. *The Journal of Biological Chemistry*, *298*(6), 101976. https://doi.org/10.1016/j.jbc.2022.101976

Kühbacher, U., & Duxin, J. P. (2020). How to fix DNA-protein crosslinks. *DNA Repair*, *94*, 102924. https://doi.org/10.1016/j.dnarep.2020.102924

Kumari, A., Lim, Y. X., Newell, A. H., Olson, S. B., & McCullough, A. K. (2012). Formaldehyde-Induced Genome Instability is Suppressed by an XPF-dependent Pathway. *DNA Repair*, *11*(3), 236–246. https://doi.org/10.1016/j.dnarep.2011.11.001

Lantz-McPeak, S., Guo, X., Cuevas, E., Dumas, M., Newport, G. D., Ali, S. F., Paule, M. G., & Kanungo, J. (2015). Developmental toxicity assay using high content screening of zebrafish embryos. *Journal of Applied Toxicology : JAT*, *35*(3), 261–272. https://doi.org/10.1002/jat.3029

Larsen, N. B., Gao, A. O., Sparks, J. L., Gallina, I., Wu, R. A., Mann, M., Räschle, M., Walter, J. C., & Duxin, J. P. (2019). Replication-Coupled DNA-Protein Crosslink Repair by SPRTN and the Proteasome in Xenopus Egg Extracts. *Molecular Cell*, *73*(3), 574-588.e7. https://doi.org/10.1016/j.molcel.2018.11.024

Lascaux, P., Hoslett, G., Tribble, S., Trugenberger, C., Antičević, I., Otten, C., Torrecilla, I., Koukouravas, S., Zhao, Y., Yang, H., Aljarbou, F., Ruggiano, A., Song, W., Peron, C., Deangeli, G., Domingo, E., Bancroft, J., Carrique, L., Johnson, E., … Ramadan, K. (2024). TEX264 drives selective autophagy of DNA lesions to promote DNA repair and cell survival. *Cell*, *187*(20), 5698-5718.e26. https://doi.org/10.1016/j.cell.2024.08.020

Leinonen, H., Cheng, C., Pitkänen, M., Sander, C. L., Zhang, J., Saeid, S., Turunen, T., Shmara, A., Weiss, L., Ta, L., Ton, T., Koskelainen, A., Vargas, J. D., Kimonis, V., & Palczewski, K. (2021). A p97/Valosin-Containing Protein Inhibitor Drug CB-5083 Has a Potent but Reversible Off-Target Effect on Phosphodiesterase-6. *The Journal of Pharmacology and Experimental Therapeutics*, *378*(1), 31–41. https://doi.org/10.1124/jpet.120.000486

Lessel, D., Vaz, B., Halder, S., Lockhart, P. J., Marinovic-Terzic, I., Lopez-Mosqueda, J., Philipp, M., Sim, J. C. H., Smith, K. R., Oehler, J., Cabrera, E., Freire, R., Pope, K.,

Nahid, A., Norris, F., Leventer, R. J., Delatycki, M. B., Barbi, G., von Ameln, S., … Kubisch, C. (2014). Mutations in SPRTN cause early onset hepatocellular carcinoma, genomic instability and progeroid features. *Nature Genetics*, *46*(11), 1239–1244. https://doi.org/10.1038/ng.3103

Li, F., Raczynska, J. E., Chen, Z., & Yu, H. (2019). Structural Insight into DNA-Dependent Activation of Human Metalloprotease Spartan. *Cell Reports*, *26*(12), 3336-3346.e4. https://doi.org/10.1016/j.celrep.2019.02.082

Li, Q., Qian, W., Zhang, Y., Hu, L., Chen, S., & Xia, Y. (2023). A new wave of innovations within the DNA damage response. *Signal Transduction and Targeted Therapy*, *8*(1), 338. https://doi.org/10.1038/s41392-023-01548-8

Lieschke, G. J., & Currie, P. D. (2007). Animal models of human disease: Zebrafish swim into view. *Nature Reviews Genetics*, *8*(5), 353–367. https://doi.org/10.1038/nrg2091

Lopez-Mosqueda, J., Maddi, K., Prgomet, S., Kalayil, S., Marinovic-Terzic, I., Terzic, J., & Dikic, I. (2016). SPRTN is a mammalian DNA-binding metalloprotease that resolves DNA-protein crosslinks. *eLife*, *5*, e21491. https://doi.org/10.7554/eLife.21491

Maddi, K., Sam, D. K., Bonn, F., Prgomet, S., Tulowetzke, E., Akutsu, M., Lopez-Mosqueda, J., & Dikic, I. (2020). Wss1 Promotes Replication Stress Tolerance by Degrading Histones. *Cell Reports*, *30*(9), 3117-3126.e4. https://doi.org/10.1016/j.celrep.2020.02.018

Magnaghi, P., D'Alessio, R., Valsasina, B., Avanzi, N., Rizzi, S., Asa, D., Gasparri, F., Cozzi, L., Cucchi, U., Orrenius, C., Polucci, P., Ballinari, D., Perrera, C., Leone, A., Cervi, G., Casale, E., Xiao, Y., Wong, C., Anderson, D. J., … Isacchi, A. (2013). Covalent and allosteric inhibitors of the ATPase VCP/p97 induce cancer cell death. *Nature Chemical Biology*, *9*(9), 548–556. https://doi.org/10.1038/nchembio.1313

Maskey, R. S., Flatten, K. S., Sieben, C. J., Peterson, K. L., Baker, D. J., Nam, H.-J., Kim, M. S., Smyrk, T. C., Kojima, Y., Machida, Y., Santiago, A., van Deursen, J. M., Kaufmann, S. H., & Machida, Y. J. (2017). Spartan deficiency causes accumulation of Topoisomerase 1 cleavage complexes and tumorigenesis. *Nucleic Acids Research*, *45*(8), 4564–4576. https://doi.org/10.1093/nar/gkx107

Maskey, R. S., Kim, M. S., Baker, D. J., Childs, B., Malureanu, L. A., Jeganathan, K. B., Machida, Y., van Deursen, J. M., & Machida, Y. J. (2014). Spartan deficiency causes genomic instability and progeroid phenotypes. *Nature Communications*, *5*, 5744. https://doi.org/10.1038/ncomms6744

Maslov, A. Y., Lee, M., Gundry, M., Gravina, S., Strogonova, N., Tazearslan, C., Bendebury, A., Suh, Y., & Vijg, J. (2012). 5-Aza-2′-deoxycytidine-induced genome rearrangements are mediated by DNMT1. *Oncogene*, *31*(50), 5172–5179. https://doi.org/10.1038/onc.2012.9

Masters, J. R. (2002). HeLa cells 50 years on: The good, the bad and the ugly. *Nature Reviews Cancer*, *2*(4), 315–319. https://doi.org/10.1038/nrc775

Modzelewski, A. J., Chen, S., Willis, B. J., Lloyd, K. C. K., Wood, J. A., & He, L. (2018). Efficient mouse genome engineering by CRISPR-EZ (CRISPR RNP Electroporation of Zygotes) technology. *Nature Protocols*, *13*(6), 1253–1274. https://doi.org/10.1038/nprot.2018.012

Mohni, K. N., Wessel, S. R., Zhao, R., Wojciechowski, A. C., Luzwick, J. W., Layden, H., Eichman, B. F., Thompson, P. S., Mehta, K. P. M., & Cortez, D. (2019). HMCES maintains genome integrity by shielding abasic sites in single strand DNA. *Cell*, *176*(1–2), 144-153.e13. https://doi.org/10.1016/j.cell.2018.10.055

Mórocz, M., Zsigmond, E., Tóth, R., Enyedi, M. Z., Pintér, L., & Haracska, L. (2017). DNA-dependent protease activity of human Spartan facilitates replication of DNA–protein crosslink-containing DNA. *Nucleic Acids Research*, *45*(6), 3172–3188. https://doi.org/10.1093/nar/gkw1315

Mosbech, A., Gibbs-Seymour, I., Kagias, K., Thorslund, T., Beli, P., Povlsen, L., Nielsen, S. V., Smedegaard, S., Sedgwick, G., Lukas, C., Hartmann-Petersen, R., Lukas, J., Choudhary, C., Pocock, R., Bekker-Jensen, S., & Mailand, N. (2012). DVC1 (C1orf124) is a DNA damage-targeting p97 adaptor that promotes ubiquitin-dependent responses to replication blocks. *Nature Structural & Molecular Biology*, *19*(11), 1084–1092. https://doi.org/10.1038/nsmb.2395

Moulton, J. D. (2007). Using morpholinos to control gene expression. *Current Protocols in Nucleic Acid Chemistry*, *Chapter 4*(1), Unit 4.30. https://doi.org/10.1002/0471142700.nc0430s27

Muller, P. Y., Janovjak, H., Miserez, A. R., & Dobbie, Z. (2002). Processing of gene expression data generated by quantitative real-time RT-PCR. *BioTechniques*, *32*(6), 1372–1374, 1376, 1378–1379.

Na, J., Newman, J. A., Then, C. K., Syed, J., Vendrell, I., Torrecilla, I., Ellermann, S., Ramadan, K., Fischer, R., & Kiltie, A. E. (2021). SPRTN protease-cleaved MRE11 decreases DNA repair and radiosensitises cancer cells. *Cell Death & Disease*, *12*(2), 165. https://doi.org/10.1038/s41419-021-03437-w

Nakamura, J., & Nakamura, M. (2020). DNA-protein crosslink formation by endogenous aldehydes and AP sites. *DNA Repair*, *88*, 102806. https://doi.org/10.1016/j.dnarep.2020.102806

Nakano, T., Miyamoto-Matsubara, M., Shoulkamy, M. I., Salem, A. M. H., Pack, S. P., Ishimi, Y., & Ide, H. (2013). Translocation and Stability of Replicative DNA Helicases upon Encountering DNA-Protein Cross-links. *The Journal of Biological Chemistry*, *288*(7), 4649–4658. https://doi.org/10.1074/jbc.M112.419358

Nandi, P., DeVore, K., Wang, F., Li, S., Walker, J. D., Truong, T. T., LaPorte, M. G., Wipf, P., Schlager, H., McCleerey, J., Paquette, W., Columbres, R. C. A., Gan, T., Poh, Y.-P., Fromme, P., Flint, A. J., Wolf, M., Huryn, D. M., Chou, T.-F., & Chiu, P.-L. (2024). Mechanism of allosteric inhibition of human p97/VCP ATPase and its disease mutant by triazole inhibitors. *Communications Chemistry*, *7*(1), 177. https://doi.org/10.1038/s42004-024-01267-3

Nawaji, T., Yamashita, N., Umeda, H., Zhang, S., Mizoguchi, N., Seki, M., Kitazawa, T., & Teraoka, H. (2020). Cytochrome P450 Expression and Chemical Metabolic Activity before Full Liver Development in Zebrafish. *Pharmaceuticals*, *13*(12), 456. https://doi.org/10.3390/ph13120456

Nie, M., Oravcová, M., Jami-Alahmadi, Y., Wohlschlegel, J. A., Lazzerini-Denchi, E., & Boddy, M. N. (2020). FAM111A induces nuclear dysfunction in disease and viral

restriction. *The EMBO Reports*, *22*(2), EMBR202050803. https://doi.org/10.15252/embr.202050803

Nitiss, J. L. (2009). Targeting DNA topoisomerase II in cancer chemotherapy. *Nature Reviews. Cancer*, *9*(5), 338–350. https://doi.org/10.1038/nrc2607

Noireterre, A., & Stutz, F. (2024). Cdc48/p97 segregase: Spotlight on DNA-protein crosslinks. *DNA Repair*, *139*, 103691. https://doi.org/10.1016/j.dnarep.2024.103691

Oka, Y., Nakazawa, Y., Shimada, M., & Ogi, T. (2024). Endogenous aldehyde-induced DNA–protein crosslinks are resolved by transcription-coupled repair. *Nature Cell Biology*, *26*(5), 784–796. https://doi.org/10.1038/s41556-024-01401-2

Otten, C., Kutnjak, M., Supina-Pavic, C., Anticevic, I., Medved, V., & Popovic, M. (2025). *ACRC/GCNA is an essential protease that repairs DNA-protein crosslinks during vertebrate development* (p. 2023.03.07.531502). bioRxiv. https://doi.org/10.1101/2023.03.07.531502

Palani, S., Machida, Y., Alvey, J. R., Mishra, V., Welter, A. L., Cui, G., Bragantini, B., Botuyan, M. V., Cong, A. T. Q., Mer, G., Schellenberg, M. J., & Machida, Y. J. (2024). Dimerization-dependent serine protease activity of FAM111A prevents replication fork stalling at topoisomerase 1 cleavage complexes. *Nature Communications*, *15*(1), 2064. https://doi.org/10.1038/s41467-024-46207-w

Park, J.-M., Zhang, H., Nie, L., Wang, C., Huang, M., Feng, X., Tang, M., Chen, Z., Xiong, Y., Lee, N., Li, S., Yin, L., Hart, T., & Chen, J. (2023). Genome-Wide CRISPR Screens Reveal ZATT as a Synthetic Lethal Target of TOP2-Poison Etoposide That Can Act in a TDP2-Independent Pathway. *International Journal of Molecular Sciences*, *24*(7), 6545. https://doi.org/10.3390/ijms24076545

Pei, D.-S., & Strauss, P. R. (2013). Zebrafish as a model system to study DNA damage and repair. *Mutation Research - Fundamental and Molecular Mechanisms of Mutagenesis, DNA Repair and Genetic Instability*, *743–744*, 151–159. https://doi.org/10.1016/j.mrfmmm.2012.10.003

Perry, M., & Ghosal, G. (2022). Mechanisms and Regulation of DNA-Protein Crosslink Repair During DNA Replication by SPRTN Protease. *Frontiers in Molecular Biosciences*, *9*. https://doi.org/10.3389/fmolb.2022.916697

Pommier, Y. (2009). DNA Topoisomerase I Inhibitors: Chemistry, Biology and Interfacial Inhibition. *Chemical Reviews*, *109*(7), 2894–2902. https://doi.org/10.1021/cr900097c

Pommier, Y., Huang, S. N., Gao, R., Das, B. B., Murai, J., & Marchand, C. (2014). Tyrosyl-DNA-phosphodiesterases (TDP1 and TDP2). *DNA Repair*, *19*, 114–129. https://doi.org/10.1016/j.dnarep.2014.03.020

Pontifex, C. S., Zaman, M., Fanganiello, R. D., Shutt, T. E., & Pfeffer, G. (2024). Valosin-Containing Protein (VCP): A Review of Its Diverse Molecular Functions and Clinical Phenotypes. *International Journal of Molecular Sciences*, *25*(11), 5633. https://doi.org/10.3390/ijms25115633

Prasad, R., Horton, J. K., Dai, D.-P., & Wilson, S. H. (2019). Repair pathway for PARP-1 DNA-protein crosslinks. *DNA Repair*, *73*, 71–77. https://doi.org/10.1016/j.dnarep.2018.11.004

Ramadan, K., Bruderer, R., Spiga, F. M., Popp, O., Baur, T., Gotta, M., & Meyer, H. H. (2007). Cdc48/p97 promotes reformation of the nucleus by extracting the kinase Aurora B from chromatin. *Nature*, *450*(7173), 1258–1262. https://doi.org/10.1038/nature06388

Ray, A., & Opyrchal, M. (2025). Targeting PARP1: A Promising Approach for Next-Generation Poly (ADP-ribose) Polymerase Inhibitors. *Current Breast Cancer Reports*, *17*(1), 22. https://doi.org/10.1007/s12609-025-00582-5

Reinking, H. K., Hofmann, K., & Stingele, J. (2020). Function and evolution of the DNA-protein crosslink proteases Wss1 and SPRTN. *DNA Repair*, *88*, 102822. https://doi.org/10.1016/j.dnarep.2020.102822

Ribas, L., & Piferrer, F. (2014). The zebrafish (Danio rerio) as a model organism, with emphasis on applications for finfish aquaculture research. *Reviews in Aquaculture*, *6*(4), 209–240. https://doi.org/10.1111/raq.12041

Ribeiro, J., & Crossan, G. P. (2023). GCNA is a histone binding protein required for spermatogonial stem cell maintenance. *Nucleic Acids Research*, *51*(10), 4791–4813. https://doi.org/10.1093/nar/gkad168

Rodríguez-Acebes, S., Martín-Rufo, R., Gómez-Moya, A., Churcher, S. B., Fernández-Llorente, A., de la Vega-Barranco, G., Perona, A., Oroz, P., Martín-Doncel, E., Toledo, L. I., Méndez, J., & Lecona, E. (2025). DNA polymerase α/primase extraction from chromatin by VCP/p97 restricts ATR activation during unperturbed DNA replication. *Nature Communications*, *16*(1), 5706. https://doi.org/10.1038/s41467-025-60077-w

Ruggiano, A., & Ramadan, K. (2021). DNA–protein crosslink proteases in genome stability. *Communications Biology*, *4*(1), 1–11. https://doi.org/10.1038/s42003-020-01539-3

Ruggiano, A., Vaz, B., Kilgas, S., Popović, M., Rodriguez-Berriguete, G., Singh, A. N., Higgins, G. S., Kiltie, A. E., & Ramadan, K. (2021). The protease SPRTN and SUMOylation coordinate DNA-protein crosslink repair to prevent genome instability. *Cell Reports*, *37*(10), 110080. https://doi.org/10.1016/j.celrep.2021.110080

Saha, L. K., Murai, Y., Saha, S., Jo, U., Tsuda, M., Takeda, S., & Pommier, Y. (2021). Replication-dependent cytotoxicity and Spartan-mediated repair of trapped PARP1–DNA complexes. *Nucleic Acids Research*, *49*(18), 10493–10506. https://doi.org/10.1093/nar/gkab777

Santi, D. V., Norment, A., & Garrett, C. E. (1984). Covalent bond formation between a DNA-cytosine methyltransferase and DNA containing 5-azacytosine. *Proceedings of the National Academy of Sciences*, *81*(22), 6993–6997. https://doi.org/10.1073/pnas.81.22.6993

Schellenberg, M. J., Lieberman, J. A., Herrero-Ruiz, A., Butler, L. R., Williams, J. G., Muñoz-Cabello, A. M., Mueller, G. A., London, R. E., Cortés-Ledesma, F., & Williams, R. S. (2017). ZATT (ZNF451)-Mediated Resolution of Topoisomerase 2 DNA-Protein Crosslinks. *Science (New York, N.Y.)*, *357*(6358), 1412–1416. https://doi.org/10.1126/science.aam6468

Schneider, C. A., Rasband, W. S., & Eliceiri, K. W. (2012). NIH Image to ImageJ: 25 years of image analysis. *Nature Methods*, *9*(7), 671–675. https://doi.org/10.1038/nmeth.2089

Serbyn, N., Noireterre, A., Bagdiul, I., Plank, M., Michel, A. H., Loewith, R., Kornmann, B., & Stutz, F. (2020). The Aspartic Protease Ddi1 Contributes to DNA-Protein Crosslink

Repair in Yeast. *Molecular Cell*, *77*(5), 1066-1079.e9. https://doi.org/10.1016/j.molcel.2019.12.007

Shi, Y., Mowery, R. A., Ashley, J., Hentz, M., Ramirez, A. J., Bilgicer, B., Slunt-Brown, H., Borchelt, D. R., & Shaw, B. F. (2012). Abnormal SDS-PAGE migration of cytosolic proteins can identify domains and mechanisms that control surfactant binding. *Protein Science : A Publication of the Protein Society*, *21*(8), 1197–1209. https://doi.org/10.1002/pro.2107

Simon, P. (2003). Q-Gene: Processing quantitative real-time RT-PCR data. *Bioinformatics*, *19*(11), 1439–1440. https://doi.org/10.1093/bioinformatics/btg157

Song, W., Zhao, Y., Ruggiano, A., Redfield, C., Newman, J. A., Zhu, X., García-Flores, M., Cruz-Migoni, A., Roddan, R., Pérez-Ràfols, A., McHugh, P. J., Elliott, P. R., & Ramadan, K. (2025). The dual ubiquitin binding mode of SPRTN secures rapid spatiotemporal proteolysis of DNA–protein crosslinks. *Nucleic Acids Research*, *53*(13), gkaf638. https://doi.org/10.1093/nar/gkaf638

Standley, A., Xie, J., Lau, A. W., Grote, L., & Gifford, A. J. (2024). Working with Miraculous Mice: Mus musculus as a Model Organism. *Current Protocols*, *4*(10), e70021. https://doi.org/10.1002/cpz1.70021

Stingele, J., Bellelli, R., Alte, F., Hewitt, G., Sarek, G., Maslen, S. L., Tsutakawa, S. E., Borg, A., Kjær, S., Tainer, J. A., Skehel, J. M., Groll, M., & Boulton, S. J. (2016). Mechanism and Regulation of DNA-Protein Crosslink Repair by the DNA-Dependent Metalloprotease SPRTN. *Molecular Cell*, *64*(4), 688–703. https://doi.org/10.1016/j.molcel.2016.09.031

Stingele, J., Bellelli, R., & Boulton, S. J. (2017). Mechanisms of DNA–protein crosslink repair. *Nature Reviews Molecular Cell Biology*, *18*(9), 563–573. https://doi.org/10.1038/nrm.2017.56

Stingele, J., & Jentsch, S. (2015). DNA–protein crosslink repair. *Nature Reviews Molecular Cell Biology*, *16*(8), 455–460. https://doi.org/10.1038/nrm4015

Stingele, J., Schwarz, M. S., Bloemeke, N., Wolf, P. G., & Jentsch, S. (2014). A DNA-Dependent Protease Involved in DNA-Protein Crosslink Repair. *Cell*, *158*(2), 327–338. https://doi.org/10.1016/j.cell.2014.04.053

Sukted, J., Junsuntonpass, A., Homchan, A., Mongkolsuk, S., Pakotiprapha, D., & Matangkasombut, O. (2025). Wss1 and Ddi1 DNA-Protein crosslink repair proteases protect Saccharomyces cerevisiae and Candida albicans against oxidative stress. *Scientific Reports*, *15*(1), 26758. https://doi.org/10.1038/s41598-025-12238-6

Sun, Y., Miller Jenkins, L. M., Su, Y. P., Nitiss, K. C., Nitiss, J. L., & Pommier, Y. (2020). A conserved SUMO pathway repairs topoisomerase DNA-protein cross-links by engaging ubiquitin-mediated proteasomal degradation. *Science Advances*, *6*(46), eaba6290. https://doi.org/10.1126/sciadv.aba6290

Supina Pavić, C. (2023). *The role of ACRC protease and nucleotide excision repair pathway in the repair of DNA-protein crosslinks (DPCs)*. https://www.croris.hr/crosbi/publikacija/ocjenski-rad/918664

Swan, R. L., Cowell, I. G., & Austin, C. A. (2021). A role for VCP/p97 in the processing of drug-stabilised TOP2-DNA covalent complexes. *Molecular Pharmacology*, *100*(1), 57–62. https://doi.org/10.1124/molpharm.121.000262

Thomas, P., & Smart, T. G. (2005). HEK293 cell line: A vehicle for the expression of recombinant proteins. *Journal of Pharmacological and Toxicological Methods, Electrophysiological Methods in Neuropharmacology*, *51*(3), 187–200. https://doi.org/10.1016/j.vascn.2004.08.014

Tiwari, P., Kaila, P., & Guptasarma, P. (2019). Understanding anomalous mobility of proteins on SDS-PAGE with special reference to the highly acidic extracellular domains of human E- and N-cadherins. *ELECTROPHORESIS*, *40*(9), 1273–1281. https://doi.org/10.1002/elps.201800219

Tom, R., Bisson, L., & Durocher, Y. (2008). Transfection of Adherent HEK293-EBNA1 Cells in a Six-Well Plate with Branched PEI for Production of Recombinant Proteins. *Cold Spring Harbor Protocols*, *2008*(3), pdb.prot4978. https://doi.org/10.1101/pdb.prot4978

Tomaskovic, I., Prieto-Garcia, C., Boskovic, M., Glumac, M., Tsai, T.-L., Mosler, T., Kazi, R., Rathore, R., Andrade, J., Hoffmann, M., Giuliani, G., Jacomin, A.-C., Pereira, R. S., Knop, E., Wachsmuth, L., Beli, P., Husnjak, K., Pasparakis, M., Ablasser, A., … Dikic, I. (2026). DNA-protein cross-links promote cGAS-STING–driven premature aging and embryonic lethality. *Science*, *391*(6784), eadx9445. https://doi.org/10.1126/science.adx9445

Tompa, P. (2002). Intrinsically unstructured proteins. *Trends in Biochemical Sciences*, *27*(10), 527–533. https://doi.org/10.1016/S0968-0004(02)02169-2

Torrecilla, I., Ruggiano, A., Kiianitsa, K., Aljarbou, F., Lascaux, P., Hoslett, G., Song, W., Maizels, N., & Ramadan, K. (2024). Isolation and detection of DNA–protein crosslinks in mammalian cells. *Nucleic Acids Research*, *52*(2), 525–547. https://doi.org/10.1093/nar/gkad1178

Tretyakova, N. Y., Groehler, A., & Ji, S. (2015). DNA-Protein Cross-links: Formation, Structural Identities, and Biological Outcomes. *Accounts of Chemical Research*, *48*(6), 1631–1644. https://doi.org/10.1021/acs.accounts.5b00056

Unger, S., Górna, M. W., Le Béchec, A., Do Vale-Pereira, S., Bedeschi, M. F., Geiberger, S., Grigelioniene, G., Horemuzova, E., Lalatta, F., Lausch, E., Magnani, C., Nampoothiri, S., Nishimura, G., Petrella, D., Rojas-Ringeling, F., Utsunomiya, A., Zabel, B., Pradervand, S., Harshman, K., … Superti-Furga, A. (2013). FAM111A Mutations Result in Hypoparathyroidism and Impaired Skeletal Development. *American Journal of Human Genetics*, *92*(6), 990–995. https://doi.org/10.1016/j.ajhg.2013.04.020

van den Boom, J., Wolf, M., Weimann, L., Schulze, N., Li, F., Kaschani, F., Riemer, A., Zierhut, C., Kaiser, M., Iliakis, G., Funabiki, H., & Meyer, H. (2016). VCP/p97 extracts sterically trapped Ku70/80 rings from DNA in double strand break repair. *Molecular Cell*, *64*(1), 189–198. https://doi.org/10.1016/j.molcel.2016.08.037

van Sluis, M., Yu, Q., van der Woude, M., Gonzalo-Hansen, C., Dealy, S. C., Janssens, R. C., Somsen, H. B., Ramadhin, A. R., Dekkers, D. H. W., Wienecke, H. L., Demmers, J. J. P. G., Raams, A., Davó-Martínez, C., Llerena Schiffmacher, D. A., van Toorn, M., Häckes, D., Thijssen, K. L., Zhou, D., Lammers, J. G., … Marteijn, J. A. (2024). Transcription-coupled DNA–protein crosslink repair by CSB and CRL4CSA-mediated degradation. *Nature Cell Biology*, *26*(5), 770–783. https://doi.org/10.1038/s41556-024-01394-y

Vaz, B., Popovic, M., Newman, J. A., Fielden, J., Aitkenhead, H., Halder, S., Singh, A. N., Vendrell, I., Fischer, R., Torrecilla, I., Drobnitzky, N., Freire, R., Amor, D. J., Lockhart, P. J., Kessler, B. M., McKenna, G. W., Gileadi, O., & Ramadan, K. (2016). Metalloprotease SPRTN/DVC1 Orchestrates Replication-Coupled DNA-Protein Crosslink Repair. *Molecular Cell*, *64*(4), 704–719. https://doi.org/10.1016/j.molcel.2016.09.032

Vaz, B., Popovic, M., & Ramadan, K. (2017). DNA–Protein Crosslink Proteolysis Repair. *Trends in Biochemical Sciences*, *42*(6), 483–495. https://doi.org/10.1016/j.tibs.2017.03.005

Wang, P., Henning, S. M., & Heber, D. (2010). Limitations of MTT and MTS-based assays for measurement of antiproliferative activity of green tea polyphenols. *PloS One*, *5*(4), e10202. https://doi.org/10.1371/journal.pone.0010202

Weickert, P., Li, H.-Y., Götz, M. J., Dürauer, S., Yaneva, D., Zhao, S., Cordes, J., Acampora, A. C., Forne, I., Imhof, A., & Stingele, J. (2023). SPRTN patient variants cause global-genome DNA-protein crosslink repair defects. *Nature Communications*, *14*(1), 352. https://doi.org/10.1038/s41467-023-35988-1

Wendorff, T. J., Schmidt, B. H., Heslop, P., Austin, C. A., & Berger, J. M. (2012). The structure of DNA-bound human topoisomerase II alpha: Conformational mechanisms for coordinating inter-subunit interactions with DNA cleavage. *Journal of Molecular Biology*, *424*(3–4), 109–124. https://doi.org/10.1016/j.jmb.2012.07.014

White, R. M., & Patton, E. E. (2023). Adult zebrafish as advanced models of human disease. *Disease Models & Mechanisms*, *16*(8), dmm050351. https://doi.org/10.1242/dmm.050351

Wilson, B. T., Stark, Z., Sutton, R. E., Danda, S., Ekbote, A. V., Elsayed, S. M., Gibson, L., Goodship, J. A., Jackson, A. P., Te Keng, W. ik, King, M. D., McCann, E., Motojima, T., Murray, J. E., Omata, T., Pilz, D., Pope, K., Sugita, K., White, S. M., & Wilson, I. J. (2016). The Cockayne Syndrome Natural History (CoSyNH) study: Clinical findings in 102 individuals and recommendations for care. *Genetics in Medicine*, *18*(5), 483–493. https://doi.org/10.1038/gim.2015.110

Wojtaszek, J. L., & Williams, R. S. (2024). From the TOP: Formation, Recognition and Resolution of Topoisomerase DNA Protein Crosslinks. *DNA Repair*, *142*, 103751. https://doi.org/10.1016/j.dnarep.2024.103751

Yang, X., Li, Y., Gao, Z., Li, Z., Xu, J., Wang, W., & Dong, Y. (2017). Structural analysis of Wss1 protein from saccharomyces cerevisiae. *Scientific Reports*, *7*(1), 8270. https://doi.org/10.1038/s41598-017-08834-w

Yip, M. C. J., Bodnar, N. O., & Rapoport, T. A. (2020). Ddi1 is a ubiquitin-dependent protease. *Proceedings of the National Academy of Sciences of the United States of America*, *117*(14), 7776–7781. https://doi.org/10.1073/pnas.1902298117

Zhang, H., Xiong, Y., & Chen, J. (2020). DNA-protein cross-link repair: What do we know now? *Cell & Bioscience*, *10*, 3. https://doi.org/10.1186/s13578-019-0366-z

Zhang, Y.-W., Regairaz, M., Seiler, J. A., Agama, K. K., Doroshow, J. H., & Pommier, Y. (2011). Poly(ADP-ribose) polymerase and XPF–ERCC1 participate in distinct pathways for the repair of topoisomerase I-induced DNA damage in mammalian cells. *Nucleic Acids Research*, *39*(9), 3607–3620. https://doi.org/10.1093/nar/gkq1304

Zhao, W., Chen, Y., Hu, N., Long, D., & Cao, Y. (2024). The uses of zebrafish (*Danio rerio*) as an in vivo model for toxicological studies: A review based on bibliometrics. *Ecotoxicology and Environmental Safety*, *272*, 116023. https://doi.org/10.1016/j.ecoenv.2024.116023

Zhu, Y., Zhang, X., Gao, M., Huang, Y., Tan, Y., Parnas, A., Wu, S., Zhan, D., Adar, S., & Hu, J. (2024). Coordination of transcription-coupled repair and repair-independent release of lesion-stalled RNA polymerase II. *Nature Communications*, *15*, 7089. https://doi.org/10.1038/s41467-024-51463-x

7. SUMMARY

DNA-protein crosslinks (DPCs) are frequent, highly heterogeneous, and strongly cytotoxic DNA lesions that obstruct replication, transcription, and other DNA-dependent processes, yet many aspects of their repair remain insufficiently understood. This work examined the roles of the ACRC and SPRTN proteases and the p97 segregase in DPC repair at the cellular and organismal levels, using human cell lines and zebrafish (*Danio rerio*) as complementary model systems. The main objectives were to determine whether ACRC functions in vertebrate DPC repair and whether its putative protease core is required for protein function, to define the contribution of p97 to DPC repair in human cells and zebrafish embryos, and to examine whether functional coupling between SPRTN and p97 is important for the removal of endogenous DPCs. These questions were addressed using modified RADAR-based isolation of DPCs, biochemical detection of total and specific DPC species, pharmacological inhibition and morpholino-mediated silencing of p97, genetic analysis of zebrafish *acrc* mutants, and rescue experiments with SPRTN and Acrc constructs. The results showed that Acrc is essential during early vertebrate development and strongly support its role in endogenous DPC repair. Zebrafish *acrc* mutants with mutations in the SprT domain showed early embryonic lethality, and the catalytic core of the SprT domain proved crucial for Acrc function. Importantly, *acrc* mutant embryos accumulated endogenous DPCs before overt lethality, including increased levels of Dnmt1-, Top1-, Top2-, histone H3-, Parp1-, Polr3a-, and Mcm2-DPCs, indicating that Acrc contributes to the repair of multiple endogenous DPCs *in vivo*. A broad role for p97 in DPC repair was also revealed. In HeLa cells, acute inhibition of p97 led to accumulation of total cellular DPCs and multiple specific endogenous DPC species, including the structural DPCs histone H3- and Ku80-DPCs and the enzymatic DPCs PARP1-, TOP1-, DNMT1-, and TOP2-DPCs. In zebrafish embryos, pharmacological inhibition of p97 caused developmental abnormalities together with increased DPC levels, whereas morpholino-mediated silencing increased DPC levels without causing an overt morphological phenotype. Analysis of the SPRTN-p97 interaction yielded more context-dependent results. In human-cell rescue systems, no firm evidence was obtained that the p97-interacting SHP motif of SPRTN is essential for endogenous DPC repair under physiological conditions. In contrast, zebrafish embryo rescue experiments suggested that the SPRTN-p97 interaction may be important for the repair of some endogenous DPCs, particularly Parp1-, Top1-, and Dnmt1-DPCs. Overall, the findings identify ACRC as an essential vertebrate DPC repair protease and establish p97 as a broad contributor to endogenous DPC repair in human cells and zebrafish.

8. SAŽETAK

Unakrsne veze DNA i proteina (DPC-ovi) česta su, vrlo raznolika i izrazito citotoksična oštećenja DNA koja smetaju replikaciji, transkripciji i drugim procesima ovisnim o DNA, no brojni aspekti njihova popravka još uvijek nisu dovoljno razjašnjeni. U ovom radu istražene su uloge proteaza ACRC i SPRTN te segregaze p97 u popravku DPC-ova na razini stanice i organizma, pri čemu su kao komplementarni modelni sustavi korištene stanične linije čovjeka i zebrica (*Danio rerio*). Glavni ciljevi bili su utvrditi sudjeluje li ACRC u popravku DPC-ova u kralježnjaka i je li za njegovu funkciju nužna pretpostavljena proteazna jezgra, zatim odrediti doprinos p97 popravku DPC-ova u stanicama čovjeka i embrijima zebrice te ispitati je li funkcionalna povezanost SPRTN-a i p97 važna za uklanjanje endogenih DPC-ova. U tu svrhu korištena je modificirana metoda RADAR za izolaciju DPC-ova, biokemijska detekcija ukupnih i specifičnih vrsta DPC-ova, farmakološka inhibicija i utišavanje p97 pomoću morfolina, genetička analiza zebrica mutanata za *acrc* te pokusi nadoknade funkcije konstruktima SPRTN i Acrc. Rezultati su pokazali da je Acrc nužan tijekom ranog razvoja kralježnjaka te snažno podupiru njegovu ulogu u popravku endogenih DPC-ova. Mutanti zebrice za *acrc* s mutacijama u domeni SprT pokazivali su ranu embrionalnu letalnost, a katalitička jezgra domene SprT pokazala se ključnom za funkciju proteina Acrc. U mutantnim embrijima nakupljali su se endogeni DPC-ovi već prije pojave jasne letalnosti, uključujući povišene razine Dnmt1-, Top1-, Top2-, histon H3-, Parp1-, Polr3a- i Mcm2-DPC-ova, što upućuje na to da Acrc sudjeluje u popravku više vrsta endogenih DPC-ova *in vivo*. Pokazana je i važna uloga p97 u popravku DPC-ova. U HeLa stanicama akutna inhibicija p97 uzrokovala je nakupljanje ukupnih staničnih DPC-ova i više specifičnih vrsta endogenih DPC-ova, uključujući strukturne histon H3- i Ku80-DPC-ove te enzimske PARP1-, TOP1-, DNMT1- i TOP2-DPC-ove. U embrijima zebrice farmakološka inhibicija p97 uzrokovala je razvojne poremećaje praćene povišenim razinama DPC-ova, dok je utišavanje p97 morfolinom povećalo razine DPC-ova bez očitog morfološkog fenotipa. Analiza interakcije SPRTN-a i p97 dala je rezultate koji ovise o modelnom sustavu. U sustavima za nadoknadu funkcije u stanicama čovjeka nije dobiven čvrst dokaz da je SHP motiv SPRTN-a, odgovoran za interakciju s p97, nužan za popravak endogenih DPC-ova u fiziološkim uvjetima. Pokusi nadoknade funkcije u embrijima zebrice uputili su na to da bi interakcija SPRTN-a i p97 mogla biti važna za popravak nekih endogenih DPC-ova, osobito Parp1-, Top1- i Dnmt1-DPC-ova. Naposljetku, rezultati identificiraju ACRC kao esencijalnu proteazu uključenu u popravak DPC-ova u kralježnjaka te utvrđuju p97 kao važan čimbenik popravka endogenih DPC-ova u stanicama čovjeka i zebrici.

9. CURRICULUM VITAE

Marin Kutnjak is currently a Research Assistant and PhD student at the Ruđer Bošković Institute in Zagreb, and is enrolled in the Interdisciplinary Doctoral Programme of Molecular Biosciences jointly organized by the Ruđer Bošković Institute, Josip Juraj Strossmayer University of Osijek, and the University of Dubrovnik. His doctoral research centers on the roles of the proteases ACRC and SPRTN and the segregase p97 in DNA-protein crosslink repair.

He completed his Master of Science in Molecular Biology at the Faculty of Science, University of Zagreb, in 2021, graduating *summa cum laude*. His master's thesis, supervised at the Ruđer Bošković Institute, examined the role of ACRC in DNA-protein crosslink repair in zebrafish. Before that, he earned his Bachelor of Science in Molecular Biology at the same faculty in 2019, graduating *magna cum laude*, with a bachelor's thesis on RNA silencing in the regulation of gene expression and plant defense against pathogens. During his studies, he also gained experience as a practice demonstrator in cell biology and completed laboratory training both at the Faculty of Science and at the Ruđer Bošković Institute.

Since joining the Ruđer Bošković Institute, Marin Kutnjak has participated in research projects related to DNA-protein crosslink repair, including the Slovenian-Croatian bilateral project Structural characterization of factors involved in DNA-protein crosslink repair and the ongoing project The repair of topoisomerase DNA-protein crosslinks *in vivo* using zebrafish model. His work has been presented at national and international scientific meetings, including EMBO workshops, the Chromosomal Instability as a Driver of Human Disease Conference, the FEBS Congress, and the FEBS3+ Meeting, where he presented both poster and oral communications on ACRC, SPRTN, and p97 in DNA-protein crosslink repair.

For his academic and research achievements, he received the Rector's Award of the University of Zagreb for an individual scientific paper in 2021, as well as the University of Zagreb Scholarship for excellence in study and two STEM scholarships from the Croatian Ministry of Science and Education. He was also awarded several travel grants and conference bursaries, including support for EMBO and FEBS meetings. He is a member of several scientific and professional societies and networks, including the European Association for Cancer Research, the European Zebrafish Society, the Croatian Society of Biochemistry and Molecular Biology, the Croatian Association for Cancer Research, the Croatian Genetic Society,

the Croatian Biophysical Society, the Zebrafish Information Network, Association Penkala, the Independent Science and Higher Education Union, and Young European Biologists. He is fluent in Croatian and English and has working knowledge of German.

Publications

1. Otten, C.*, Kutnjak, M.*, Supina-Pavic, C., Anticevic, I., Medved, V., & Popovic, M. (2025). ACRC/GCNA is an essential protease that repairs DNA-protein crosslinks during vertebrate development (2026) (p. 2023.03.07.531502). bioRxiv. https://doi.org/10.1101/2023.03.07.531502 (*equal contribution). In press in Nucleic Acids Research (DOI: 10.1093/nar/gkag324)

2. Lončar, J., Žaja, R., Mihaljević, I., Višević, J. D., Vujica, L., Kutnjak, M., Otten, C., & Smital, T. (2026). Zebrafish Abcg2a mutant line as an *in vivo* model for evaluation of the interaction of Abcg2a with drugs and contaminants. Aquatic Toxicology, 291, 107709. https://doi.org/10.1016/j.aquatox.2026.107709

3. Vujica, L., Dragojević, J., Lončar, J., Otten, C., Kutnjak, M., Babić, S., Mihaljevic, I., & Smital, T. (2026). Differential toxicity of perfluorooctane sulfonate (PFOS) in wild-type and Oatp1d1 mutant zebrafish larvae. Chemico-Biological Interactions, 428, 111955. https://doi.org/10.1016/j.cbi.2026.111955

4. Vuković, M.*, Kutnjak, M.*, Vitko, S., Tkalec, M., & Vidaković-Cifrek, Ž. (2025). Heat Priming Modifies Heat Stress Response in *BPM1*-Overexpressing *Arabidopsis thaliana* (L.) Heynh. Journal of Plant Growth Regulation, 44(4), 1695–1712. https://doi.org/10.1007/s00344-024-11337-4 (*equal contribution)

5. In preparation: Bembic, P.[1], Kutnjak, M.[1], Otten, C., Kisovec, M., Ivic, N., Kezar, A., Anticevic, I., Adamek, M., Popovic, M.*, & Podobnik, M.* (2026). Structural and functional insights into the molecular interplay between the DNA-protein crosslink repair enzymes p97 and SPRTN ([1]equal contribution, *correspondence)